INVESTIGATION OF ROAD BASE SHEAR STRAINS USING IN-SITU INSTRUMENTATION

A thesis
submitted in partial fulfilment
of the requirements for the Degree
of
Master of Engineering (Transportation)
in the
University of Canterbury
by

Benjamin J. Hayward

University of Canterbury
2006

ABSTRACT

The large majority of New Zealand's road network is constructed from thin surfaced unbound flexible pavements where a granular layer provides the main structural strength of the pavement. The current New Zealand empirical design theory states that permanent deformation should largely be attributed to the subgrade and that shape loss in the granular layers is simply a consequence of a previously deformed subgrade. However, recent research and field trials have indicated that basecourse shear strains may be a large contributor to rutting in unbound granular layers.

The purpose of this investigation was to determine whether the shear strains induced under heavy vehicle loads can be accurately measured using in-situ induction coils and whether the shear strains are related to permanent pavement deformation.

In this investigation a rosette configuration of free floating induction coils was designed to measure principal basecourse shear strains. The principal strains were then used to construct Mohr's circle of strain in order to calculate the maximum shear strain occurring in the granular layer. The rosettes were installed in two full scale test pavements at the Canterbury Accelerated Pavement Testing Indoor Facility (CAPTIF). The pavements were loaded with an 8 tonne dual wheel axle load for 1 million and 600,000 load applications respectively and strain and rut depth testing occurred periodically throughout the test life.

The research showed that the rosette coil arrangement was a feasible and accurate device for measuring in-situ shear strains in granular pavement layers. Finite element modelling confirmed the accuracy of the system.

The results from the two CAPTIF pavements showed that there was a strong linear relationship between the magnitude of the basecourse shear strain and the rut depth at the end of the post construction compaction period. The investigation also showed that shear strain magnitudes in the region of 5000με result in rapid shear failure in the granular layer. In addition, after the post construction compaction period had finished, the rate of change of shear strain was proportional to the rate of change of rut development. The results indicated

that there was approximately a 4:1 ratio between the rate of change in rut depth and the rate of change in shear strain after the initial post construction period.

Investigations into the effect of load magnitude on the magnitude of the basecourse shear strain showed that a linear relationship existed between the two parameters. Further to this, load location testing revealed that for a dual wheel configuration, 50mm of lateral wheel variation either side of a point of interest was the maximum allowable movement that would result in similar strain measurements.

The research highlighted the dominance of the longitudinal tensile strain and shear strain over the vertical compressive strain within granular layers. As a result, these pavement responses should be considered in further granular pavement research in addition to the commonly used vertical compressive strains.

ACKNOWLEDGEMENTS

I wish to acknowledge the assistance of the following people:

Associate Professor Rob Douglas, as supervisor, for his guidance, encouragement, valuable oversight and genuine enthusiasm for the research.

Dr Bryan Pidwerbesky, as associate supervisor, for initially stimulating my interest in this field of research. Without Dr Pidwerbesky's professional interest and constant support, this research would not have been possible.

Dr James Mackechnie, as associate supervisor, for his interest and contribution to the research.

Alan Fussell and Frank Adams for their assistance on my work at CAPTIF and valuable advice.

David Alabaster for his technical advice and assistance throughout the project.

Frank Greenslade for his assistance with the emu electronics, computer programming and laboratory work.

Dr Bruce Steven, Dr Sabine Werkmeister and Alvaro Gonzalez for their advice and technical assistance.

Fulton Hogan LTD, for their financial assistance and for their genuine commitment to wider research and development in the transport engineering field.

DEDICATION

I wish to dedicate this thesis to my parents for their constant support and encouragement throughout this period of my life.

This page is intentionally left blank.

TABLE OF CONTENTS

LIST OF FIGURES

LIST OF TABLES

CHAPTER 1

INTRODUCTION

1.1 General New Zealand Conditions

More than 95% of New Zealand's roads have flexible unbound pavements. A typical cross section of this type of pavement is shown in Figure 1.1. A flexible unbound pavement consists of three major elements. The first element is the subgrade which is the natural ground on which the rest of the pavement is constructed. Typically the top 150mm of this natural layer is scarified and compacted to the desirable density. The second element is the basecourse and this layer is constructed from unbound granular material that is usually crushed quarried rock or locally sourced aggregate. The third element is the surface course which is a thin layer (usually not exceeding 50mm) comprised of either hot mix asphalt or 20 to 50mm of chip seal. The stresses caused by external loading are not resisted by the pavement structure itself, but rather the pavement serves to distribute these stresses over a large area so that the subgrade only resists a small proportion of the original surface load. The pavement layers are therefore designed to reduce the stresses and strains affecting the subgrade layer.

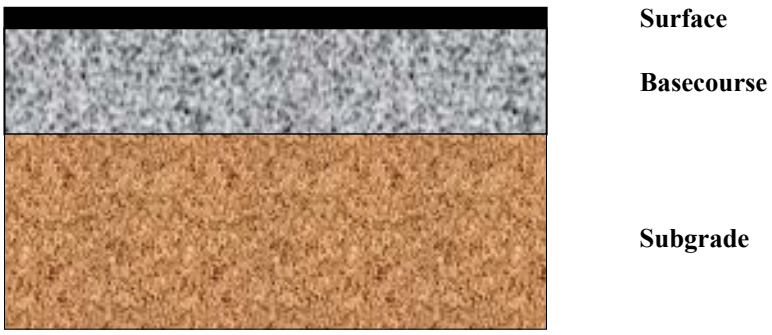

Figure 1.1 Typical cross section of a New Zealand flexible pavement.

This type of pavement structure has predominantly been used in New Zealand due to the large availability of aggregate throughout the country and the low construction cost of this type of pavement compared to other types of pavements. Therefore, overseas research and methodologies developed for structural hot mix asphalt or concrete road pavements are not applicable to the preponderance New Zealand roads.

The current New Zealand design methodology for flexible unbound pavements is based upon the 2004 AUSTROADS empirical and mechanistic design process (AUSTROADS 2004). This design method identifies two critical failure modes for unbound pavements, namely asphalt fatigue and rutting or shape loss. The first failure mode occurs due to tensile strain at the bottom of the asphalt layer, whilst the second mode of failure is stated to be caused by vertical compressive strain at the top of the subgrade. Based on these failure modes, the thickness of the basecourse layer is designed purely to minimise the stresses on the top of the subgrade. The design process therefore implies that as long as the basecourse is a high quality material that meets Transit New Zealand's (TNZ) specifications, the basecourse layer will not fail over the pavements design life. However, field evidence suggests this may not be a completely faithful picture of the behaviour.

1.2 Statement of the Problem

The current New Zealand unbound pavement design theory implies that rutting and shape loss will be caused by subgrade failure due to excessive vertical compressive strains. However, field surveys have shown that significant amounts of pavement rutting have occurred within the basecourse layers of some flexible pavements whilst the subgrade remains in good structural condition. In addition to this, pavement research on typical New Zealand roads has shown that lateral movement within the basecourse can occur under heavy vehicle loads. Based on these findings it appears that shear strains can occur within the basecourse layer and these repeated strains could result in the permanent deformation of this layer. They need to be accounted for in design procedures or in the picture of behaviour.

1.3 Need for Research

As the urban population of New Zealand continues to grow, the increase in motorway and highway traffic, especially with respect to heavy vehicles, will continue to rise. It is therefore essential for New Zealand authorities to continue to increase their practical knowledge in the area of flexible pavement design in order to construct the most structurally appropriate new roads and rehabilitated sections.

There is a genuine need for a method of in-situ field measurement of basecourse shear strains caused by heavy vehicle loading. This should be able to show the actual affects that vehicle

loads have on basecourse shear strains, which are currently not well understood. The results obtained from test using this method could be compared to both repeat load tri-axial test results and the measured permanent deformation of the test roads to verify whether the current design theory is sufficient. In addition to this, research should be able to provide field results showing the effect of different axle loads on the basecourse shear strains in order that conclusions could be drawn on the road asset consumption by various vehicle weights. A greater understanding of this type of stress within granular pavement layers could lead to significantly improved basecourse layer designs and improved rehabilitation methods and schedules.

1.4 Objectives

Based on this context, there were three main objectives developed for this investigation. The first was to experimentally determine the most appropriate induction coil matrix configuration to measure basecourse shear strains. The second was to measure basecourse strains under varying axle loads to investigate the relationship between vehicle loads and shear strain. The final objective was to attempt to relate the measured basecourse strains to any permanent deformation that occurred within the pavement. Based on the last two objectives, conclusions were to be drawn on the ability to quantify heavy vehicle consumption of unbound flexible pavements using measured basecourse shear strains.

1.5 Scope of the Research

To fulfil the objectives stated above, a literature review was conducted in order to investigate previous work undertaken on shear failure within flexible unbound granular pavements. In addition, the geotechnical theory behind shear strains and shear failure was investigated including a review of shear failure considerations in modern pavement design guides. The outcome of this literature study was that research indicated that shear failure was prominent in granular layers of unbound pavements and often in these situations the subgrade layer was structurally sound. However, the New Zealand design guide does not consider basecourse shear failure within the design process and assumes that so long as a granular material that meets TNZ M/4 (Transit NZ 2005) specifications is used, the structural layer will perform adequately. In addition, the literature search indicated that no form of instrumentation had been used to measure unbound materials' in-situ shear strength under heavy vehicle loads.

Based on this study, a method of measuring basecourse shear strains using in-situ free floating induction coils and the Canterbury Accelerated Pavement Testing Indoor Facility (CAPTIF) [1] emu soil strain measuring system (Steven 2005) was developed.

Accelerated pavement testing was conducted on two test pavements at CAPTIF during 2005 and 2006. Over the duration of the accelerated testing, basecourse shear strain measurements and rut measurement were taken at regular intervals at three stations around the track.

The measured data was used to investigate the relationship between basecourse shear strain and rut development over the test duration. In addition to this, a smaller investigation was undertaken to investigate the effect of vehicle load and wheel location on the magnitude of the in-situ shear strains.

Based on the two test pavements, relationships between shear strain magnitude and rut development were proposed and a linear relationship between vehicle load and shear strain was also presented.

[1] www.transit.govt.nz/technical/captif.jsp. CAPTIF. Transit New Zealand. Visited 16.9.2006

CHAPTER 2

LITERATURE REVIEW

2.1 Introduction

This chapter outlines the construction of flexible unbound pavements in New Zealand with an emphasis on basecourse failure due to shear forces generated by traffic loads. A review of the mechanical theory behind the development of shear strains within granular materials is presented, including the use of the Mohr-Coulomb failure envelope to define critical combinations of principal and shear stresses and the use of Mohr's circle to determine shear strains from measured principal strains.

This chapter also summarises the current New Zealand design methodology for unbound flexible pavements and highlights the lack of consideration for basecourse failure within this design method. In particular, the argument that basecourse shear strain may be a dominant factor in causing permanent deformation in the pavement is presented and supported by reference to field investigations and accelerated testing research.

2.2 Unbound Flexible Pavements

The vast majority of New Zealand roads are constructed as flexible unbound pavements with the base course covered by either chip seals or a thin asphalt concrete (AC) layer. As opposed to rigid pavements, unbound materials have no tensile strength since the unbound particles can provide no form of tensile resistance. Instead, their loading bearing capacity is derived from the interlock forces between adjacent aggregate particles. Tensile strength can only be generated by modifying the granular layers by adding lime, cement or bitumen. Figure 2.1 shows a typical cross section of a flexible pavement.

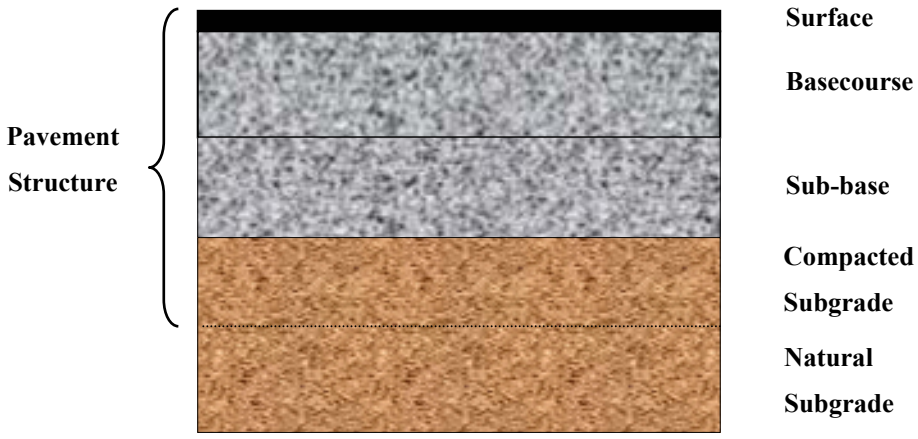

Figure 2.1 Cross section of a flexible unbound pavement.

The top layer is known as the surface course. This thin layer (usually not exceeding 50 mm) is comprised of either hot mix asphalt or 20 to 50 mm of chip seals. This is the surface that a vehicle travels along and its primary purpose is to provide a pleasant and safe driving surface for the driver and to protect the lower load bearing layers from moisture infiltration. In most cases in New Zealand this layer serves no structural purpose.

The next two layers directly beneath the surface course are the basecourse and the sub-base. The main function of these unbound granular layers is to distribute the applied load and reduce moisture transfer to the subgrade. These layers are the structural layers of the pavement and are usually made up of unbound granular material. Tensile strength can be given to these layers by modifying them with bitumen, cement or lime resulting in a bound granular layer. The distinction between the sub-base and the basecourse is that the sub-base is generally made a of lower quality material for economic reasons. This is acceptable because the stresses are lower in the sub-base due to its relative position within the pavement structure and thus the sub-base can have a lower bearing capacity compared with the basecourse. Many flexible pavements in New Zealand do not require a sub-base because the thickness of the granular layers is not large enough to warrant two distinct layers. See Figure 1.1 for a typical New Zealand pavement structure.

The final layer is the subgrade. This element of the road is natural ground on which the pavement structure will be constructed, although the upper 150mm of this layer are compacted and sometimes modified to create a stronger foundation layer. The stresses caused

by external loading are not resisted by the pavement structure itself, in the sense of flexure or shear as in flexible pavements or rigid pavement. Rather, the pavement serves to distribute these stresses over a large area so that the subgrade is subjected to reduced stresses. The pavement layers are therefore designed to reduce the stresses and strains affecting the subgrade layer.

2.3 Unbound Flexible Pavement Failure Mechanisms

The three main components of a flexible pavement can all fail independently resulting in either total pavement failure (due to a significant loss of serviceability) or further failure within other sections of the pavement. The following sub-sections outline the main mechanisms of failure within pavements' layers and the causes of these failures.

2.3.1 Asphalted Concrete Layer Failure

Asphalted concrete (AC) surface layers usually fail in tension, whereby cracks propagate through the layer until the layer's serviceability is unacceptable and failure is deemed. This is known as fatigue cracking and is one of the predominant methods of failure in AC layers. The critical pavement response for this type of failure mode is tensile strain at the bottom of the asphalt layer. This tensile strain is caused by the bending of the flexible surface course by traffic loading and the inadequate structural support from the underlying structural basecourse layer. Therefore, AC layers should perform satisfactorily so long as they are designed correctly and the basecourse layer prevents excessive bending.

2.3.2 Subgrade Failure

Subgrade failure by vertical compressive strain is considered one of the critical flexible pavement responses by the Austroads Pavement Design Guide (AUSTROADS 2004). The subgrade soil usually fails in shear when its shear capacity is exceeded by the applied load. Therefore, the failure is not a result of a poor subgrade, but rather the inability of the overlying pavement to distribute the applied load in order that the stresses at the top of the subgrade do not exceed its shear capacity. The strain induced at the top of the subgrade is mainly elastic. However, a small amount of plastic strain (non-recoverable strain) is induced with each loading cycle and therefore after a significant number of load applications

permanent deformation occurs within the subgrade. The compressive strain at the top of the subgrade pavement response is correlated to the rutting mode of failure for unbound pavements (AUSTROADS 2004).

2.3.3 Basecourse Failure

The basecourse layer within unbound flexible pavements is subject to independent failure, however, once the basecourse begins to fail it usually results in subgrade or surface course failure as described above. Permanent deformation of the basecourse layer is caused by the granular material having insufficient stability to cope with the prevailing loading and environmental conditions (AUSTROADS 2004). This situation is often caused by poor drainage conditions resulting in an increase in the moisture content within the granular layer. Consequently the particle-to-particle interlock forces are reduced and thus the bearing capacity of the main structural layer is compromised. This type of densification failure results in both rutting and shoving and is visible at the pavement surface.

Shear failure is also possible within granular layers whereby small lateral translation of the aggregate is caused by unequal strains in different directions. This involves the aggregate being horizontally translated due to the applied loads and consequently particle rearrangement is possible. This can ultimately result in permanent deformation by rutting or shoving at the surface (Vuong 2004). However, although this mode of failure has been recognized and considered within flexible pavement design in the Austroads Pavement Design Guide, there is no suitable model to accurately predict rut development due to basecourse failure and therefore it is not included within the design process.

2.4 Shear Stress in Soils and Granular Materials

The following section outlines the fundamental theory of shear strain within soil and granular materials and methods of quantifying this strain.

2.4.1 Mohr-Coulomb Failure Criterion

The resistance of a soil or granular material to support external loading is determined by the material shear strength. Hence the basecourse and sub-base material shear strength is critical

in highway design to ensure that the main structural layers can sufficiently support the vehicle loads and distribute the stresses evenly over the underlying subgrade.

In the early 1900's Otto Mohr developed a theory that stated that materials fail due to a critical combination of both shear stress and normal stress. The relationship between shear stress and normal stress on a given failure plane was expressed as a linear approximation (Equation 1) and is commonly known as the Mohr-Coulomb failure criterion. The line this equation forms is referred to as the failure envelope.

$$\tau_f = c + \sigma \tan\phi \quad (1)$$

Where:

τ_f = Shear strength (kN/m^2)

c = Cohesion (kN/m^2)

ϕ = Angle of internal friction (degrees)

σ = Normal stress on the failure plane (kN/m^2)

The shear strength of a soil is defined as the internal resistance per unit area that the soil mass can offer to resist failure and sliding along any plane inside it (Das 2002). Figure 2.2b visually illustrates the Mohr-Coulomb failure envelope, whereby if the magnitudes of the given stresses (shown in Figure 2.2a) on the failure plane are at point A then shear failure will not occur. However, if the magnitudes of the stresses are represented by point B then failure will, occur along the plane.

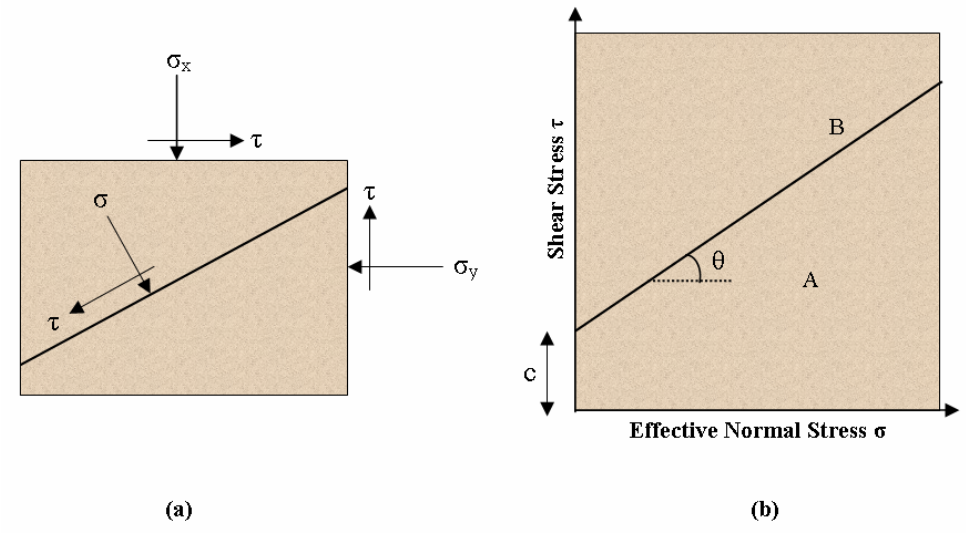

Figure 2.2 Mohr-Coulomb failure criterion.

Mohr's circle can be used to determine the inclination angle of the failure plane (θ) so long as the major and minor principal stresses (σ_1 and σ_2) are known. The principal stresses are stresses that occur on two sets of orthogonal planes with no shear stress (τ) and compressive stresses are considered positive.

2.4.2 Mohr's Circle

The magnitude of shear stress and normal stress vary throughout a soil element depending on the angle of the plane under consideration. The stresses on a plane inclined at an angle θ to the direction of the plane on which σ_1 acts can be obtained be considering the equilibrium of the forces acting on a soil element (such as Figure 2.2a). Resolving these forces in the direction of $\sigma_{n\theta}$ results in Equation 2 and Equation 3 (Parry 1995).

$$\sigma_{n\theta} = \sigma_x \cos^2\theta + \sigma_y \sin^2\theta + \tau_{xy} \sin 2\theta \tag{2}$$

$$\tau_\theta = \frac{1}{2}(\sigma_y - \sigma_z)\sin 2\theta + \tau_{xy} \cos 2\theta \tag{3}$$

By using the relationships

$$\cos^2\theta = \frac{1+\cos 2\theta}{2}$$

$$\sin^2\theta = \frac{1-\cos 2\theta}{2}$$

Equation 2 can take on the form

$$\sigma_{n\theta} - \frac{1}{2}(\sigma_x + \sigma_y) = \frac{1}{2}(\sigma_x - \sigma_y)\cos 2\theta + \tau_{xy} \sin 2\theta \tag{4}$$

If equations 3 and 4 are squared and added and some algebraic manipulation is conducted, Equation 5 can be formed.

$$\left[\sigma_{n\theta} - \frac{1}{2}(\sigma_x + \sigma_y)\right]^2 + \tau^2{}_\theta = \left[\frac{1}{2}(\sigma_x - \sigma_y)\right]^2 + \tau^2{}_{xy} \tag{5}$$

Setting $$s = \frac{1}{2}(\sigma_x + \sigma_y)$$

$$r^2 = \left[\frac{1}{2}(\sigma_x - \sigma_y)\right]^2 + \tau^2{}_{xy}$$

Then Equation 5 can be simplified to form Equation 6 which is the general form a circle with radius r and centre point s.

$$(\sigma_{n\theta} - s)^2 + \tau^2{}_{\theta} = r^2 \qquad (6)$$

Therefore if these varying stress values relating to a specific plane angle (θ) are plotted on a coordinate system with shear stress on the vertical axis and normal stress on the horizontal axis, a circle is formed. For example, the soil element shown in Figure 2.3 has a major principal stress of σ_1 and a minor principal stress of σ_3. In addition to this a plane at an angle θ is shown on the element.

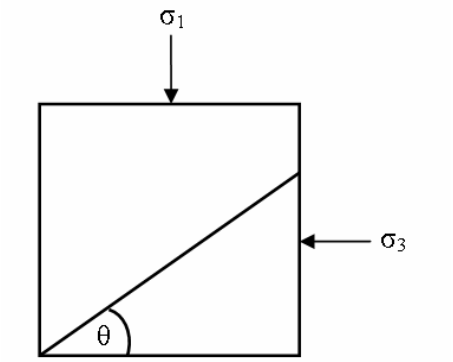

Figure 2.3 Representation of principal stresses on a soil element.

These two principal stresses can then be plotted forming Mohr's circle (Figure 2.4) for the specific soil element shown. Based on this circle, the shear and normal stress on the plane with angle θ can be interpreted. However, to determine these stresses from Mohr's circle an angle of 2θ must be used because the central angle of a circle is twice that of the original soil element.

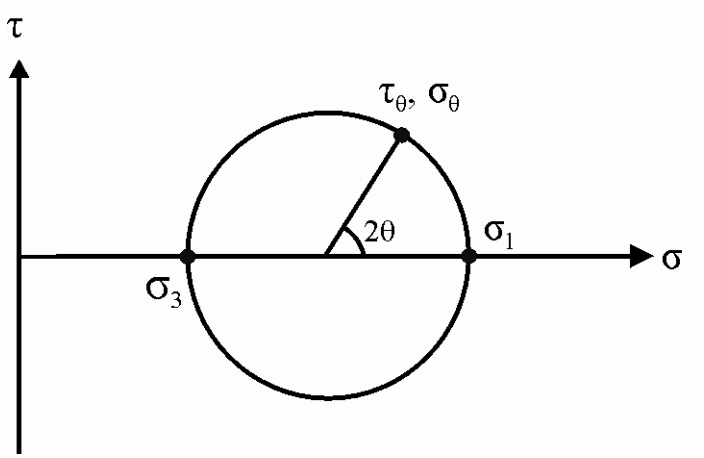

Figure 2.4 Mohr's Circle plot of soil element stresses

Multiple Mohr's circle plots determined from repeat load tri-axial tests can be used to experimentally determine the Mohr-Coulomb failure envelope discussed in Section 2.4.1. This results in a failure envelope for a specific material. Based on this envelope it can be determined whether or not a material will fail due to any specific combination of normal and shear stress. An example of multiple tri-axial test Mohr's circles and the subsequent failure envelope is shown in Figure 2.5. This plot clearly shows that failure does not always occur when the shear stress is at a maximum but rather at critical combinations of shear stress and normal stress.

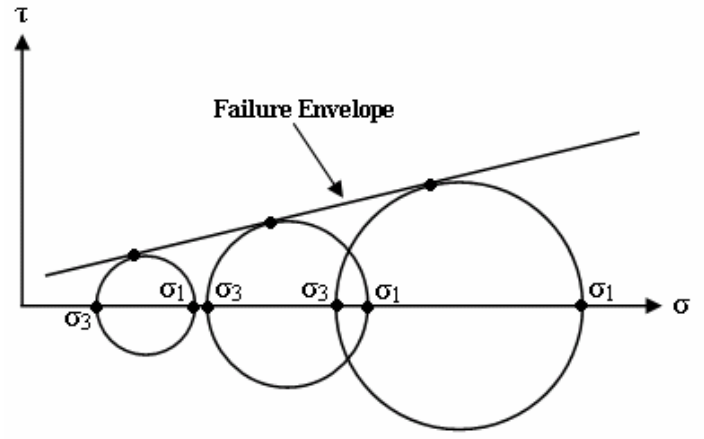

Figure 2.5 Example of multiple Mohr's circles from tri-axial tests forming the failure envelope.

In the same way that Mohr's circle of stress can be determined by knowing and plotting the principal stresses, a circle of strain can also be plotted based on known strains in an element. The circle of strain is based on Equation 7 which is simply a strain transformation of Equation 5.

$$\left[\varepsilon_\theta - \left(\frac{\varepsilon_x + \varepsilon_y}{2}\right)\right]^2 + \left[\frac{\gamma_\theta}{2} - 0\right]^2 = \left[\sqrt{\left(\frac{\varepsilon_x - \varepsilon_y}{2}\right)^2 + \left(\frac{\gamma_{xy}}{2}\right)^2}\right]^2 \quad (7)$$

Where:

γ = engineering shear strain.

The engineering shear strain (for example γ_{xy}) is the total shear distortion of the element and this represents the total measure of shear strain in the x–y plane (Parry 1995). Therefore:

$$\gamma = \varepsilon_{yx} + \varepsilon_{xy} = 2\varepsilon_{xy}$$

This is in contrast to shear strain (ε_{xy}) which is the average of the shear strain on the x face along the y direction, and on the y face along the x direction.

Since engineers almost always work in terms of engineering shear strain (sometimes known as volumetric strain), engineering shear strain (γ) will be used throughout the thesis.

Figure 2.6 shows how the principal strains (ε_1, ε_1) on the element can be plotted to form Mohr's circle of strain. In addition to this, the maximum shear strain (γ_{max}) can be determined from the circle and the angle that this shear strain occurs at can be measured and related back to the soil element. In this specific example, the maximum shear strain occurs on two complementary 45º planes (90º and 270º on the circle due to the central angle) and the magnitude of this shear strain is equal to the diameter of the circle. It should be noted that compressive strains are considered positive and tensile strains are negative.

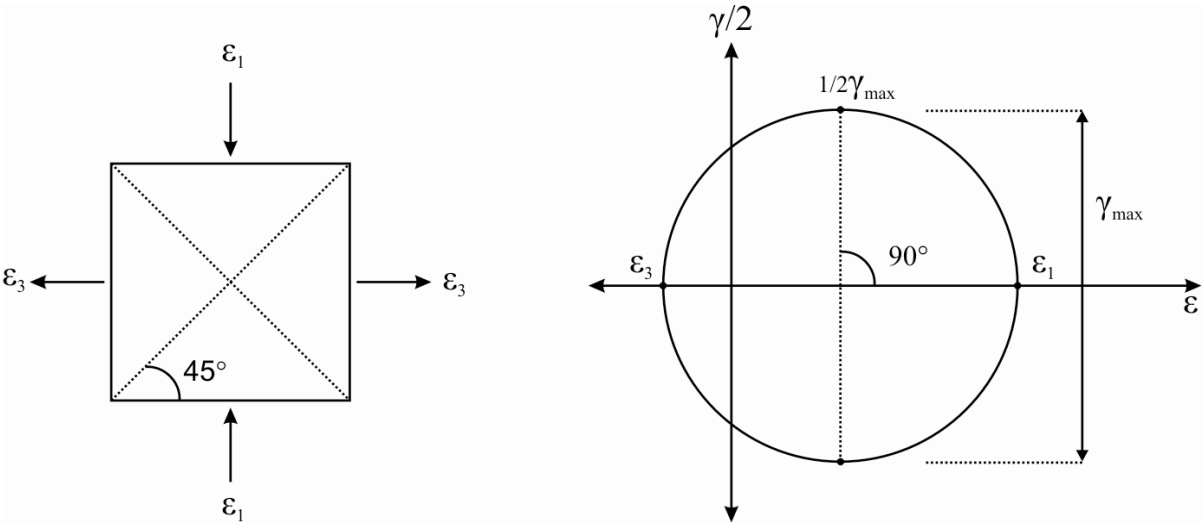

Figure 2.6 Soil element with principal strains and corresponding Mohr's circle of strain

2.4.3 Shear Strain in Pavement Basecourse

As opposed to pure shear failure along a clearly defined failure plane as previously described, basecourse shear failure results from cyclic lateral translation of a section of the granular material (usually under the wheel path) that leads to rutting or heave at the surface. This type of failure is often known as shallow shear failure and is usually assumed to only occur when the basecourse layer is under-compacted or has a high moisture content, both of which reduce the particle to particle interlock forces. An example of the typical aggregate movement (shear strain) induced by heavy vehicle loading is shown in Figure 2.7.

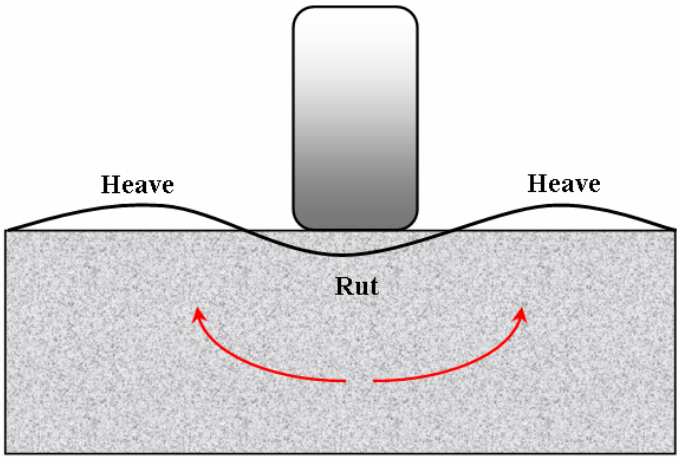

Figure 2.7 Basecourse shear movement and consequent permanent deformation.

However, pavement research and field excavations have suggested that this type of basecourse shear strain can occur within well-constructed flexible pavements. Unfortunately, the current New Zealand design code doesn't account for it.

2.5 Current New Zealand Flexible Pavement Design Process

Australian roads are designed and constructed very similar to those in New Zealand because of the availability of high quality aggregate deposits. The Association of Australian and New Zealand Road Traffic and Transport Authorities (AUSTROADS) is involved in a significant amount of flexible pavement research, publication of guides and manuals and a comprehensive knowledge-sharing network. For this reason New Zealand's State highway authority (Transit New Zealand) became a participating member of AUSTROADS[2]. In 1995 Transit New Zealand adopted the AUSTROADS document *Pavement Design – A Guide to the Structural Design of Road Pavements (1992)*, subsequently referred to in this report as the Austroads Pavement Design Guide. In addition to this, Transit New Zealand publishes a New Zealand supplement to the AUSTROADS document incorporating Transit New Zealand's material specifications and other considerations unique to New Zealand. Transit New Zealand has recently adopted the revised 2004 edition of the Austroads Pavement Design Guide (AUSTROADS 2004).

The Austroads Pavement Design Guide follows an empirical design procedure for unbound flexible pavements with thin asphalt (less than 40mm) or chip sealed surfaces. The Guide also contains a mechanistic design procedure for flexible pavements with thick asphalt surfaces and stabilised basecourse layers. However, this later type of pavement design will not be considered in this investigation.

2.5.1 Flexible Unbound Empirical Design Method

The AUSTROADS empirical flexible pavement design process evolves determining the basecourse thickness using a design chart where the required input data is the design traffic and the subgrade California bearing ratio (CBR).

[2] http://www.austroads.com.au/about_us.html. About Austroads. AUSTROADS. Visited 18.9.2005.

The design traffic value represents the number of equivalent standard axles (ESA) that the pavement is estimated to experience during its design life. An ESA represents one pass of a single axle with dual wheels carrying 80kN.

The subgrade CBR is a value that expresses the strength of the in-situ material. This value can be used with correlation charts to convert the value to a resilient modulus value which is a more common expression of a material's stiffness. The CBR value is most accurately determined by conducting a penetration test where a standard piston with an area of 1935mm^2 is pushed into the soil at a standard rate of 1.3mm per minute. The pressure at each 2.5mm interval is recorded up to 12.7mm. The ratio between the tested material's bearing capacity and a standard premium crushed rock is then calculated at 2.5mm and 5.0mm penetration. The maximum ratio value is the CBR value for the tested material.

Using both the subgrade CBR and the design traffic value, the thickness of the basecourse layer is determined using the design chart shown in Figure 2.8 (AUSTROADS 2004). This design process is based around subgrade deformation being the critical failure mode. The basecourse design chart is only used to ensure the depth of the granular layer is sufficient to distribute the applied vehicle stresses to such a degree that the vertical compressive strain at the top of the subgrade is minimized to an acceptable level (Jameson 2003). There is no consideration of shear capacity within the granular layers. The New Zealand supplement to the Austroads Pavement Design Guide states that it is assumed that base layers have sufficient shear strength to withstand the proposed traffic loading so long as the materials comply with the appropriate Transit New Zealand M/4 specifications (Transit NZ 2000).

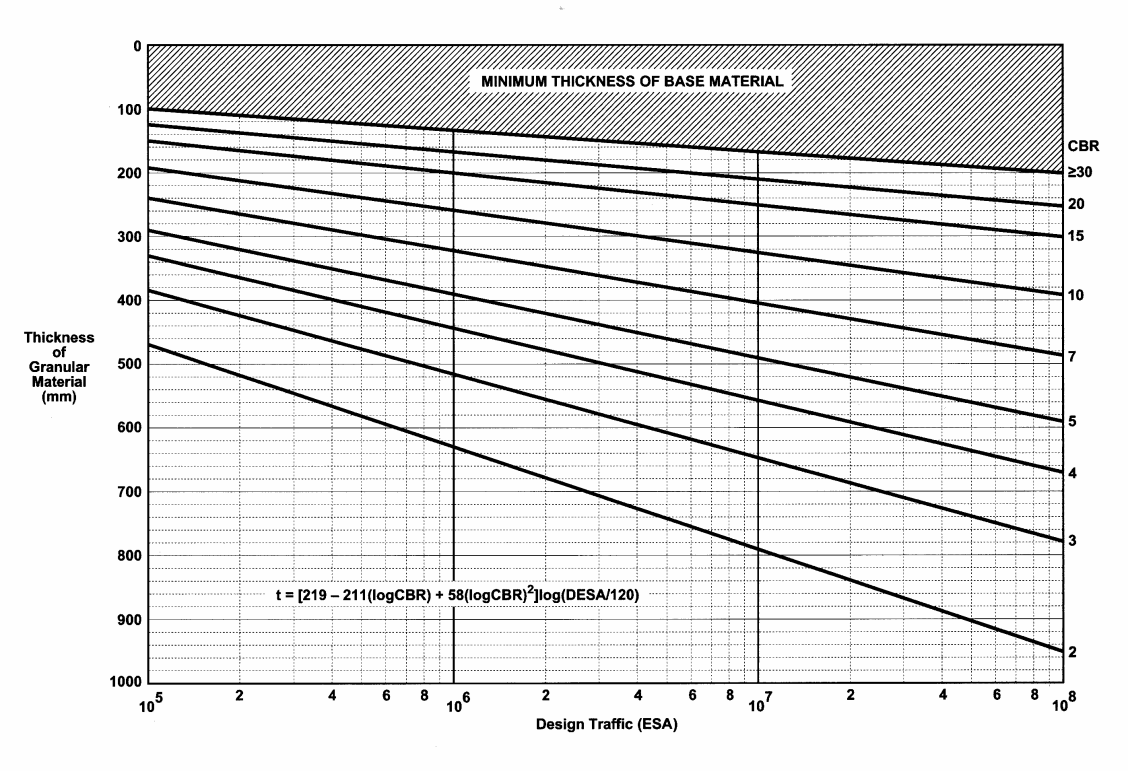

Figure 2.8 Design chart for granular pavements with thin surfaces (AUSTROADS, 2004).

Some alternative pavement design guides that are based on road types similar to New Zealand pavements, such as the South African Mechanistic-Empirical Design Method (SAMDM), have considered shear stress as a critical failure parameter within basecourse layers. The SAMDM utilises safety factor equations, developed by Maree in 1978, to determine the ratio of the material's shear strength divided by the applied stress causing shear. The safety factors are calculated from the Mohr-Coulomb shear strength parameters of the granular material (cohesion and internal angle of friction) and the major and minor principle stresses around the point of interest in the layer. The safety factor is then used in one of four different transfer equations (depending on the class or function of the road) to calculate the allowable number of load applications until shear failure occurs (Theyse et al. 1996). This method has been questioned as to whether there is a lack of understanding of the nature of shear strength and shear failure within granular materials. For example, the safety factor equation does not take into consideration construction density or the degree of saturation of the material. This has been highlighted in South Africa where sections of consistently designed road failed in shear in certain places but remain in good structural condition in other areas (Theyse 2004).

2.6 Observed Flexible Pavement Responses

The current design theory assumes that as long as a high quality basecourse aggregate is used during construction and the required thickness and compaction are achieved then basecourse deformation should not occur. Attention with respect to rutting would thus shift to the subgrade. However, research by Douglas (1997) has indicated that improved performance of unbound granular pavements is more due to the response of the basecourse than the subgrade. This conclusion was drawn by comparing the performance of the pavement's overall structural performance and subgrade vertical compressive strains. Douglas' research showed that decreasing heavy vehicles tyre inflation pressure resulted in an improved performance of the overall pavement but had minimal effect on the subgrade's vertical compressive strain. This therefore indicated that the performance was a result of the behaviour of the basecourse. Douglas thus concluded that rut development can be viewed as an indication of base behaviour under loading, if there is no appreciable subgrade consolidation.

Subsequent research by Dawson (Dawson 2002) provides positive evidence to support the basecourse failure theory, with numerous test site photographs showing significant basecourse rutting whilst the subgrade remained in good structural condition. Figure 2.9 and Figure 2.10 (Dawson 2002) show examples of unbound pavement exhumations in Galloway, Scotland, where the basecourse had rutted but the subgrade remained generally undeformed.

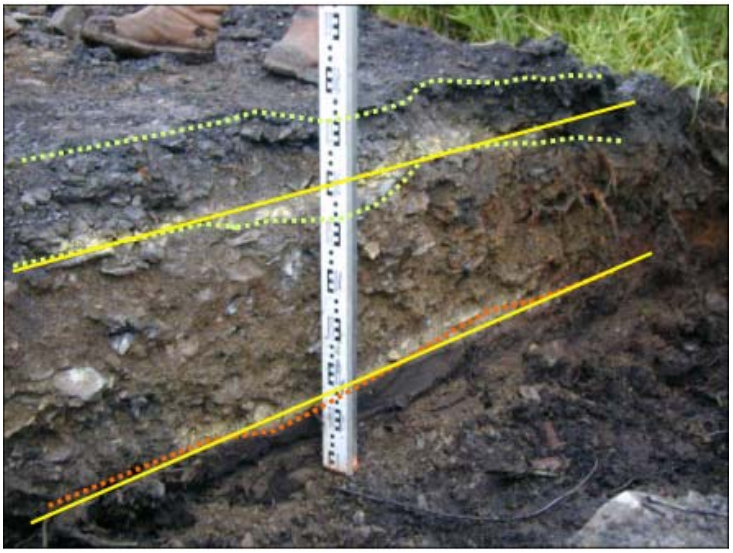

Figure 2.9 Forestry road basecourse rutting is dominant to subgrade rutting (Dawson, 2002).

Figure 2.10 Large basecourse rutting and heaving with minimal subgrade deformation (Dawson, 2002).

Therefore in certain cases, "the typical assumption that the aggregate moves bodily downwards on a deforming subgrade is inappropriate" (Dawson 1997). Dawson identified three modes of rutting failure within pavements. The first mode has local shear close to the wheel path occurring in the basecourse. Shear in this context is more appropriately described as a lateral translation of the aggregate resulting in dilative heave parallel to the wheel path. This mode of failure is also known as shallow shear failure.

In addition to this, field investigations by New Zealand roading contractors including Fulton Hogan have shown cases where significant pavement rutting has occurred where the subgrade remains in good condition, but, the basecourse has been deformed (Pidwerbesky 2005). This phenomenon does not comply with the current design theory and therefore it is suggested that basecourse shear stains may be a major cause of permanent pavement deformation.

Research by Pidwerbesky at the CAPTIF facility revealed that during testing, shallow shear appeared to be occurring in the basecourse (Pidwerbesky 1996). Vertical coil pairs within both wheel paths of the basecourse had been installed and were separated by 600mm to sense strain. It was observed that when the wheel load passed over the first coil pair, the coils moved closer together as elastic deformation occurred. The coils did not completely return to their original position, but rather a small amount of permanent vertical compression remained as shown in Figure 2.11. When the wheel load passed over the second coil pair in the alternative wheel path, the second pair of coils compressed vertically in the same way as the

first coil pair, but, as this occurred, the first coil pair expanded slightly and returned to their original position (see Figure 2.12). Pidwerbesky (Pidwerbesky 1996) related this expansion to shallow shear forces created by the wheel load in the alternative wheel path. It was stated that these forces "could affect the degradation of the aggregate in the pavement" (Pidwerbesky 1996).

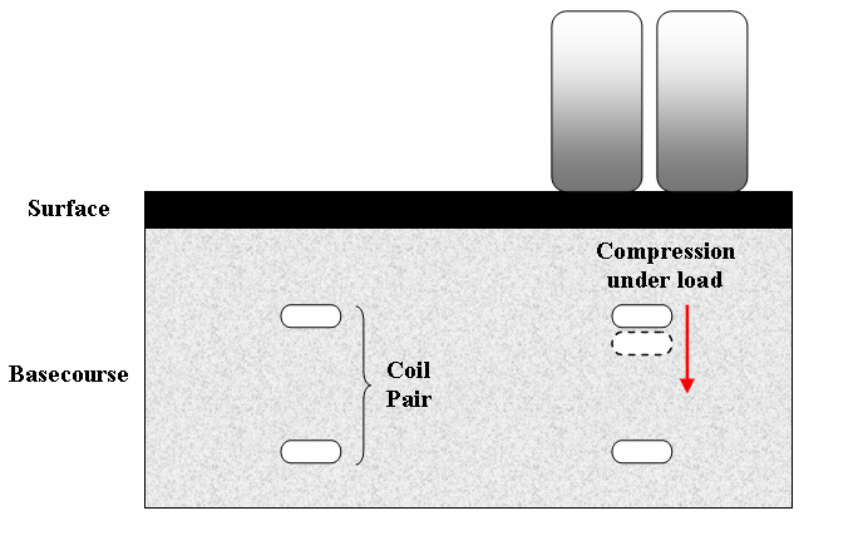

Figure 2.11 Stage 1- Vertical compression of the coils under the wheel load resulting in a final small permanent compression.

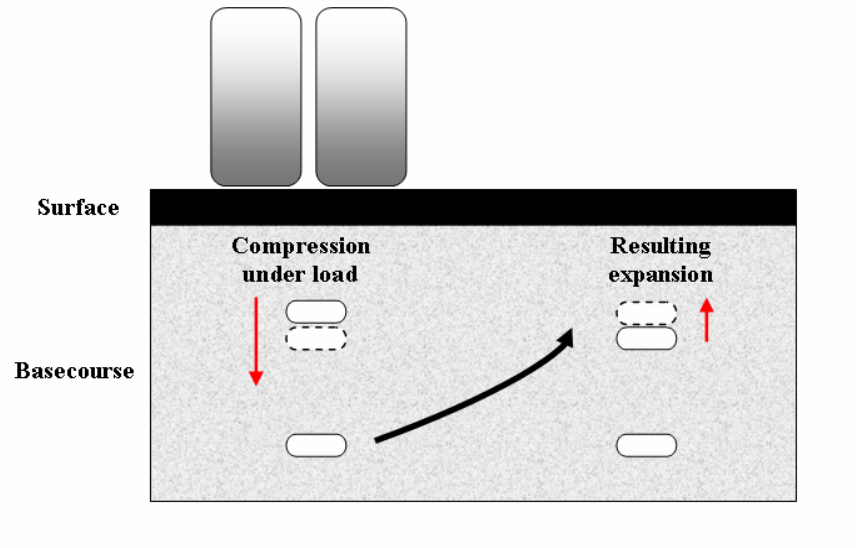

Figure 2.12 Stage 2 - Vertical compression of loaded coils and vertical expansion of previously permanently compressed coils caused by lateral basecourse movement.

In summary, Douglas' (1997) research could be considered negative evidence against the current design theory by inferring that distortion causing rutting is not in the subgrade, but rather in the base. Conversely, Dawson's (2002) observations of basecourse rutting without permanent subgrade deformation and Pidwerbesky's (1996) observations of lateral basecourse movement both provide positive evidence for considering basecourse shear as a major factor leading to permanent pavement deformation. These two forms of evidence provide solid justification for the proposed research.

2.7 Chapter Summary

The vast majority of New Zealand roads are flexible unbound pavements which are designed using an empirical design method. This design method involves determining the granular layer thickness from an empirical chart using the known subgrade bearing capacity and the estimated design traffic. This design method assumes that failure by way of permanent deformation will only occur if the vertical compressive strains at the top of the subgrade repeatedly exceed a critical limit. This model of behaviour assumes that permanent deformation is largely attributed to subgrade strain and that shape loss in the granular layers is simply a consequence of the deformation of the subgrade.

Current research has indicated that subgrade deformation may make a significantly smaller contribution to surface rutting than the model assumes (Douglas 1997). In addition to this, flexible unbound pavement exhumations have shown many cases where there has been a substantial amount of basecourse rutting with minimal to no subgrade deformation (Dawson 2002). It has been suggested that this basecourse deformation is due to the lateral translation of basecourse material, otherwise known as shallow shear strains (Pidwerbesky 1996).

CHAPTER 3

INDUCTION COIL CONFIGURATION DESIGN

In order to measure shear strains within granular layers, free floating induction coils were used due to their ability to accurately measure vertical and horizontal stains in granular layers (Hayward 2004). However, as opposed to previous investigations that have utilised induction coils to measure only sub-surface vertical and horizontal strains, a method was required to measure shear strains. The following chapter introduces the theory behind free floating induction coils as well as detailing the laboratory investigation that was conducted in order to finalise a feasible method of measuring in-situ shear strains.

3.1 Strain Measurement Using Free-Floating Induction Coils

Induction coils, originally developed by Bison Instruments in Minnesota, are simply small, flat, circular disks with wire wound around their perimeter. Pavement response data collection relies on the concept of induced voltage, whereby by one of the two disks separated by a nominal distance, has an alternating voltage applied to it. This coil is known as the transmitter and the voltage creates an electro-magnetic field around the coil. This magnetic field induces a voltage in the second coil which is called the receiver and the magnitude of this induced voltage is proportional to the distance between the coils (Paterson 1972). An illustration of the operation principles are shown in Figure 3.1.

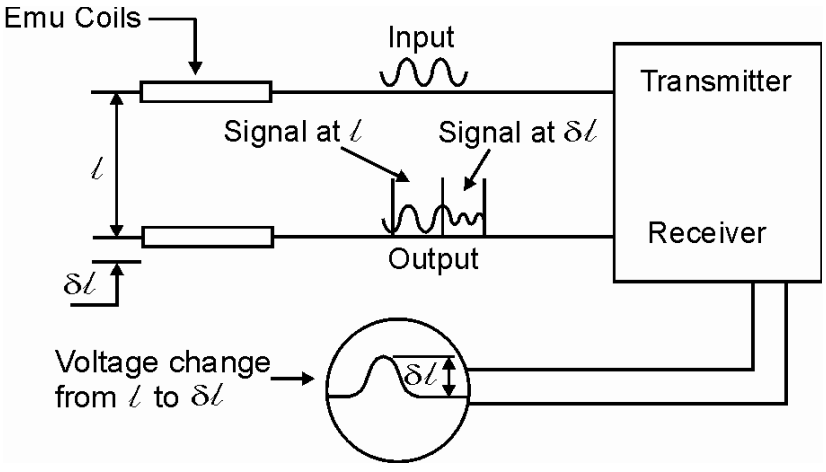

Figure 3.1 Principle of induction coil strain measurement system.

These coils are highly practical for pavement response investigation in that they can be set in place at any location throughout the pavement structure and at any stage during of construction, thus giving a clear indication of how different sections of the pavement respond to applied loads. The coils also have the benefit of being able to be installed during the construction of the road. The disk that holds the coil is generally made from structurally reliable plastic that does not puncture during the compaction of unbound layers and thus pavement disruption after construction can be avoided. The induction coil's minimally intrusive nature also suggests that an accurate representation of the pavement response can be expected since there is a minimal "zone of disturbance" during installation Figure 3.2. Research by Janoo, Irwin and Knuth (Janoo et al. 2000) has also shown that slight disruption of the coil alignment has minimal effects on the calculated strains, with 10-degree rotational misalignment being the acceptable limit, and one tenth of the strain gauge length being the lateral misalignment limit. These results confirm the findings of Patterson (1972).

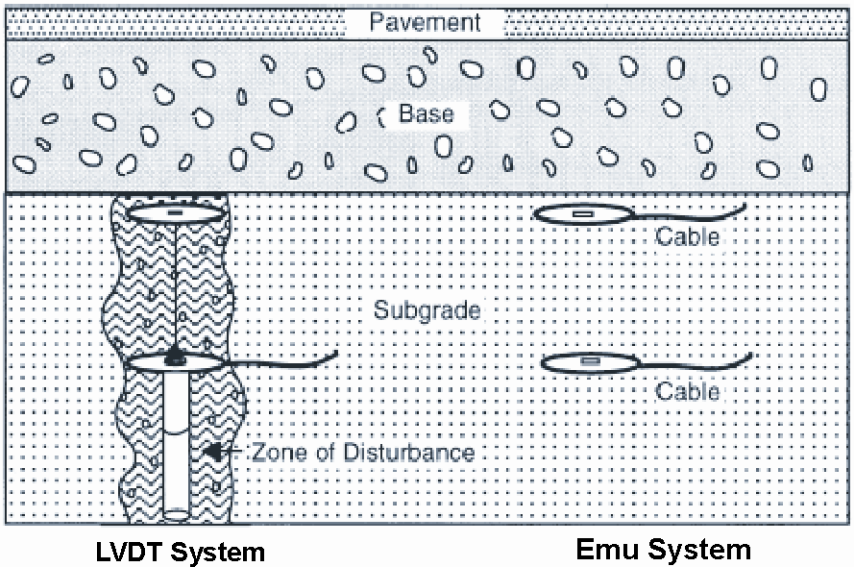

Figure 3.2 Comparison of LVDT's and induction coils intrusive nature (Janoo et al. 2000).

One disadvantage of this system is that the induction coils are more sensitive to external electrical noise than linear variable differential transducers (LVDT) which are common for measuring strain in pavements. However the "ε-mu" Soil Strain Measurement System developed at the University of Nottingham has reduced this phenomenon to an acceptable level, where the inferred strain produced by external noise is insignificant compared to the strain produced by live loading.

Research conducted at the U.S. Army Cold Regions Laboratory and the University of Nottingham has produced accurate results, indicating that in-situ induction coils are a feasible method of determining strain measurements within pavement layers (Janoo et al. 2000). Research has also been conducted by Pidwerbesky (1996) at the University of Canterbury and the Canterbury Accelerated Pavement Indoor Testing Facility (CAPTIF) on the behaviour of unbound granular pavements using this same strain measurement method, once again producing accurate sub surface strain measurements to within ± 50με.

3.2 Coil Configuration Designs

In order to measure basecourse shear strains, two coil configuration designs were initially suggested. It was intended that both of these designs would be installed in the first test pavement and that the measured shear strains would be compared to verify the systems. Based on the results from the first test pavement one of the designs was to be selected to be used in the subsequent test pavements. The choice of this final design would be based on the accuracy of the measured strains and the ease of installation. However, laboratory testing revealed that one of the concept designs was not feasible.

3.2.1 Rosette Design

The first of the two concept coil configuration designs was called a *Rosette*. This design involved three pairs of co-axial coils separated by 75mm measuring the three principal strains within hypothetical cube of granular material. Using the measured principal strains, Mohr's circle of strain can be plotted in order to determine the maximum shear strain on two planes. This type of analysis is based on the assumption that there is no shear strain acting on the faces of the material cube. Obviously small shear strains on the cube faces will be present due to the torque caused by the tyre and therefore the compressive and tensile strains measured by the coils are not the true principal strains. However, these strains are assumed to be small enough that neglecting them will not have a significant effect on the magnitude of the calculated maximum shear strain within the soil element. Refer to Section 7.1.1 for finite element analysis verification of this assumption.

The coil configuration initially had one 50mm diameter coil sitting flat on each of the six sides of a 75mm square cube. However, it was later decided that six coils (including the

insulated leads) within this close proximity of each other may result in the in-situ cube of material being reinforced. Therefore it was decided to change the design by separating the pairs and spacing them out at 200mm along the wheel path Figure 3.3.

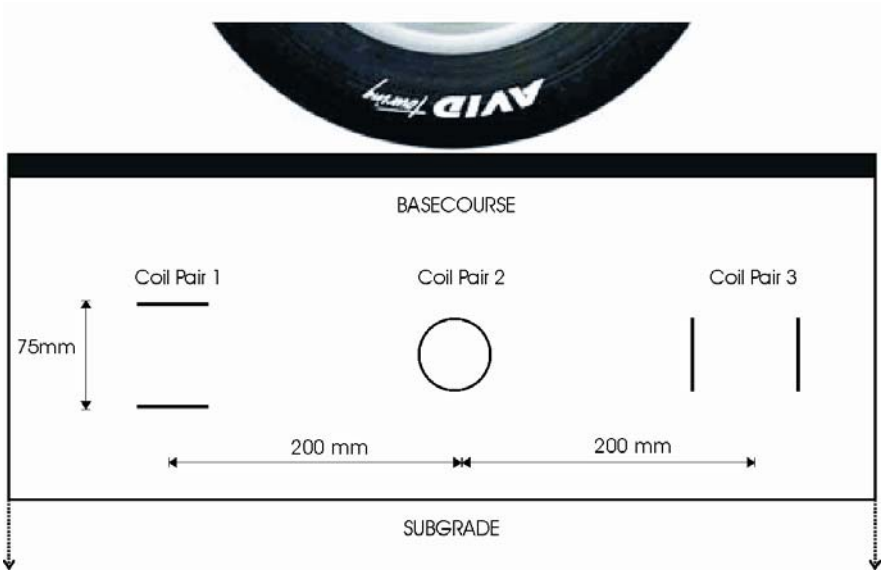

Figure 3.3 Side elevation of a pavement with rosette general design

Based on the known speed of the test vehicle and the 200mm spacing between the coils, the measured strain profiles for each of the three coil pairs can be translated back to one specific point. This would result in the same measurements that would have occurred if all three coil pairs were located around the same in-situ cube of material. A visual illustration of this is shown in Figure 3.4 and Figure 3.5.

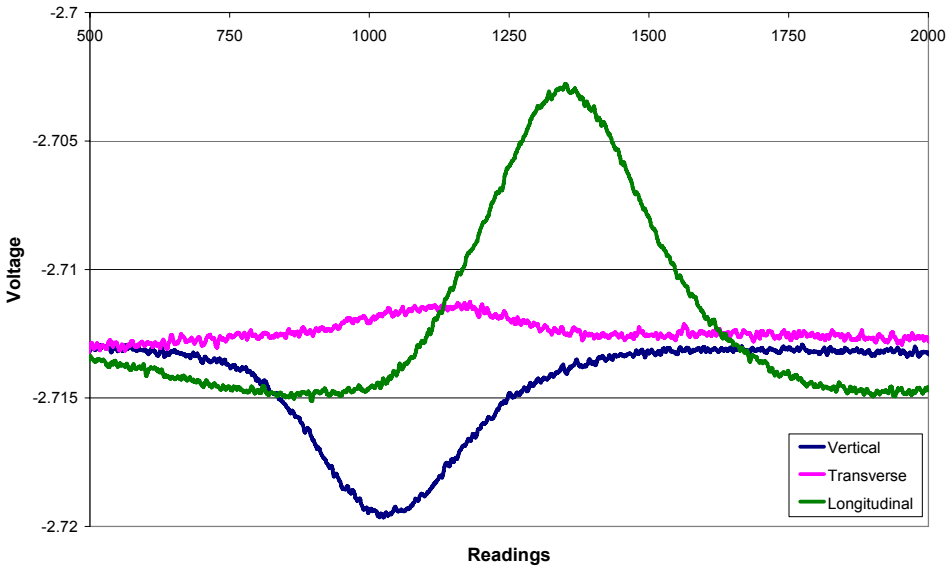

Figure 3.4 Example of original voltage traces from a rosette

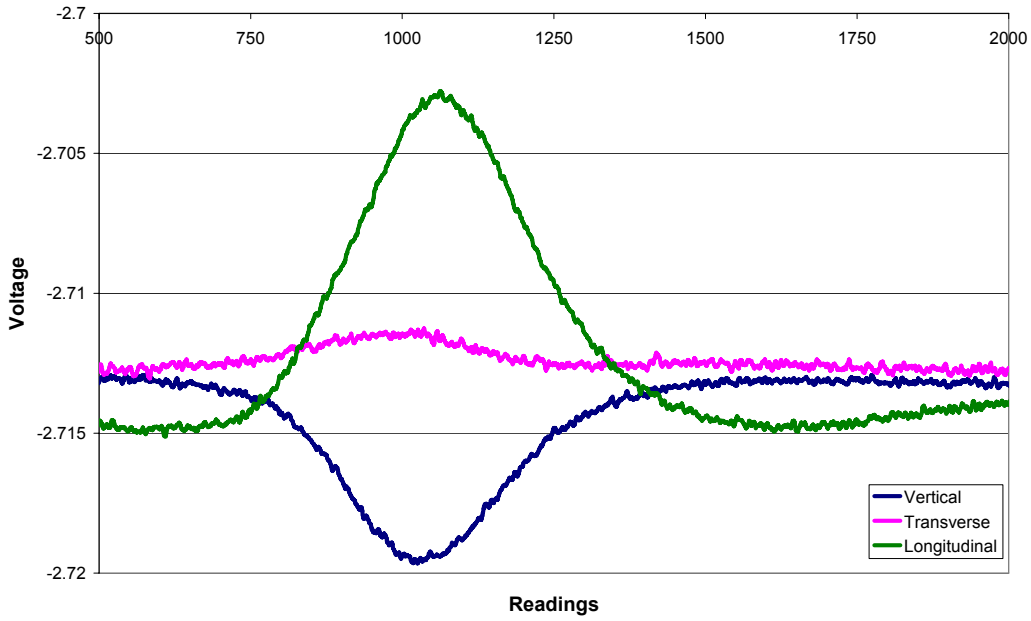

Figure 3.5 Example of transverse and longitudinal voltage traces translated back to vertical trace

3.2.2 Shear Strain Calculation from Rosettes

The basecourse shear strength in a well constructed pavement ensures that combinations of shear strains and normal strains induced by vehicle loads are significantly below the Mohr Coulomb failure criterion (otherwise rapid failure would occur). Likewise, the magnitudes of the shear strains measured in this investigation at CAPTIF are significantly below the critical shear strains defined by the Mohr Coulomb failure criterion. The three coil pairs that make up one rosette measure the three principal strains around the in-situ granular cube as shown in Figure 3.6. The vertical, transverse and longitudinal strains are represented by ε_v, ε_t, ε_l respectively.

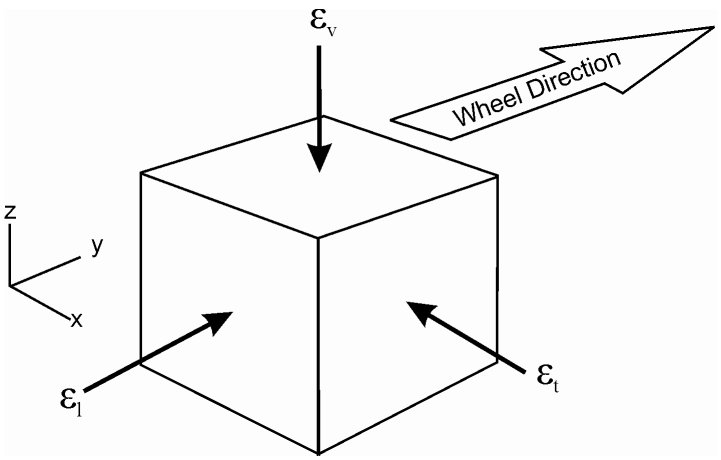

Figure 3.6 Principal strains measured by rosette in CAPTIF.

Using the vertical and longitudinal principal strains and the vertical and transverse principal strains, two Mohr's circles can be constructed to determine the combination of normal and shear strains at any angle on the yz and xy planes. In addition to this, the magnitude of the maximum shear strain can be determined from the plot, where this value is equal to the diameter of the circle. For example, Figure 3.7 shows an element of soil with the vertical and longitudinal strains measured. Based on these principal strains, Mohr's circle of strain is constructed and the maximum shear strain is determined. In addition to this, the circle indicates that this maximum shear strain occurs on a 45 degree plane within the element (shown by the dashed line on the element with shear arrows).

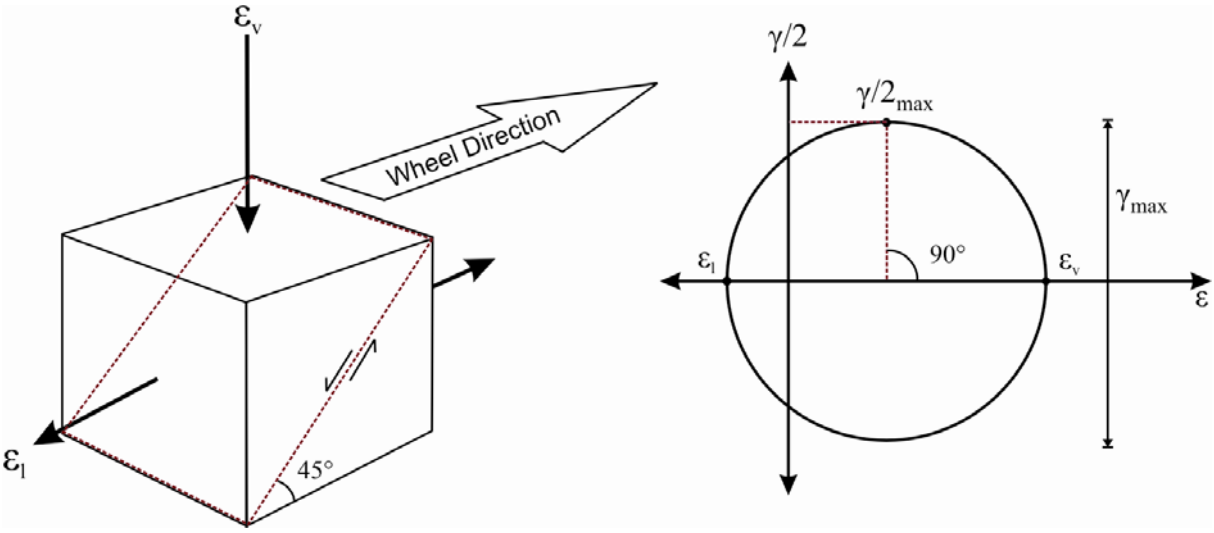

Figure 3.7 Two measured principal strains and corresponding Mohr's circle of strain showing maximum shear strain and the plane this shear strain acts on – Longitudinal Shear Strain.

Throughout this work, shear strains measured at CAPTIF are referred to as either longitudinal shear strains or transverse shear strains. Longitudinal shear strain is the strain that would cause shearing along a plane at an angle (e.g.45º) to the yz plane in the direction of wheel travel (such as shown in Figure 3.7). The longitudinal shear strain is determined using the principal vertical strain and the principal longitudinal strain. Similarly, the transverse shear strain occurs along a plane at an angle to the xy plane (perpendicular to the direction of travel) and this strain is determined using the principal vertical strain and the principal transverse strain. The maximum shear strain is therefore the greater of either the longitudinal or transverse shear strains. This method of determining the maximum shear strain is based on the Tresca criterion (Chen and Saleed 1994) whereby although three principal strains are known, only the two strains with the greatest difference are used to calculate the maximum shear

strain. This is illustrated in Figure 3.8 where although three principal strains are known, the smaller compressive strain (ε_t) is not used to calculate the maximum shear strain.

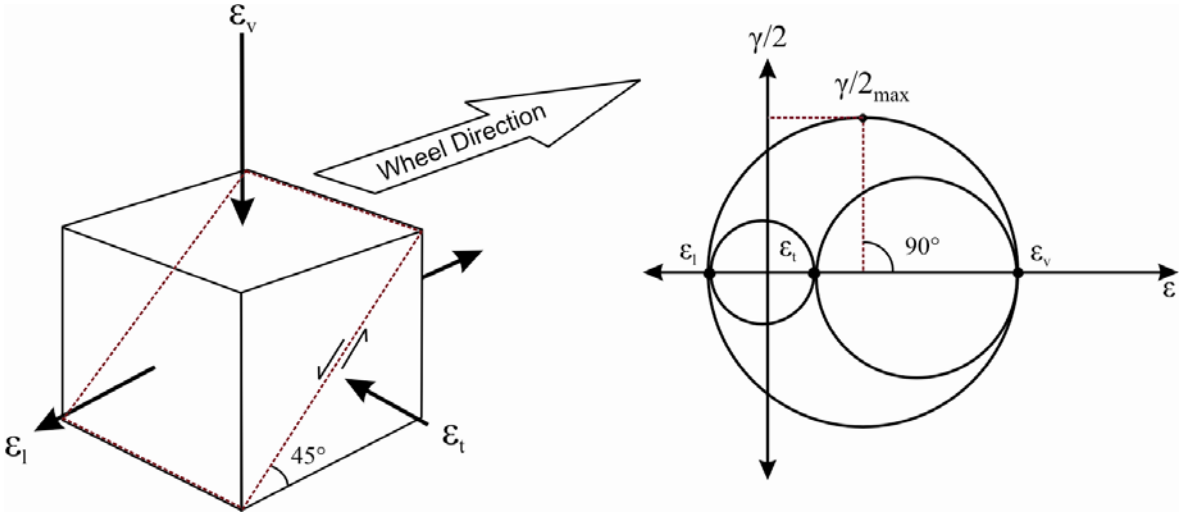

Figure 3.8 Maximum shear strain using Tresca failure criterion

More advanced models can be used to calculate the maximum shear strain by incorporating the third principal strain such as Von Mises' criterion (Timoshenko 1953) which incorporates all three principal strains to determine a less conservative maximum shear strain. However, the Von Mises criterion is normally used to determine the yield criteria for ductile materials. The Von Mises criterion has been extended to deal more with soils such as the Drucker-Prager model (Chen and Saleed 1994). However, the maximum difference between shear strains calculated using Tresca and Von Mises is approximately 15% and this only occurs when two principal strains are equal and opposite. In many other cases, the shear strains calculated using the two methods are much closer. For the purpose of this investigation, shear strain will be calculated using the Tresca criterion whereby the maximum shear strain is a function of maximum difference between two principal strains. It is assumed that the small amount of additional accuracy gained by using a Von Mises based model is not needed in this investigation for the following reasons:

1. Inaccuracies in strain measurement due to instrumental error and the assumption that there is no plane shear will counteract the slightly higher shear strains calculated using Von Mises criterion.
2. The additional accuracy gained using a Von Mises based model is not critical within the confines of this investigation. It is the variation of strain with respect to load applications that is of interest as opposed to determining one specific critical failure

value. Thus any errors resulting from using only two principal strains will be consistent throughout the entire test phase. This would only result in a slightly conservative strain progression relationship with respect to load applications.

3. If the shear strain results were to be used in pavement modelling programs, material assumptions such as Poisson's ratio, anisotropic behaviour, homogeneous materials and elastic behaviour are likely to overshadow the errors created by using Tresca's strain criterion.
4. If the rosette system shows that one shear strain (either transverse or longitudinal) is consistently more dominant than another, then one of the three coil pairs would become redundant. Therefore if the system was to be utilised for commercial testing, the redundant coils would not be installed.

3.2.3 Coil Cube Matrix Design

The second concept design was the *Coil Cube Matrix*. This design (Figure 3.9) involved eight coils placed at the centre of a 75mm cube. Due to the fact that induction coils can measure strains in either a co-axial or co-planar orientation, strains could be measured between any two coils within the cube. It was intended that shear strains (or lateral basecourse movement) would be measured using diagonal coils on the vertical faces.

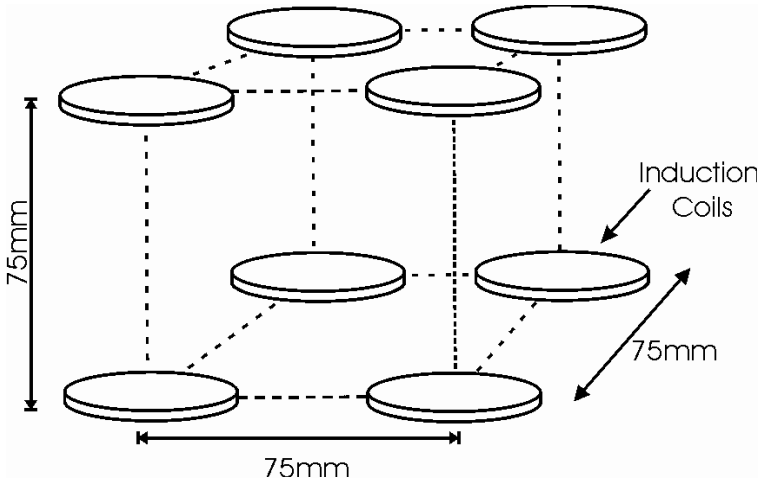

Figure 3.9 Coil cube matrix conceptual design.

The coil cube matrix design was appealing because the strain measured between diagonal coils on the vertical cube faces would give a true measure of the lateral movement of material. However, because previously induction coils have only been used in either a purely co-axial

or co-planer orientation, it was unknown whether the offset angle between coils of equal distance would affect the results. Therefore, a laboratory experiment was conducted to investigate the effect of the offset angle between two coils on the measured voltage.

3.3 Offset Angle Investigation

To investigate the effect of the offset angle between two induction coils an experiment was conducted using a standard induction coil calibration jig. Firstly, a transmitter coil was set up in a fixed position at the left hand end of the calibration jig. A second receiver coil was then set up at the right hand end of the jig. This receiver coil could be positioned at horizontal distances of 72, 75 or 78mm above the transmitter coil. This was achieved by using the existing movable support on the calibration jig. In addition to this, the receiver coil could be located vertically either 72, 75 or 78mm away from the transmitter coil. This was achieved by manufacturing three extension rods (72, 75 and 78mm in length) that could be attached to the existing moveable support on the jig. This resulted in nine possible locations for the receiver coil to be fixed. A photograph showing two coils separated 75mm horizontally and 72mm vertically is shown in Figure 3.10.

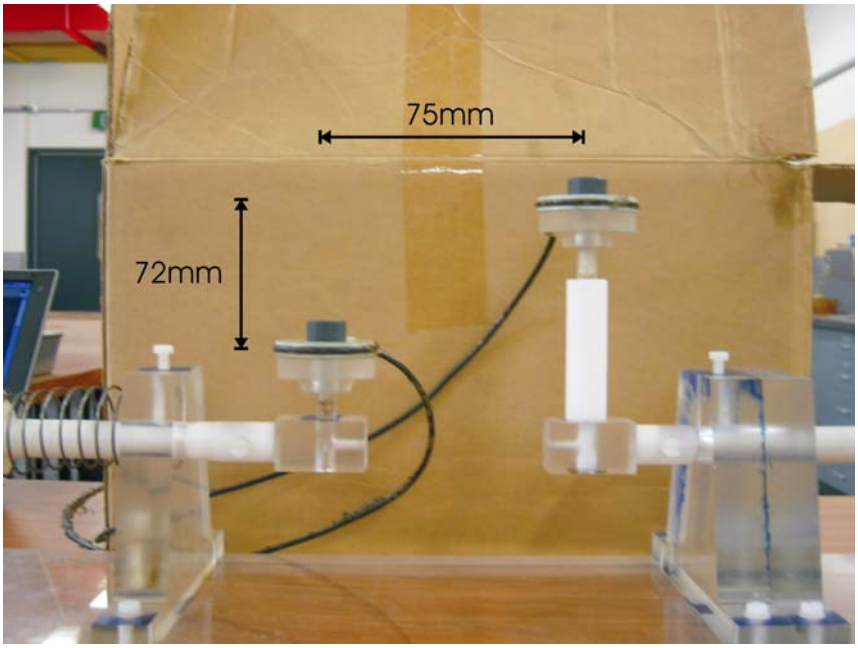

Figure 3.10 Calibration jig with vertical extension rod (Photo:Hayward).

A static voltage measurement was recorded between the permanent transmitter coil and the nine independent receiver coils using a portable emu soil strain measuring system. The

horizontal and vertical separation distances, total separation distance and measured static voltage values are shown in Table 3.1.

Table 3.1 Measured voltages for various offset angles

			Trial 1	Trial 2	Trial 3	Average
Height	Width	Distance	Voltage	Voltage	Voltage	Voltage
72	78	106.15	0.244	0.245	0.244	0.244
72	75	103.97	0.298	0.298	0.298	0.298
72	72	101.82	0.358	0.359	0.359	0.359
75	78	108.21	0.261	0.261	0.261	0.261
75	75	106.07	0.311	0.31	0.311	0.311
75	72	103.97	0.369	0.369	0.369	0.369
78	78	110.31	0.274	0.274	0.274	0.274
78	75	108.21	0.322	0.321	0.321	0.321
78	72	106.15	0.376	0.376	0.376	0.376

Based on the results from Table 3.1, a plot was made of the measured voltages against the diagonal separation distance (Figure 3.11). This figure shows three series of values which consist of the three measured voltages with a constant vertical displacement.

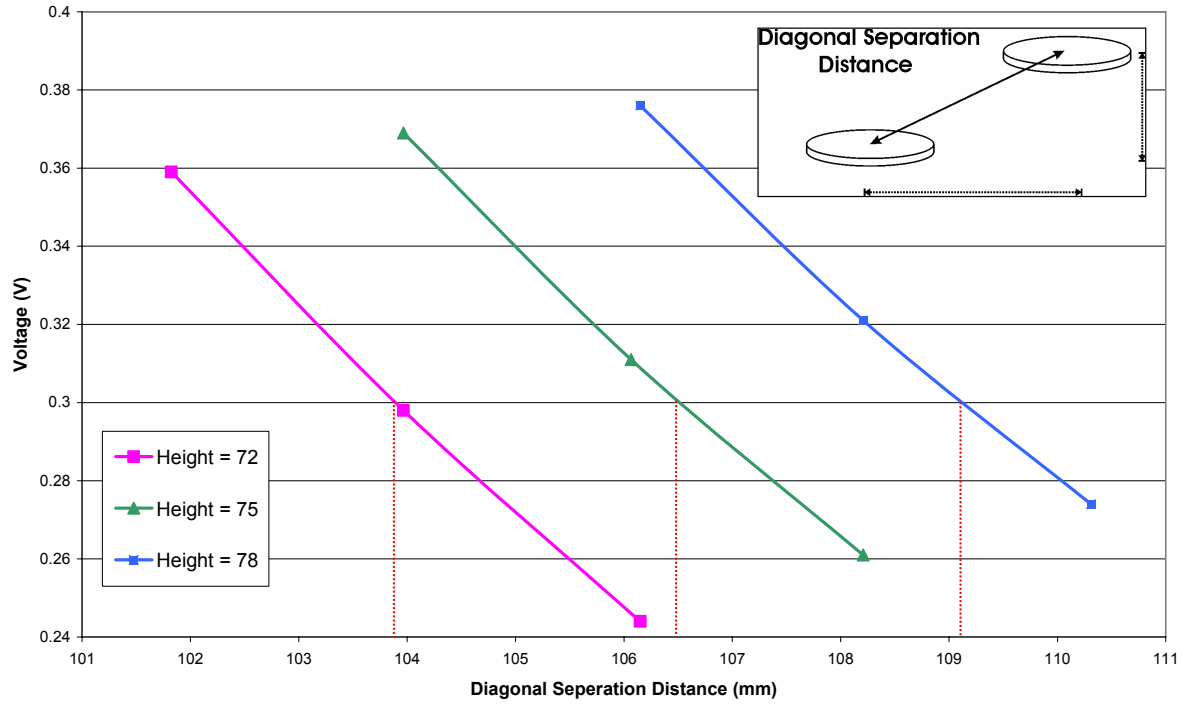

Figure 3.11 Measured voltages versus diagonal separation distance for nine receiver coils.

The discussion below only refers to coils within the same vertical plane (as was conducted in the experiment). Therefore the terms co-axial and co-planar refer to the position of the coil pair. A purely co-axial pair is where one coil is directly above the other thus sharing the same central axis. A purely co-planar coil pair is where each coil pair is at the same vertical elevation. The discussion is therefore based on a two dimensional case and the term co-planar should not be confused with the planes on a hypothetical soil cube.

The results shown in Figure 3.11 confirm with what would normally be expected for two coils aligned within the same vertical plane, namely:

- As the coils become more co-axial, the voltage increases. This is indicated by the upper values for each of the three series of data.
- As the coils become more co-planar, the voltage decreases. This is indicated by the bottom three values for each of the three series of data.

The experiment clearly shows that the angle between coils of equal distance does have a large effect on the measured voltages. This is largely due to the fact that co-planar coil pairs have a voltage measurement of significantly less than co-axial coil pairs (with the same separation distance).

Based upon the results of this experiment, the coil cube matrix concept design initially suggested will be significantly more difficult to interpolate and calibrate. This is because a voltage measurement between diagonal coils on one hypothetical surface plane (similar to the experiment) could be reached by the coils moving in a variety of different paths. For example, if a value of 0.3 was measured and analysed using Figure 3.11, three different separation distances could be assumed (in reality an infinite amount of solutions occur). Therefore, without assuming that some coils do not move under loading and therefore relating other coils movement back to a fixed datum, it will be very difficult to accurately determine the actual movement pattern of diagonal coils. These coils are the most important since shear strain is the critical pavement response being measured. Therefore it was decided that the rosette design with 200mm spacing between the pairs was to be implemented within the test pavements.

CHAPTER 4

EXPERIMENTAL INVESTIGATIONS

The following chapter presents a detailed description of the test facility and the various methods of measuring and analysing the received data. In addition to this, an outline of the experimental test schedule is described.

4.1 CAPTIF Test Facility

The test pavements were constructed and tested at the Canterbury Accelerated Pavement Testing Indoor Facility (CAPTIF) which is located in Christchurch, New Zealand. The testing facility comprises a ring shaped concrete tank that is 1.5m deep and 4m wide. This concrete tank forms the stiff confining sides of the pavements that are built inside as well as preventing moisture percolating into and out of the test pavement. The ring shaped track has an average diameter of 18.5m giving a circumference of 58.1m. The inside and outside concrete edges of the track have markings that evenly divide the track into 58 one metre sections (measured at the centre line) from 00 through to 57. A cross section of the CAPTIF tank and a typical pavement are shown in Figure 4.1.

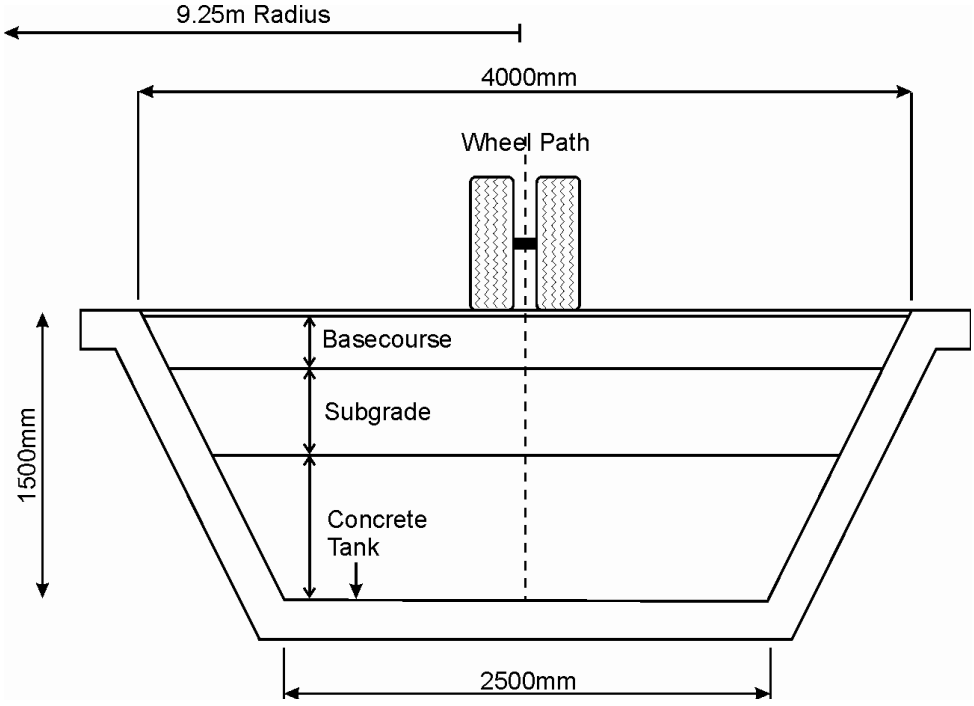

Figure 4.1 CAPTIF tank and typical pavement cross section.

Pavements are constructed using typical field construction methods. The subgrade is usually placed in lifts not exceeding 200mm in depth. Each lift is then compacted using a sheep's foot roller. Basecourse lifts are formed by either using a grader or an asphalt paving machine and the lifts are later compacted using a steel drum and rubber tyred roller. These construction methods ensure that the test pavements model field pavements as best as possible. The facility is fully enclosed by a corrugated iron building in order to minimise environmental effects on pavement during construction and testing.

4.1.1 Loading Apparatus

The tests pavements are loaded using the Simulated Loading and Vehicle Emulator (SLAVE). The SLAVE consists of a central platform located at the centre of the circular track. Two diametrically opposed truss arms radiate from the central platform and the half axle wheel assemblies are connected to the ends of these arms (usually at the centre of the pavement). Figure 4.2 shows the SLAVE operating on a test pavement at CAPTIF.

Figure 4.2 SLAVE operating at CAPTIF.

The SLAVE allows loading parameters to be modified in order to analyse different loading conditions. The half axle wheel assemblies can consist of either single wheels with loads ranging from 23kN to 30kN or dual wheels with loads ranging from 23kN to 50kN. The wheel assembly loads are increased in 2.75kN increments by attaching steel load plates to the front and back of the wheel assembly frame. The wheel assembly also allows for lateral

movement of up to 1m and different suspension types. The wheels are driven thus providing realistic traction forces. The rig can be operated at speeds ranging from 1 km/h up to 50 km/h in increments of 1 km/h.

4.1.2 Data Acquisition System

Sub-surface strains induced by the SLAVE are measured using free floating induction coils and the emu soil strain measurement system. The emu system uses the inductive coil principal (refer to Section 3.1) and measures the induced voltage signal between two coils for a short period of time, including the loading pulse. CAPTIF pavements are typically divided into five sections with coils installed within each section. Each site has a separate emu unit, a 36 channel multiplexer for coil connection, an industrial computer with a National Instruments PCI 6025E, 16 channel, 12 bit analog-to-digital converter and 8 channels of digital input/output (Steven 2005). During testing only one coil pair is energised by the emu system and the continuous voltage signal between the two coils before, during and after loading is measured using the emu system. Each coil pair is loaded and voltage signals measured for five vehicle passes to generate an average voltage signal during loading. Throughout this investigation, the voltage was sampled 2000 times per second for a duration of four seconds resulting in 8000 data points. A typical voltage signal measured using the emu system is shown in Figure 4.3. The increase in voltage (i.e. becoming more negative) between the vertical coils shown, corresponds to the coils moving closer together as the load is applied.

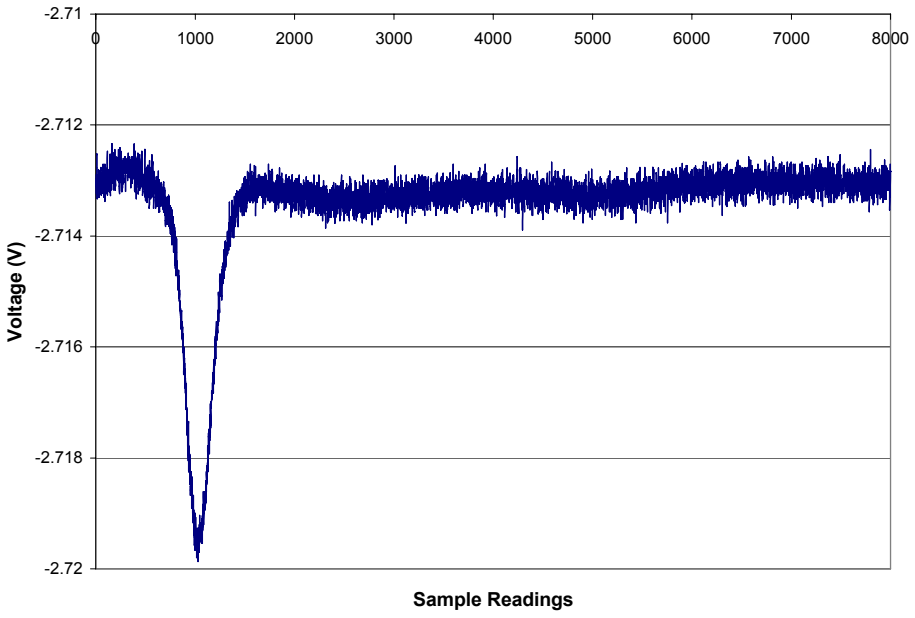

Figure 4.3 Typical voltage signal measured by emu system from a pair of coaxial vertical coils.

After the data has been measured by the emu system and stored on the CAPTIF server it is processed using CAPTIF software developed by Bruce Steven (CAPTIF research associate) and David Alabaster (CAPTIF manager). The software conducts the following steps on each voltage signal:

- The continuous raw voltage signal is filtered using a 4 pole Butterworth filter with a cut off frequency of 40 Hz in order to reduce the signal noise (Steven 2005).
- The new filtered voltage signal is converted to the relative separation distance of the specific coil pair using the calibration files. (see Section 5.1)
- The unloaded separation distance of the coil pair is determined by averaging the first 100 readings of the new filter signal.
- The maximum strains are calculated based on the peak of the voltage signal.
- The five traces for each coil pair are averaged resulting in a final value for the unloaded static separation distance of the coil pair, the maximum separation distance during loading and the corresponding strain value.

4.1.3 Transverse Profile Measurements

Complete transverse profiles of the test pavements were used to measure the degree of rutting over the pavements life. The transverse profile was measured using the CAPTIF Profilometer. This device consists of an aluminium beam that straddles the width of the track and a carriage that is driven along the beam by a small motor. An LVDT with a small rolling wheel at the bottom is attached to the moving carriage so that as the carriage moves along the beam, the small wheel rolls across the pavement surface and the LVDT displaces as the surface profile changes. The electronic measurements are recorded by a Psion Organiser computer and are accurate to ± 1mm. It should be noted that throughout this work, all rut depths are expressed as a vertical surface deformation (VSD) as opposed to a straight edge value. The VSD is the maximum permanent surface displacement from the original surface profile prior to testing.

4.2 Pavement Testing Summary

The following section outlines the objectives of the pavement testing and provides a summary of the test methods used within the experimental phases of the investigation. A detailed description of each pavement's construction, instrumentation and test conditions can be found in Chapter 5 and Chapter 6.

The two main objectives of the testing were to:

- Measure the magnitude of shear strains occurring in the basecourse of two different pavements and to relate the measured shear strains to the observed permanent deformation over the pavements' test lives.
- Investigate the effect of different load conditions on the magnitude of basecourse shear strains.

To complete these objectives, the testing of each pavement was divided into two different tasks. These two tasks were not run in series but rather occurred in parallel with each other. The first task involved measuring vertical and horizontal basecourse strains and surface rutting profiles at regular intervals throughout the pavements' life. The vertical and horizontal basecourse strains were then converted to shear strain values and the relationship between shear strain and basecourse rutting over the pavements' lives were investigated. The second task involved varying the axle load, wheel configuration and load position over the coils, to investigate the effect of loading parameters on the magnitude of the shear strains in the basecourse.

The exact loading parameters used in pavement testing by CAPTIF vary with each project, however, typical pavement testing involves applying a 40kN load at the end of the truss arms on the SLAVE. Typically a dual tyre wheel configuration is used resulting in a 20kN tyre load. The SLAVE is operated continuously at 40km/hr during testing and stoppages only occur for pavement condition and response testing such as strain and profile measurements or pavement rehabilitation work. The term *accelerated testing* will be used to denote when the SLAVE is operating at full speed (40km/hr) with the sole purpose of rapidly accumulating laps to wear the pavement. The accelerated test life is the number of loading laps that a pavement is subjected to in order to capture enough data to drawn conclusions on the long term performance of the pavement. This will vary depending on the design and construction of each test pavement. A typical pavement's accelerated test life involves 500,000 full revolutions of the SLAVE with its two wheel assemblies, resulting in 1,000,000 load applications due to the dual arm on the SLAVE.

Throughout this thesis, pavement loading will be described in terms of applied laps not load repetitions since this is the convention at CAPTIF. In addition to this, unless otherwise stated, the term *wheel load* will be used to denote the SLAVE's half axle dual wheel load. For example a 40kN *wheel load* is the 40kN load applied over the dual wheel assembly at one end of the SLAVE arm, corresponding to a trucks axle load of 80kN.

Therefore 1 lap = 2 load repetitions = 2 x 40kN load applications.

4.2.1 Test Task 1 – Shear Strain and Permanent Deformation

The purpose of this task within the pavements accelerated test life was to investigate the relationship between basecourse shear strain and permanent deformation within the granular layer. This task in the testing schedule was conducted at regular intervals throughout the accelerated test life. A detailed test description for each pavement including measurement schedule, tyre proprieties and pavement properties can be found in Chapter 5 and Chapter 6.

Task 1 involved taking dynamic basecourse strain readings at regular intervals throughout the accelerated test life. During strain testing, the standard dual wheel load was applied to the pavement at a rate of 10km/h. The speed was reduced from 40km/h during accelerated testing to 10km/h during strain testing is because higher speeds result in more vertical bounce of the wheel and consequently a greater variation in the applied load. Research at CAPTIF has shown has shown that 10km/hr is the minimum speed the SLAVE can be operated at to ensure a consistent speed and therefore this speed was chosen for strain testing. The dual wheels were centred directly over the longitudinal axis of the strain coil rosettes. This ensured that a symmetrical load was applied to the coils.

After the series of strain measurements were taken at the various intervals over the pavement life, transverse surface profiles were taken of the test sections so that rut accumulation could be determined. Based upon the measured basecourse strains and the rut development over the pavement's accelerated testing life, the relationship between these two pavement properties was investigated.

4.2.2 Task 2 – Shear Strain under Different Loading Conditions

Task 2 involved modifying the loading conditions in order to investigate the effect of wheel assembly configuration, load location and tyre load on the magnitude of the shear strains in the basecourse layer. This test task was conducted at approximately the half way point during the accelerated testing life in order to minimise any pavement damage caused by the testing.

Arnold et al. (2004) categorised CAPTIF aggregates as having either class A, B or C rutting behaviour. Class A represents a material where its incremental increase of permanent strains (permanent deformation) is decreasing during load cycling. Class C represents a material with unstable behaviour and the incremental increase of permanent strain increases rapidly during the early stages of load cycling resulting in rutting failure. Class B behaviour lies between the other two classes. These permanent deformation behaviour classes are illustrated in Figure 4.4.

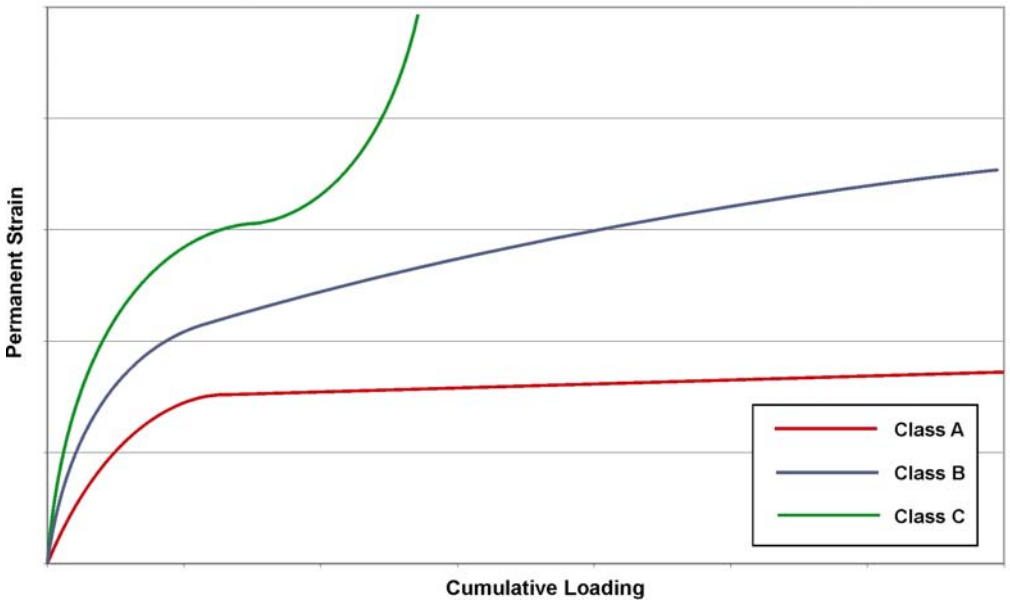

Figure 4.4 Three material behaviour classes for unbound granular materials

Based on both the research of Arnold et al. (2004) and Transit New Zealand M/4 specifications (Transit NZ 2000), it was assumed that the unbound aggregate used in the CAPTIF pavements tested in this investigation would exhibit either Class A or Class B behaviour. Therefore, based on the gradient of the permanent strain accumulation lines shown in Figure 4.4, the rate of strain accumulation for Class A and Class B behaviour is most stable after the initial rapid plastic strain development has occurred during the initial stages of

loading. If failure does occur it would most likely happen towards the end of the proposed accelerated test life. Therefore, based on the conservative assumption that rutting failure would occur, the most appropriate time to apply a range of different loads to the pavement would be at approximately the mid point of the test life.

During this task, three variables (tyre load, load location and the wheel assembly) were independently modified in order to investigate the effect of the loading parameters on the in-situ shear strains. Task 2 testing comprised three different investigations namely:

1. Task 2A – Single wheel with varied load location.
2. Task 2B – Dual wheel with varied load.
3. Task 2C – Dual wheel with varied load location.

Table 4.1 shows a summary of the loading parameters during each sub task test with the variable parameter in each test highlighted.

Table 4.1 Task 2 loading conditions

Sub Task Test	Tyre Type	Load (kN)	Load Location
Task 2A	Single	23	Centre of tyre directly centred over coils.
Task 2A	Single	23	Quarter point of tyre directly centred over coils
Task 2A	Single	23	Edge of tyre directly centred over coils.
Task 2B	Dual	23	Centre of gap in duals directly centred over coils.
Task 2B	Dual	32	Centre of gap in duals directly centred over coils.
Task 2B	Dual	40	Centre of gap in duals directly centred over coils.
Task 2B	Dual	51	Centre of gap in duals directly centred over coils.
Task 2C	Dual	40	Centre of gap in duals directly centred over coils.
Task 2C	Dual	40	Centre of inside tyre directly centred over coils.
Task 2C	Dual	40	Quarter point of inside tyre directly centred over coils.
Task 2C	Dual	40	Edge of inside tyre directly centred over coils.

Based on the results of Task 2 testing the relationships between basecourse shear strain and the various loading parameters was investigated.

CHAPTER 5

FIRST PAVEMENT: SHEAR STRAIN INVESTIGATION

The following chapter provides a detailed description of the work that was conducted on the first test pavement. This includes the calibration of the coils, construction of the pavement, installation of the induction coils, the specific details of task 1 and task 2 shear strain testing and the post mortem exhumations. Work on the first pavement began in June 2005 and continued through until January 2006.

Only the first test pavement's details are described in this chapter. The second test pavement is described in Chapter 6. The two test pavements are dealt with in separate chapters because many of the design and construction details of the two pavements are similar and combining this information together had the potential to confuse the reader.

5.1 Coil Calibration

Based upon the rosette coil configuration design, three pairs of coils were required to make up one rosette (refer to Figure 3.3). It was decided that three separate rosettes would be installed in order to provide comparative data over a longer section of pavement and as a failsafe in case any coils were damaged over the testing period. Therefore a total of nine pairs of coils were to be installed in the pavement.

Each induction coil that was used was calibrated with its corresponding paired coil. Calibration is required for every pair in order to generate a specific equation relating the induced voltage between two coils and their separation distance. This involved the designated transmitter coil being fixed at the stationary end of the CAPTIF calibration jig and the designated receiver coil being fixed at the moveable end of the jig (Figure 5.1). The coils were initially separated by 85mm and the micrometer was set to a reading of 20mm. The coils were plugged into CAPTIF emu unit D and a static voltage reading was taken at 85mm separation. The coils were then moved together in 1mm increments until they were 65mm apart and a static voltage reading was taken after each incremental movement. This resulted in 20 static voltage readings that corresponded to 20 separation distances between 85mm and 65mm.

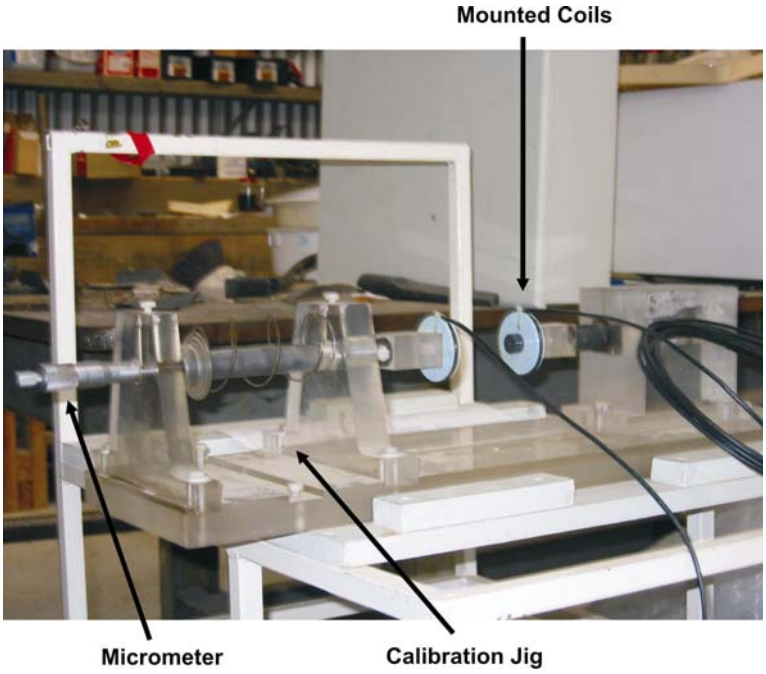

Figure 5.1 Calibration jig with two coils in process of calibration (Photo:Hayward).

A plot of the static induced voltage versus the separation distance was created for each of the 9 coil pairs and a power trend line was fitted to each graph. Using the Microsoft Excel function, the trend line equation was generated. This equation is what was used to determine the separation distance of the coils during loading base upon the measured voltages. An example of a calibration curve is shown in Figure 5.2.

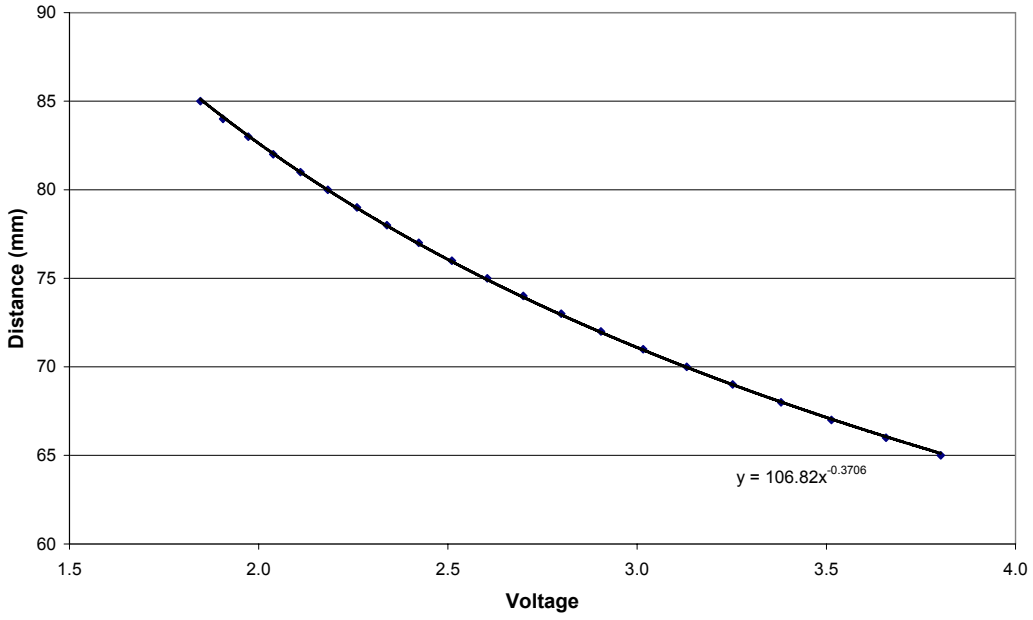

Figure 5.2 Calibration curve for coil pair 1 in the 1st pavement.

5.2 Original Pavement Design and Construction

The original test pavement was an unbound flexible pavement consisting of a clay subgrade, an unbound granular basecourse and a thin open graded porous asphalt (OGPA) surface layer. CAPTIF's main objective for the pavement was to investigate fatigue development within the OGPA surface. The track was divided into two main sections in order that both a thick and a thin pavement could be tested Figure 5.3. The thin pavement comprised a stiff subgrade with a 150mm granular layer and this pavement extended from station 55-22. The thick section had a weak subgrade with a 300mm granular layer and this pavement extended from section 23-54. A longitudinal section of the pavement design is shown in Figure 5.3.

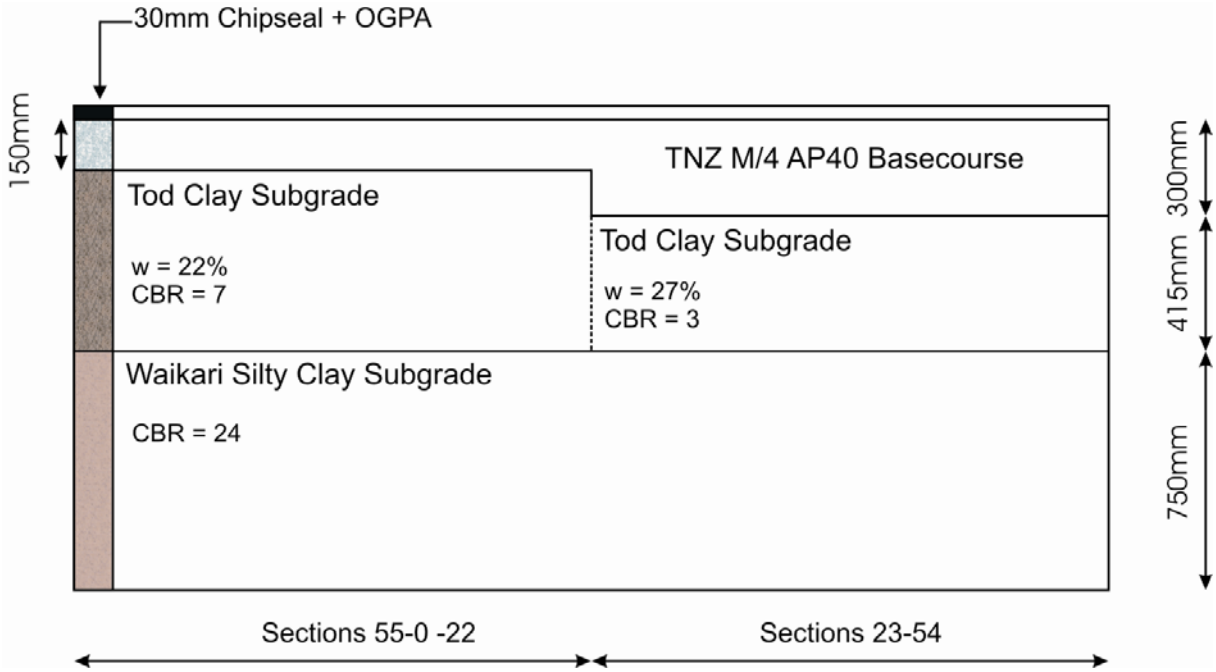

Figure 5.3 Pavement 1 - Original design - longitudinal section.

The 750mm thick Waikari clay subgrade layer was constructed for a previous pavement and was left in good structural condition after the above layers were removed. Based on 13 dynamic cone penetrometer tests, the Waikari subgrade had an inferred California Bearing Ratio (CBR) of 24. Both the weak and stiff Tod clay subgrade layers were laid in 150mm lifts and compacted using a sheep's foot roller. The stiff subgrade which extended from section 55-22 was Tod clay with 22% moisture content, which was the optimum moisture content based on NZS:4402 (1989). This layer was compacted to an average dry density of 1.512 t/m^3 and had an inferred CBR of 7. The weak Tod clay subgrade was compacted to 1.495 t/m^3 with

a final moisture content of 27% which was 5% above optimum (NZS:4402 1986) and had an inferred CBR of 3.

The basecourse material was a Transit New Zealand specification (Transit NZ 2005) M/4 AP40 basecourse. This was a greywacke crushed rock sourced from Fulton Hogan's Pound Road quarry in Christchurch. The basecourse was laid in 150mm lifts and compacted using a 750kg remote driven plate compactor. A typical vibratory roller could not be used at CAPTIF because the steel drum roller tends to separate the aggregate as it drives in a circular direction. The basecourse was compacted to an average dry density of 2.23 t/m^3, which was 99% of maximum dry density based on the NZS:4402 (1986), at 2.5% moisture content. The basecourse densities were measured using a nuclear densometer (ND) in backscatter mode. Following compaction and drying, a prime coat of cutback bitumen (1 part aviation gas oil and 3 parts kerosene) was applied to the finished basecourse surface and allowed to dry for two days. The chipseal was then applied by spraying a thin film of 180/200 penetration grade bitumen on the basecourse surface and laying the chip from a reverse driven truck. The bitumen and chipseal was applied in two coats. Initially 1 litre of bitumen per square metre of pavement surface was sprayed and a TNZ Grade 3 chip (Transit NZ 2004) (7.5-10mm aggregate stone) was applied. Following this, a further 0.8 litres of bitumen per square metre of track was sprayed and a TNZ Grade 5 chip was then applied (approximately 8mm aggregate stone). This second smaller stone acts to fill the voids between the larger 7.5-10mm chip. The chip seal surface was approximately 10mm thick after it was rolled with a steel drum and rubber tyred combination roller.

5.3 Induction Coil Installation

The three rosettes were installed in stations 50-52 in the strong section of the pavement. This section was chosen due to the thicker basecourse layer which was the pavement layer of interest in this investigation. If the thin section had been used the coils would have had to be installed near the bottom of the layer to prevent magnetic interference from moving metal in the SLAVE tyres (Paterson 1972). This would have meant that the bottom coils would be very close to the subgrade and therefore this softer layer may have contributed significantly to some of the strains measured. It was decided that the thicker layer would provide strains that would have been generated mainly due to the basecourse behaviour.

The central coil pair in each rosette (co-axial transverse coil pair) was located at the intersection of the centre line of the pavement and each station mark (50-52). The other two coil pairs for each rosette were spaced longitudinally by 200mm each side of the central pair. The upper coil in the vertical pair was located 125mm below the basecourse surface thus making the centroid of each rosette 162.5mm below the surface of the basecourse Figure 5.4. The minimum depth of installation (125mm) was a compromise between wanting the coils as high as possible within the basecourse where the strains are highest, whilst ensuring that the SLAVE wheel would not interfere with the magnetic fields.

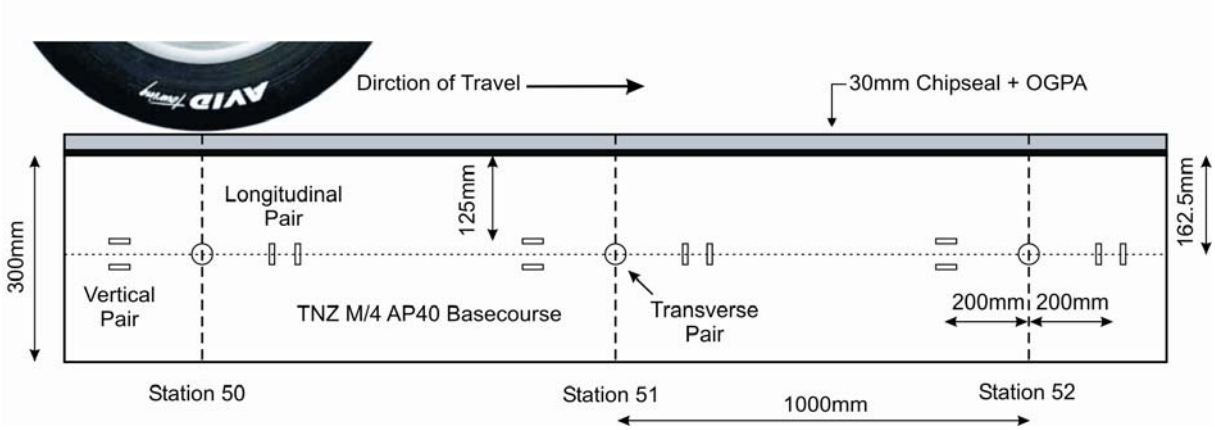

Figure 5.4 Pavement 1 side elevation section showing coil locations.

5.3.1 Placement Technique

In order to obtain accurate strain results, the precise placement of the induction coils was important. The coils were installed after the basecourse was fully constructed. The installation of each coil pair involved the excavation of some of the granular material in order that the required coil depth could be achieved.

The three vertical coil pairs were installed by excavating 164.5mm of basecourse and placing the bottom coil on a 2mm bed of AP5 crusher dust. Coil depths were measured relative to sides of the concrete tank using a level beam, a measuring tape and a laser light as shown in Figure 5.5. The bottom coil was checked for level using a finish eye level and then covered with intermediate material. The intermediate material was compacted using a vibratory compaction hammer with a 100mm diameter circular plate. The upper coil was installed in a

similar way ensuring that there was exactly 75mm of intermediate material between the lower and upper coil using the level beam and measuring tape.

The six co-axial horizontal coil pairs were installed using a similar method. However, precise placement of the coils was assured using a pair of CAPTIF coil pliers and a 72mm spacer cylinder. The pliers were used along with the spacer to hold the coil pair exactly 75mm apart (centre to centre). Once the coils were located at the correct depth using the reference beam and measuring unit, the sides of the coils were packed in place using AP5 crusher dust (Figure 5.6). Once the coils were in a stable and supported state, the covering material was back filled and compacted using the vibratory compaction hammer.

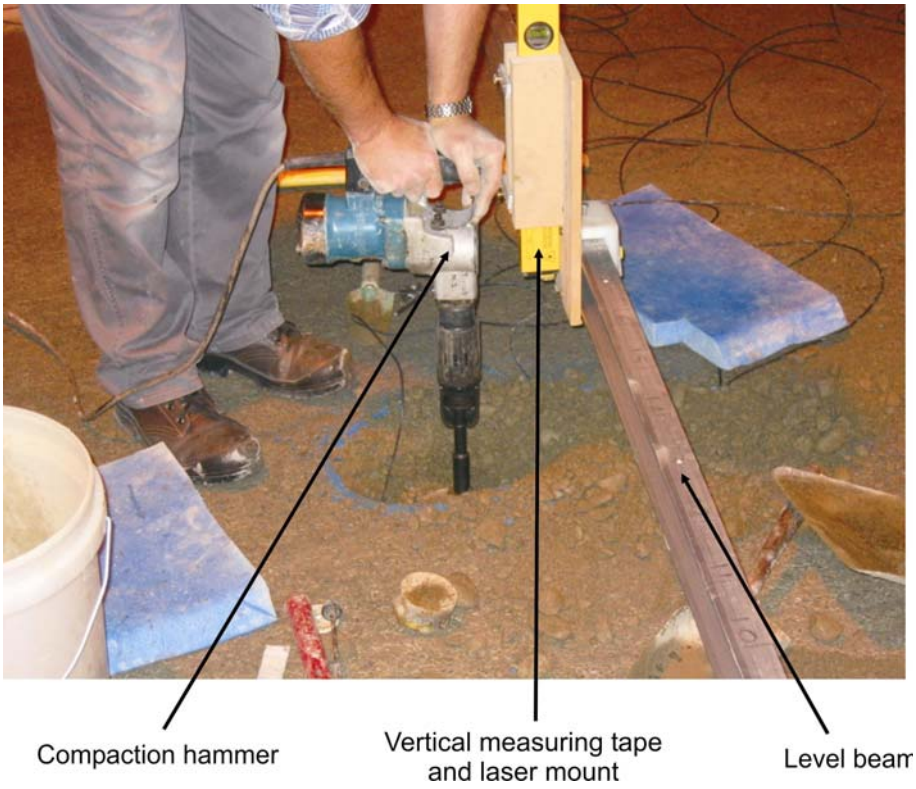

Figure 5.5 Vertical coil pair installation with reference beam shown and measuring unit (Photo:Hayward).

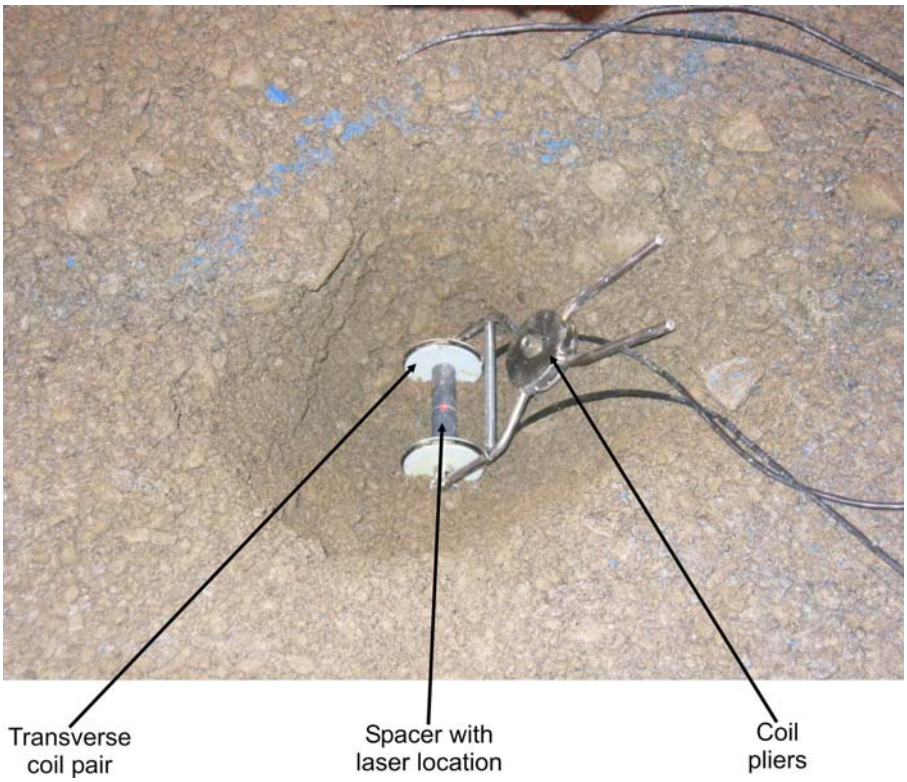

Figure 5.6 Horizontal coil installation showing CAPTIF pliers and laser location from measuring unit (Photo:Hayward).

Following the installation of the nine coil pairs, the basecourse surface was finished using AP5 granular material and a small plate compactor in order to create a level surface representative of the rest of the undisturbed pavement.

5.4 Preconditioning, Pavement Overlays and Final Pavement Design

Initially, the chipseal pavement was to have 100,000 23kN single wheel laps applied to it in order to precondition the pavement before the OGPA was applied. However, after 8000 laps, the majority of the pavement surface had moderate rutting and several isolated sections had large shoving failures. The preconditioning loading was stopped at this stage because it was clear that the pavement would fail before the planned 100,000 laps were applied. It was later concluded by the CAPTIF pavement engineer that the premature failure was due to the weak subgrade and that pavement strengthening was required.

A 70mm thick M/4 AP20 unbound granular overlay was laid over the existing pavement and compacted to an average dry density of 2.234 t/m^3 (measured using a ND in backscatter

mode). This overlay was constructed directly over the top of the existing chipseal surface. Following this, a second 10mm thick two coat chipseal (identical to the seal described previously) was applied to the surface and the preconditioning loading resumed. However, after less than 2500 laps, the chip seal began to ravel and bitumen bleeding started to occur. The ravelling occurred because of a high sand content in the chipseal caused by the contractor heating the chip in the sand plant. The contractor remedied this problem by laying a scrub coat of hot mix asphalt (HMA) over the chipseal surface so that the volume in space between the chip stones and the bitumen seal was filled with HMA. This layer was approximately 5mm thick and the end result was a HMA surface level with the top of the original chip stones. However in five different sections around the track (including test section 52) a thicker 40mm AC patch was required due to excessive ravelling and surface deterioration. Following this, 50,000 40kN dual wheel preconditioning laps were applied to the pavement after which the 25mm OGPA layer was laid. This resulted in a 25mm thick surface course comprising the chip seals and OGPA layer. This was the final state of the pavement and following the OGPA construction, loading began for the proposed 500,000 lap 40kN test. A longitudinal section of the final pavement is shown in Figure 5.7.

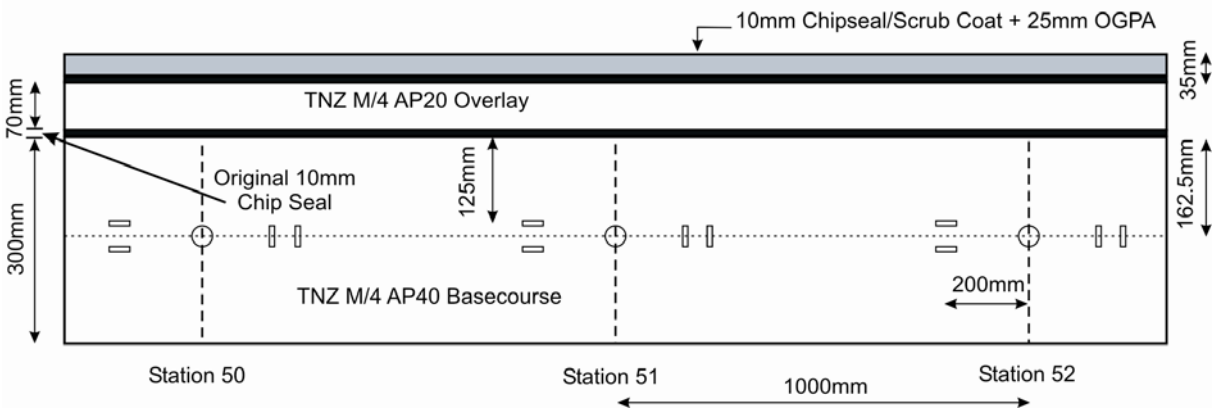

Figure 5.7 Side elevation longitudinal section of final pavement design.

5.5 Strain Measurement Test Specifications

The standard 40kN dual wheel load (Figure 5.8) was applied continuously at 40 km/h for 500,000 laps. Stoppages only occurred for pavement testing such as strain measurements and surface profiling. The location of the loads across the width of the pavement was varied by the SLAVE arm automatically moving laterally. The laterally moving arm caused the wheels

to move as far as 200mm either side of the central wheel path so that the loads were applied based on a normal distribution with a standard deviation of 1.67.

Figure 5.8 SLAVE - 40kN dual wheel load on OGPA surface (Photo:Hayward)

5.5.1 Initial Strain Testing

Task 1 strain testing and profile measurements (refer to Section 4.2) were conducted on both the original pavement before the rutting failures and on the final pavement prior to the OPGA layer being constructed. In the case of the original pavement, the testing was conducted with the single 23kN preconditioning wheel load. The overlay pavement with the chipseal was initially trafficked with the 23kN single load and later trafficked with the 40kN dual load used during the main test life.

5.5.2 Main Task Testing

Task 1 strain testing and profile measurements were conducted at twelve stages throughout the pavement life. Proportionally more testing was conducted during the first 100,000 laps because it was assumed that rutting would develop quickly during the early stages of loading as previously indicated by Figure 4.4. Task 2 strain testing was conducted after 150,000 laps when the permanent deformation accumulation rate had reached a plateau. A summary of the strain testing undertaken on the first pavement is shown in Table 5.1. It should be noted that

the load application count was reset between both the initial pavement and the overlay pavement and between the overlay pavement and the final pavement.

Table 5.1 Summary of strain tests on first pavement.

Pavement Stage	**Cumulative Laps Applied**	**Test Task**
Initial pavement	<1000	Task 1 (23kN)
Pavement Stage	**Reset Cumulative Laps Applied**	**Test Task**
Overlay pavement with chipseal	5000	Task 1 (23kN)
Overlay pavement with scrub coat	50,000	Task 1 (40kN)
Pavement Stage	**Reset Cumulative Laps Applied**	**Test Task**
Final pavement OGPA	<1000	Task 1 (40kN)
Final pavement OGPA	15,000	Task 1 (40kN)
Final pavement OGPA	30,000	Task 1 (40kN)
Final pavement OGPA	50,000	Task 1 (40kN)
Final pavement OGPA	150,000	Task 1 (40kN), Task 2
Final pavement OGPA	200,000	Task 1 (40kN)
Final pavement OGPA	300,000	Task 1 (40kN)
Final pavement OGPA	400,000	Task 1 (40kN)
Final pavement OGPA	500,000	Task 1 (40kN)

CHAPTER 6

SECOND PAVEMENT: SHEAR STRAIN INVESTIGATION

The following chapter provides a detailed description of the construction and investigative testing that was conducted on the second pavement. Work on the second pavement began in February 2006 and continued through until August 2006. Procedures that have previously been explained which are common to both projects (such as coil calibration) will not be repeated in this section.

6.1 Pavement Design and Construction

The second pavement was very similar to the first pavement. It was an unbound flexible pavement consisting of a clay subgrade, an unbound granular basecourse and a chipseal riding surface with an asphalted concrete (AC) scrub coat. CAPTIF's two objectives for this project were to investigate the effect of basecourse compaction and to investigate shoulder treatment effects. For this reason, the track was divided into two main sections. The first section which extended from station 55-22 was designed to investigate shoulder treatments. This section was not used for the shear investigation and therefore construction techniques and geometry will not be detailed.

The second section which extended from station 23-54 was made up of three different pavement designs. Each of the three pavements had the same subgrade. However, the basecourses in all three sub-sections were compacted to a different dry density because the CAPTIF project objective was to investigate the effect of poor compaction on pavement performance. The subgrade consisted of 750mm of Waikari silty clay subgrade that was left from the previous pavement. This material had a CBR of 23 based on 17 dynamic cone penetrometer tests. A 300mm weak Tod clay subgrade was constructed on top of the Waikari clay. This layer was placed in 150mm lifts and compacted using a sheep's foot roller. The subgrade layer was compacted to an average dry density of 1.529 t/m^3 with a final moisture content of 25% which was 3% above optimum based on the NZS:4402 (1989). This resulted in an inferred CBR of 3 based on 17 dynamic cone penetrometer tests.

The basecourse on all three sub-sections was a greywacke M/4 AP40 basecourse from the same Christchurch quarry as the first test pavement. The basecourse layer was 450mm thick and was laid and compacted in three separate 150mm lifts. However, each of the three sub sections was compacted to a different density in order to create three different strength pavements. The sub-sections were compacted using a 750kg vibratory plate compactor and a 3 tonne steel drum/rubber wheel combination roller. A summary of the compaction efforts and achieved densities is shown in Table 6.1. The achieved basecourse dry densities determined at CAPTIF were measured using a nuclear densometer in backscatter mode and therefore each subsequent lift will be influenced by the layer below. For example, the density taken on the finished surface (lift 3) will be a composite density based on the total basecourse depth.

Table 6.1 Second pavement basecourse compaction summary

	Lift (150mm)	Target Dry Density (% of Max NZS:4402)	Achieved Dry Density (% of Max NZS:4402)	Construction technique
Sub Section 1 (Station 24-34)	1	85	89	1 pass with static roller (3t)
	2	85	91	
	3	90	94	
Sub Section 2 (Station 34-44)	1	90	93	1 pass with 750kg plate compactor and 3 passes with vibratory roller (3t)
	2	90	93	
	3	90	94	
Sub Section 3 (Station 44-54)	1	95	99	8 passes with 750kg plate compactor and 5 passes with vibratory roller (3t).
	2	95	99	
	3	95	95	

Based on the achieved basecourse densities, it was decided that the shear strain investigation in the second pavement would be focused in sub-section 2 (stations 43-44). This was because in contrast with the first pavement, the poorly compacted granular pavement would have a high possibility of basecourse shear failure which could provide good data on the shear strain effects in a sub-standard pavement.

Sub-section 3 was compacted to a similar density as the first pavement and therefore this section was not considered due to the similarities. Conversely, sub-section 1 was compacted so poorly, it was assumed that failure could occur within the first 5000 laps which would

provide very little data for analysis and thus this section was not selected. Therefore, sub-section 2 was chosen due to its moderately poor compaction effort. A longitudinal section of the chosen test section is shown in Figure 6.1. This section was compacted to 2.093t/m^3 with a moisture content of 2%.

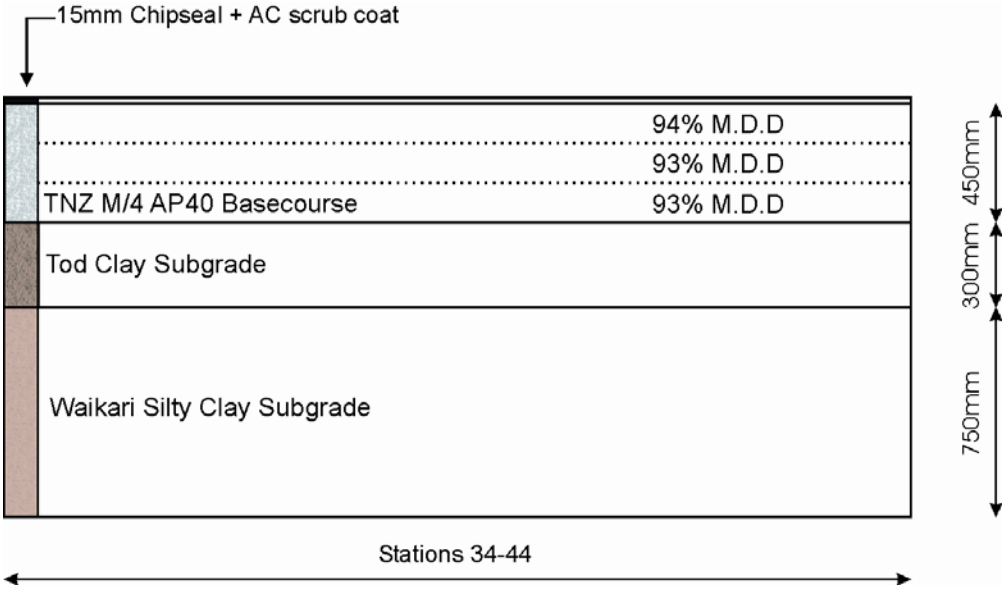

Figure 6.1 Pavement 2 - Longitudinal section of pavement layers and compaction in basecourse lifts

Following basecourse drying, a prime coat of cutback bitumen (1 part aviation gas oil and 3 parts kerosene) was applied to the finished basecourse surface and allowed to dry for two days. The chipseal was then applied by spraying a thin film of 180/200 penetration grade bitumen on the basecourse surface and laying the chip from a reverse driven truck. The bitumen and chipseal were applied in one phase. Bitumen was applied at a rate of 1.9 litres per square metre of track and a TNZ Grade 3 (Transit NZ 2004) (7.5-10mm aggregate chip) was applied to the surface. The surface was then subjected to one pass of a steel drum roller in order to bed the chips into the bitumen layer and five passes with a large rubber wheel roller to re-orientate the chips in the binder. Following this, a scrub coat of asphalt cement was placed on the surface. This additional riding surface component is simply a small amount of hot mix asphalt that fills in the voids between adjacent chip stones thus creating a smooth riding surface with the final level still equal to the height of the chip seal stones. This layer has no structural improvement on the pavement and only serves to reduce tyre wearing during testing and to minimise ravelling of the chip stones. The scrub coat was constructed by manually applying the hot mix asphalt to the chip sealed surface and smoothing the surface

using a flat rake. The total surface course consisting of the chip seal and scrub coat was approximately 25mm thick. The final pavement was then subjected to two passes with a 3 tonne steel drum roller to compact the loose asphalt and form a smooth riding surface.

Therefore, the second pavement was geometrically and structurally identical to the first pavement apart from the following features:

- The second pavement's surface layer was 15mm thinner than the first pavement's because no OPGA was applied on the second pavement. However, it was assumed that the small difference in the non structural layer would not affect the magnitude of the stresses applied to the basecourse.
- The total basecourse depth in the second pavement was 80mm greater.
- The basecourse layer under investigation (Sections 34-44) was compacted to a maximum of 94% of maximum dry density (NZS:4402 1986), 5% less than the first pavement.

Thus, the major variable in the second pavement was the stiffness of the basecourse which provided an excellent comparison with the strong basecourse structure in the first pavement.

6.2 Induction Coil Installation

The induction coils were calibrated and installed in the same way as for the first pavement. The only difference in the installation involved using the Clegg hammer to ensure the consistency of the basecourse re-compaction after the coils were installed. This technique involved taking five Clegg hammer readings on top of the basecourse within a 150mm radius area of where each coil was to be installed and an average Clegg value was determined. Following the installation of the coils, the basecourse material that was removed during installation was re-compacted and then subjected to Clegg tests to ensure that the initial average Clegg value was maintained. It was therefore assumed that the replaced basecourse material was re-compacted to a density very similar to the initial 94% maximum dry density. The Clegg hammer was used for this procedure due to its ability to be operated within the confines of the small hole excavated for the coils. The nuclear densometer which had previously been used for compacted testing was not considered for this procedure because it was assumed that the densometer would not be able to detect changes in such a small amount of re-compacted material given the large size of the base of the instrument.

The three rosettes were installed in stations 38-40 in the 450mm thick granular layer. Similar to the first pavement, the central coil within each rosette (co-axial transverse coil pair) was located at the intersection of the centre line of the pavement and each station mark. The other two coil pairs were longitudinally spaced by 200mm each side of the central pair. The centroid of each rosette was 252.5mm below the surface of the finished basecourse. This centroid depth would ensure that after the chip seal running course was applied, the coils would be located at the same depth below the pavement surface as the coils in the first pavement (after the granular overlay and OGPA was constructed). Therefore, the strains measured in this second pavement are comparable to those in the first. A profile of the coils within the basecourse is shown in Figure 6.2.

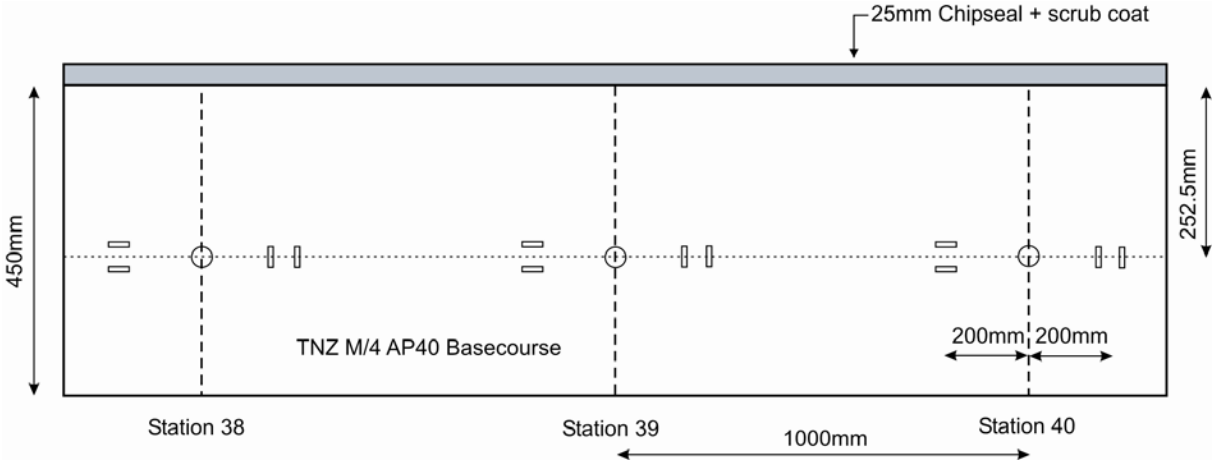

Figure 6.2 Pavement 2 longitudinal section showing coil locations.

Refer to Section 5.3.1 for specific details on coil installation techniques.

6.3 Strain Measurement Test Specifications

The standard 40kN dual wheel load was applied continuously at 50km/hr for 300,000 laps. One large loading break occurred after 187,000 laps because construction on the CAPTIF project shoulder section and epoxy open graded asphalt test was undertaken. The shoulder construction was conducted from Station 00 to Station 23 and therefore this construction would not have affected the test area relevant to this investigation. The epoxy surface trial involved milling back the AC layer from Stations 24-34 and replacing this with the new open graded mix. It is highly unlikely that this surface treatment would have disturbed the pavement structure involved in this investigation which was 5m away from the end point of

the new surface. The total break due to the construction was one month. Other stoppages only occurred at strategic pavement testing times. Similar to the first pavement, the location of the loads across the width of the pavement was varied by the SLAVE arm automatically extending and shortening laterally. The wheel was moved 200mm either side of the central wheel path so that the loads were applied based on a normal distribution with a standard deviation of 1.67. It should be noted that during strain testing the SLAVE was manually adjusted so that the wheel load was always centred directly over the coils. A summary of the strain testing undertaken on the second pavement is shown in Table 6.2. Due to the weaker basecourse, significantly more testing was undertaken in the first 100,000 laps compared to the first pavement in the order that enough data could be collected before failure occurred.

Table 6.2 Summary of strain tests on first pavement

Cumulative Laps Applied	Test Task
0	Task 1 (40kN)
1000	Task 1 (40kN)
3000	Task 1 (40kN)
5000	Task 1 (40kN)
10,000	Task 1 (40kN)
20,000	Task 1 (40kN)
50,000	Task 1 (40kN)
75,000	Task 1 (40kN)
100,000	Task 1 (40kN)
170,000	Task 1 (40kN)
187,000	Task 1 (40kN)
One Month Loading Break	No Loading or Testing
188,000	Task 1 (40kN)
204,000	Task 1 (40kN)
250,000	Task 1 (40kN)
300,000	Task 1 (40kN)

Task 2 testing was not possible on the second pavement for two reasons. Firstly, it was decided that the weak basecourse sections should not be subjected to excessive 51kN wheel loads to limit the possibility of rapid failure occurring. Secondly, due to the large shoulder section constructed from station 55 to 22, it was not possible to laterally move the SLAVE

arm to investigate the effect of load location because one of the wheel assemblies would run onto the sloping shoulder. Therefore, only Task 1 (life cycle) testing was undertaken on the second pavement.

CHAPTER 7

PRESENTATION AND ANALYSIS OF RESULTS

The following chapter presents and analyses the results collected during the two pavement tests. Initially the process of strain translation is discussed to show how the shear strains were calculated. Following this a finite element modelling investigation that was used to justify the main assumptions made is summarised. Finally the life cycle test data collected from both pavements is presented and analysed. This includes:

- Presentation of shear strain and rut development over loading laps.
- Analysis of the relationship between shear strain and rut development.
- Analysis of the effect of axle load on shear strain magnitude.
- Analysis of the effect of load location on the magnitude of shear strains.

7.1 Principal Strain Translation and Shear Strain Calculation

The following section explains how the three principal strains measured using the rosette at each pavement station were translated to a common reference point in order to investigate the presence of shear strains at one specific point in the pavement. The data used in this section as an example was taken at 500 laps, however, all the data produced similar results and the conclusions reached using this data were applicable throughout the entire test lives.

Due to the fact that each of the three coil pairs forming one rosette were separated longitudinally by 200mm, it was initially not possible to determine the magnitude of the three principal strains occurring simultaneously at one specific point of reference in the pavement. This was because the emu system began measuring voltages after the SLAVE arm intersected a permanent laser trigger each lap. Therefore, the transverse voltage trace lags the vertical voltage trace and similarly the longitudinal voltage trace lags the transverse trace by the same amount due to the 200mm and 400mm offsets respectively. An example of three voltage traces is shown in Figure 7.1.

Throughout the report, principal strains are negative for tensile strains and positive for compressive strains. However, all shear strains will be represented as positive values. In reality both negative and positive equal and opposite shear strains occur and localised material properties will determine which directional shear strain will result in failure.

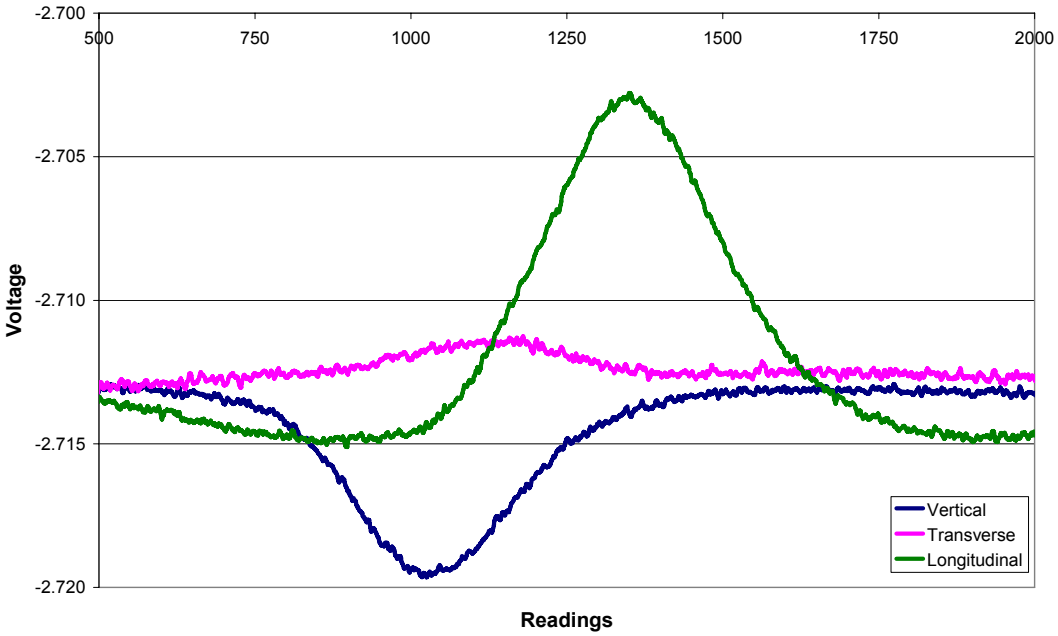

Figure 7.1 Voltage traces from one rosette showing lag in peak due to 200mm offsets.

Therefore, in order to determine the shear strains, two of the three sets of data measured had to be translated back to the first set. This was done by translating the transverse and longitudinal strain voltage profiles back to coincide with the vertical strain voltage profile. The following steps were used to determine the strains at one particular reference point:

1. Based on a vehicle speed of 10km/h (2778mm/s) it would take the SLAVE unit 0.072 seconds to cover the 200mm offset.
2. The emu data processing system was sampling voltages at a rate of 2000 readings/s. Therefore, there was a lag of 144 voltage measurements between each of the coils in the Mohr's Rosette.
3. Based on this lag, the transverse voltage trace was shifted back by 144 readings and the longitudinal trace was shifted back by 288 readings.

The translation of the voltage traces explained above is possible because the vehicle is travelling at a constant speed and also there are no tractive stresses. Therefore the strains act

on the horizontal and vertical faces of the hypothetical soil cube and there is no rotation of planes that would occur is the vehicle was accelerating or decelerating.

The resulting plots (Figure 7.2 and Figure 7.3) show the peaks and troughs of the three voltages traces occurring at almost the exact same time. The slight difference can be attributed to small variations in the vehicle speed and slight errors in the exact coil offset distance due to inconsistencies during installation. However, it can be assumed that these voltage peaks and troughs (which represent tensile and compressive strain) occur at the same point in time. That is to say, when the wheel travels over a point in the pavement, the vertical, transverse and longitudinal strain all reach a maximum value at the same time. This assumption is justified by comparing the actual transverse and longitudinal strains that correspond with the peak vertical strain with the maximum longitudinal and transverse strains occurring at the peak vertical strain. Table 7.1 and Table 7.2 show that there is only a 3% difference in strain magnitude between using the transverse and longitudinal voltages that correspond with the maximum vertical voltage and using the maximum transverse and longitudinal voltage value. Therefore, for ease of calculations, it was assumed that the vertical, transverse and longitudinal strains at a single reference point in the basecourse would all reach a maximum at the same time when loaded by the SLAVE. Thus, in order to calculate the three principal strains and subsequently the shear strain within the basecourse, only the maximum voltages were located and the corresponding strains calculated.

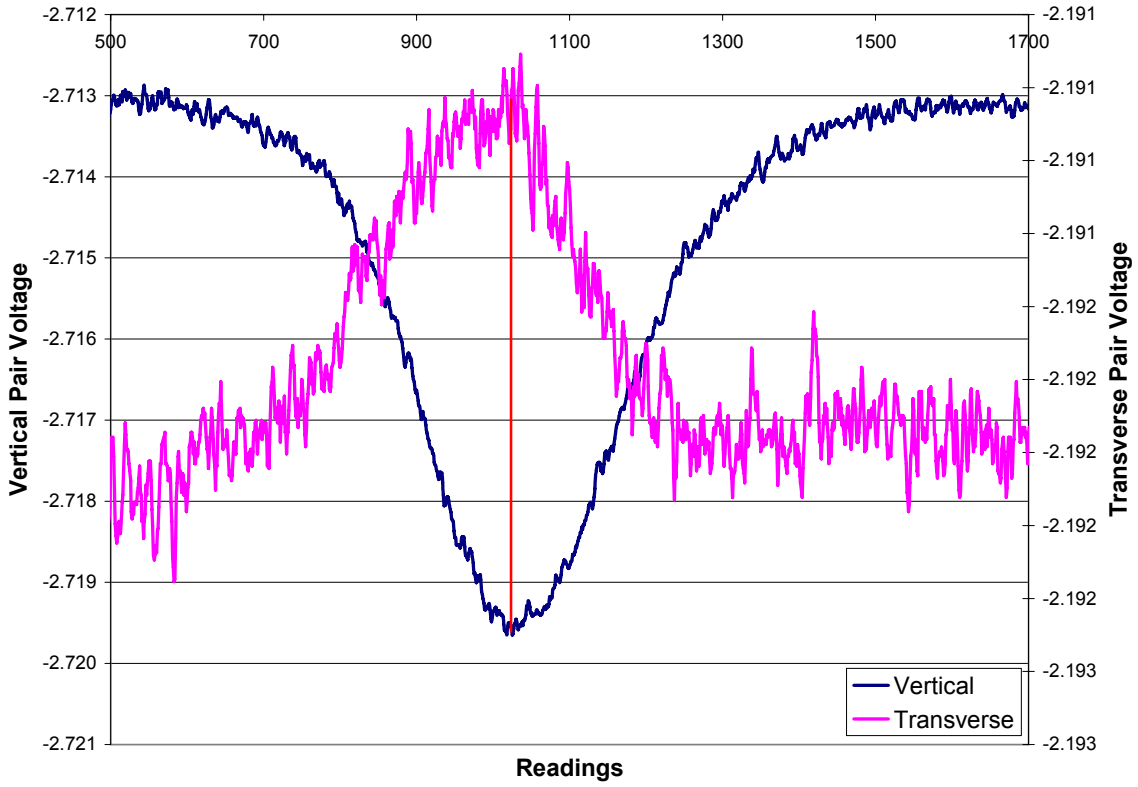

Figure 7.2 Vertical and translated transverse voltage traces with corresponding transverse value indicated

Table 7.1 Difference between true corresponding transverse strain and the assumed (max) strain

Max Vertical Voltage	Static Transverse Voltage	Corresponding Transverse Voltage	Max Transverse Voltage	Actual Corresponding Strain (με)	Max Corresponding Strain (με)	% Difference in Strain
-2.7196	-2.1922	-2.19096	-2.191	208	201	3.2

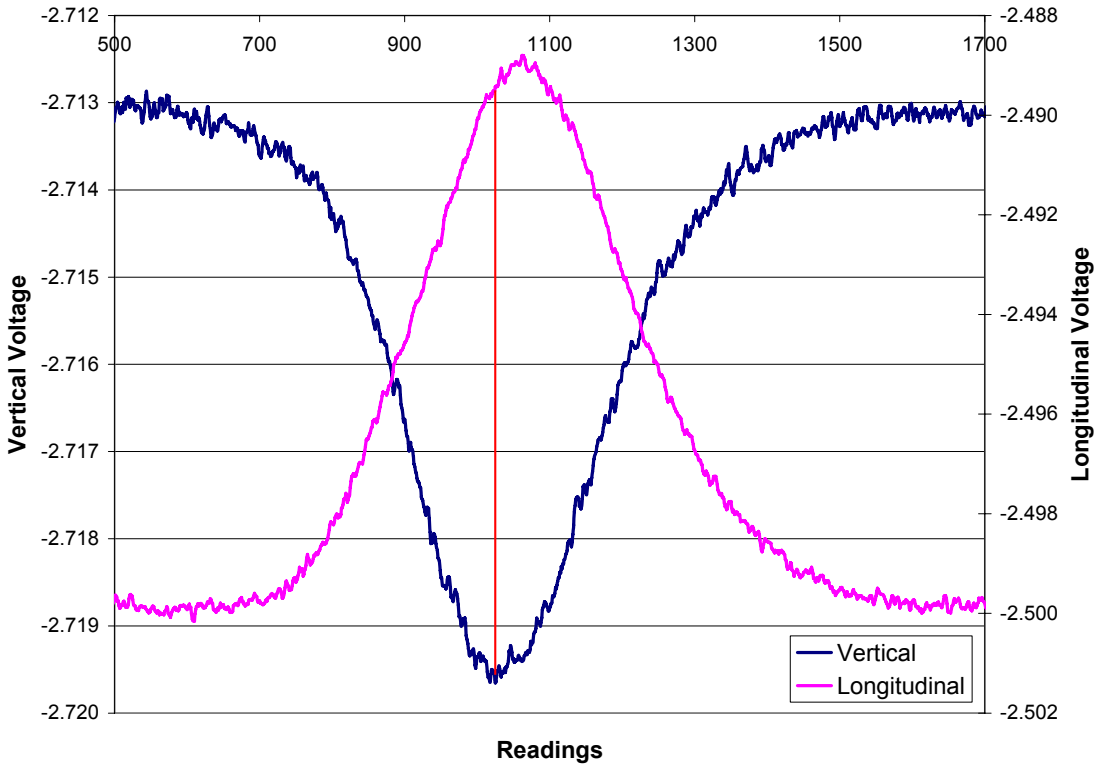

Figure 7.3 Vertical and longitudinal voltage traces with actual corresponding longitudinal value indicated

Table 7.2 Difference between true corresponding longitudinal strain and the assumed (max) strain

Max Vertical Voltage	Static Longitudinal Voltage	Corresponding Longitudinal Voltage	Max Longitudinal Voltage	Actual Corresponding Strain (με)	Max Corresponding Strain (με)	% Difference in Strain
-2.7196	-2.4982	-2.4893	-2.489	1317	1361	3.3

7.1.1 Finite Element Verification of the Principal Strain Assumption

As previously mentioned, the rosette shear strain measuring system relies on the assumption that the measured vertical and horizontal transverse and longitudinal strains are principal strains. This implies that there are no shear strains acting on the vertical and horizontal faces of the hypothetical soil cube under consideration due to the drag of the tyre.

In order to verify this assumption, finite element analysis was conducted to estimate the size of the shear strains occurring on the plane faces. ABAQUS[3], a general purpose three dimensional finite element code was used to model the first pavement and measure the strains

[3] http://www.abaqus.com/home.html. ABAQUS Homepage. ABAQUS Inc. Visited 26.9.2006

induced by a dual wheel assembly identical to the SLAVE. Finite element analysis was used as opposed to linear elastic analysis (which is more common for practitioners) in order to better simulate the non-linear stress dependent behaviour of granular materials.

The finite element model used was developed by Gonzalez (2004) and has been used to generate accurate pavement response values using CAPTIF emu strain data. The following is a brief description of the Gonzalez model for the CAPTIF specific pavement and the input parameters used to define the pavement and loading.

The modified universal model, which has been adopted by AASHTO 2002 Design Guide (AASHTO 2004), was used to model the elastic response of granular layers. This model has previously been used with CAPTIF data because it provides the best compromise between accuracy and computational stability (Gonzalez et al. 2004). Given the symmetry of the problem, a quarter-model (Figure 7.4) of the dual wheel assembly and pavement was used in order to reduce computational time. The asphalt layer was modelled using linear hexahedron elements and the basecourse and subgrade were modelled using quadratic hexahedrons. A 40kN wheel assembly load applying 700kPa of vertical pressure was used as the model load and the load area dimensions were determined from tyre print tests at CAPTIF. The asphalt was modelled as 25mm thick with an elastic modulus of 5000MPa. The 370mm thick basecourse was modelled using the modified universal model (Gonzalez et al. 2004) and the three material coefficients required for this model were determined using repeat load tri-axial tests on the CAPTIF material. The subgrade was modelled with an elastic modulus of 35MPa which was determined from CAPTIF Falling Weight Deflectometer (FWD) and light FWD back calculations. A rigid boundary was included in the model to represent the finite non-deflective concrete tank that the pavements were constructed in.

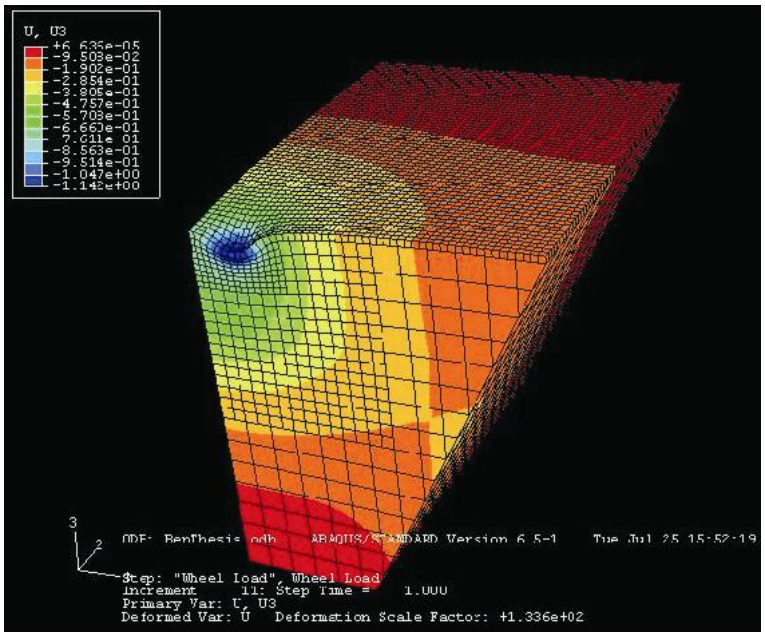

Figure 7.4 Deflection image of finite element quarter-model under 40kN SLAVE load

The model was used to analyse the strains at a node the same depth from the pavement surface as the centroid of the coil rosette. Table 7.3 shows a summary of the strains predicted by the finite element model and the strains measured at CAPTIF in the first pavement (500,000 laps). The vertical compressive strains predicted by the model are within 10% of the strains measured in Pavement 1 confirming the accuracy of the model. The horizontal normal strains vary significantly. However, historically horizontal strains have been very difficult to accurately predict using non-linear models due to difficulties in determining the anisotropic characteristics of materials from tri-axial testing. Under isotropic conditions, stresses in the lower half of an unbound aggregate base over a soft subgrade are often unrealistic (Masad et al. 2006). The concept of anisotropy will be discussed further in Chapter 8. The model shows that the three shear strains on the surfaces of the element are very small and would thus have a negligible effect on calculating the maximum shear strain. Thus, since the shear strains on the element faces are considered negligible, the assumption that the normal strains measured by the induction coils approximate the principal strains is taken to be valid.

Table 7.3 Comparisons between strains predicted by finite element model and measured CAPTIF stains

Strain	FEM Predicted Strains (με)	Measured CAPTIF Strains (με)	Abaqus Co-ordinate System
ε_3 (vertical normal)	677	609	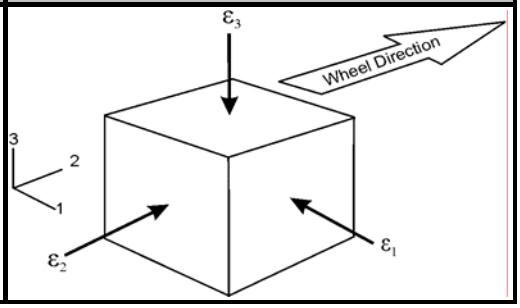
ε_2 (longitudinal normal)	-439	-2165	
ε_1 (transverse normal)	-123	-166	
ε_{12} (face shear)	-0.2	0 (assumed)	
ε_{13} (face shear)	5.4	0 (assumed)	
ε_{23} (face shear)	-5.14	0 (assumed)	

7.2 First Pavement Preconditioning Failure Results

The following strain measurements were taken after 5000 laps, of the planned 200,000 lap preconditioning period for the chipsealed pavement. After 8000 laps, the pavement was deemed to have failed due to significant rutting and heaving within the basecourse. Testing ceased at this point until the 70mm granular overlay was constructed in order to strengthen the basecourse. All strain values throughout this report are expressed in micro strain (με).

The principal strains measured under the 23kN single wheel load are shown in Table 7.4. These strain values are based on the average of five consecutive strain measurements corresponding to five load repetitions of the SLAVE arm. The coil orientation column shows the orientation of each coil within the rosette at each station.

Table 7.4 Preconditioning phase principle strains (με)

			Laps (x1000)
	Station	Coil Orientation	5
Average Principal Strains (Tension -ve)	50	Vertical	3190
		Transverse	-1084
		Longitudinal	-2240
	51	Vertical	2020
		Transverse	-635
		Longitudinal	-3201
	52	Vertical	2987
		Transverse	-910
		Longitudinal	-2467

Based on the principle strains, the maximum transverse and longitudinal shear strains were calculated using Mohr's circle of strain (refer to Section 3.2.2) whereby the maximum shear strain is equal to the diameter of the circle of strain. The calculated shear strains at each station and the corresponding surface deformation are shown in Table 7.5.

Table 7.5 Preconditioning phase average maximum transverse and longitudinal shear strains (με) with corresponding surface deformation

Station	Transverse Shear Strain	Longitudinal Shear Strain	Surface Rutting (mm)
50	4274	5430	16.5
51	2655	5221	21.5
52	3897	5454	14

Due to the fact that the pavement failed so quickly, only one data point was captured at each station and therefore the change in shear strain as rutting progressed could not be determined. However, the three data points do provide good indicators of the magnitude of shear strains that occur during rapid (Class C) basecourse failure (Section 4.2.2). Post-mortem trenches confirmed that subgrade deformation did not occur and thus basecourse shear failure was the cause of the permanent deformation (Section 7.3.2 details this analysis).

Following the placement of the 70mm granular overlay and the various hot mix asphalt patches required due to the highly ravelling second chipseal, a second set of chipseal preconditioning strains were measured. These strains are shown in Table 7.6 and are compared to the original chipseal preconditioning strains mentioned above. The strains after strengthening indicated that the thin (30mm) AC patch which extended approximately 600mm over Station 52 (covering the coils) had a substantial effect on the longitudinal tensile strain. Whereas the longitudinal tensile strains at Station 50 and 51 increased marginally, the longitudinal strain at station 52 decreased by 41%. The other principal strains over all stations changed by approximately the same relative percentage. This low longitudinal tensile strain continued to occur at station 52 throughout the Task 1 testing. Because the large longitudinal tensile strains affect the magnitude of the shear strains, Station 52's shear strain data is consistently almost half the magnitude of Station 50 and 51's. The results indicate that the AC patch had a greater structural effect than anticipated and Station 52 therefore acts as a different pavement. Statistical student t-tests (Appendix C) further confirmed that the

longitudinal strain values measured at station 52 are not part of the same population as those measured at stations 50 and 51. For this reason graphical representations and further analysis of strain data from station 52 have not been presented because it cannot be compared with the other test sections. However, the measured principal strain and calculated shear strains are presented in the tables below.

Table 7.6 Comparison of principal strains after pavement strengthening

	Station	Coil Orientation	Initial preconditioning strains	Strains after overlay and patch	% Change
Average Principal Strains (Tension -ve)	50	Vertical	3190	1220	-62%
		Transverse	-1084	-306	-72%
		Longitudinal	-2240	-2366	6%
	51	Vertical	2020	803	-60%
		Transverse	-635	-228	-64%
		Longitudinal	-3201	-3465	8%
	52	Vertical	2987	955	-68%
		Transverse	-910	-216	-76%
		Longitudinal	-2467	-1456	-41%

7.3 First Pavement and Second Pavement Task 1 Testing

The following section presents the strain and rut measurements that were taken during the 500,000 and 300,000 lap main testing phase in Pavements 1 and 2 respectively. The entire Task 1 test period involved loading with a 40kN dual wheel assembly representing the maximum dual wheel axle weight limit on New Zealand roads. Examples of measured voltage traces from both pavements are shown in Appendix A.

7.3.1 First Pavement Shear Strain Measurements

The principal strains measured at 10 points during the Task 1 life cycle testing are shown in Table 7.7. Based on these strains, Mohr's circle of strain was used to calculate the transverse and longitudinal shear strains which are shown in Table 7.8 and Table 7.9 respectively. In addition to this, each shear strain value for each station was normalised with respect to the initial shear strain calculated within the first 100 laps. This was done because the magnitudes of the raw shear strains often varied over the three sections due to the non-homogeneous nature of the pavement. The normalised shear strain values provide a better comparison of the

actual trends without taking into consideration the effect of structural inconsistencies over the three test stations.

Table 7.7 First pavement principal strains during Task 1 testing

			Laps (x1000)									
	Station	Coil	0	15	30	50	100	150	200	300	400	500
Average Strains (Tension -ve)	50	Vertical	879	835	884	880	872	787	791	760	701	743
		Transverse	-207	-208	-252	-217	-183	-178	-184	-187	-197	-192
		Longitudinal	-1414	-1376	-1649	-1572	-1675	-1716	-1749	-1913	-1609	-1939
	51	Vertical	523	565	600	553	555	534	488	500	485	475
		Transverse	-102	-106	-99	-102	-96	-91	-66	-98	-104	-131
		Longitudinal	-1407	-1721	-2045	-1876	-2085	-2119	-2203	-2364	-2047	-2390
	52	Vertical	583	617	643	652	579	523	516	541	479	501
		Transverse	-87	-162	-229	-198	-196	-152	-132	-157	-174	-174
		Longitudinal	-655	-761	-877	-572	-746	-753	-733	-797	-574	-778

Table 7.8 First pavement transverse shear strains during Task 1 testing

			Laps (x1000)									
	Station	Value	0	15	30	50	100	150	200	300	400	500
Avergage Maximum Transverse Shear Strain	50	Raw Strain	1086	1043	1136	1097	1055	965	975	947	898	935
		Normalised	1.000	0.960	1.046	1.010	0.971	0.889	0.898	0.872	0.827	0.861
	51	Raw Strain	625	671	699	655	651	625	554	598	589	606
		Normalised	1.000	1.074	1.118	1.048	1.042	1.000	0.886	0.957	0.942	0.970
	52	Raw Strain	670	779	872	850	775	675	648	698	653	675
		Normalised	1.000	1.163	1.301	1.269	1.157	1.007	0.967	1.042	0.975	1.007

Table 7.9 First pavement longitudinal shear strains during Task 1 testing

			Laps (x1000)									
	Station	Value	0	15	30	50	100	150	200	300	400	500
Avergage Maximum Longitudinal Shear Strain	50	Raw Strain	2293	2211	2533	2452	2547	2503	2540	2673	2310	2682
		Normalised	1.000	0.964	1.105	1.069	1.111	1.092	1.108	1.166	1.007	1.170
	51	Raw Strain	1930	2286	2645	2429	2640	2653	2691	2864	2532	2865
		Normalised	1.000	1.184	1.370	1.259	1.368	1.375	1.394	1.484	1.312	1.484
	52	Raw Strain	1238	1378	1520	1224	1325	1276	1249	1338	1053	1279
		Normalised	1.000	1.113	1.228	0.989	1.070	1.031	1.009	1.081	0.851	1.033

The variation in strains within structurally similar sections of the pavement, as mentioned above, was common throughout the entire pavement. Alabaster et al. (2006) undertook a

small investigation to prove that the variation was material related. Alabaster compared the central deflections from an FWD with the integrated central deflection of a wheel load calculated from the measured vertical compressive strains under a number of emu coils. This investigation showed that there was a reasonable linear relationship (R^2=0.95) between the central FWD deflection and the integrated deflection. This implied that the variation in strain readings between similar sections was related to local material variations such as slight density differences, moisture contents and material variation between the coils (Alabaster et al. 2006). The researcher further proved this relationship in Pavement 1 of the investigation by comparing the Prima 100 portable FWD composite pavement modulus values at the three stations with the initial compressive vertical strain measurements (Figure 7.5). This clearly shows that there was variation in the stiffness of the three adjacent stations and as the Prima modulus increased (relating to an increase in pavement stiffness), the vertical compressive strain decreased as expected. A similar comparison was not possible on the second pavement due to the Prima FWD not being operational.

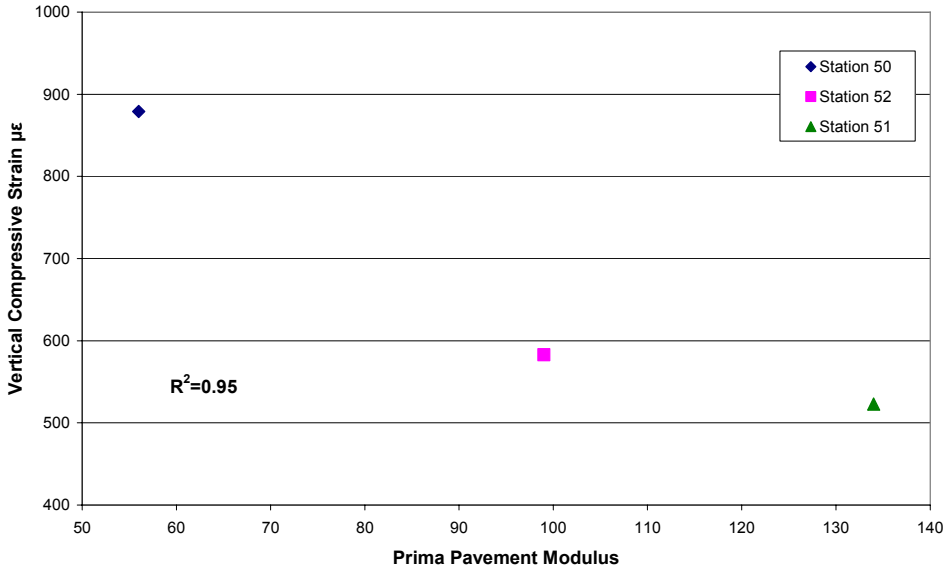

Figure 7.5 Prima FWD modulus versus vertical compressive strain at 0 laps

Plots of the calculated transverse and longitudinal shear strains over the 500,000 laps are shown in Figure 7.6 and Figure 7.7 respectively. The noticeably higher transverse shear strains at Station 50 are due to the higher vertical compressive principal strains caused by a slightly weaker local section and material variations (see Table 7.7). The higher vertical compressive strain (represented as a positive strain) creates a larger diameter on Mohr's circle

of strain compared to Station 51, thus inferring a larger maximum shear strain. The normalised plots of the two shear strains versus loading laps are shown in Figure 7.8 and Figure 7.9. These graphs show that the general trend in shear strain magnitudes versus loading laps is similar for both stations once the strains are normalised with respect to the initial zero lap value.

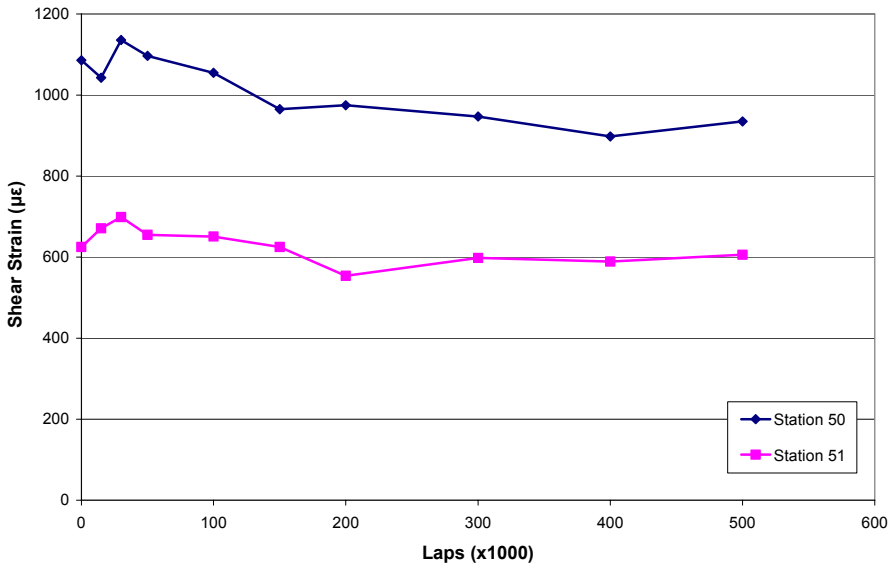

Figure 7.6 First pavement transverse shear strain versus loading laps

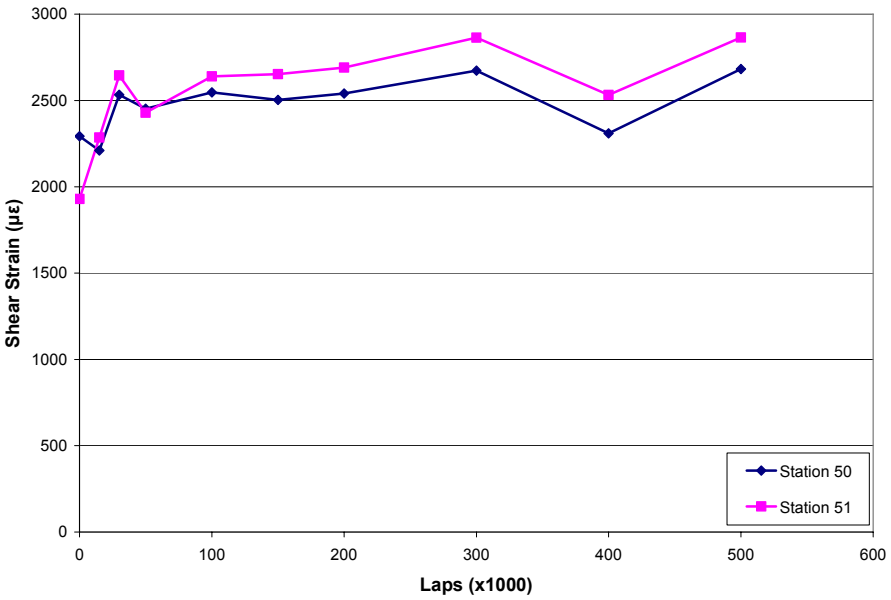

Figure 7.7 First pavement longitudinal shear strain versus loading laps

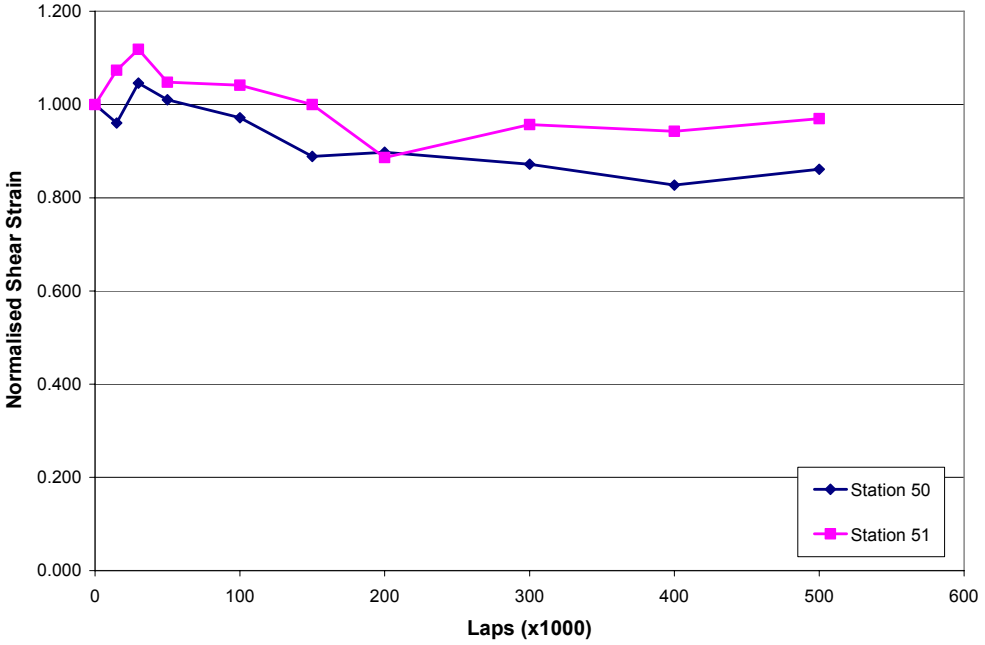

Figure 7.8 First pavement normalised transverse shear strain versus loading laps

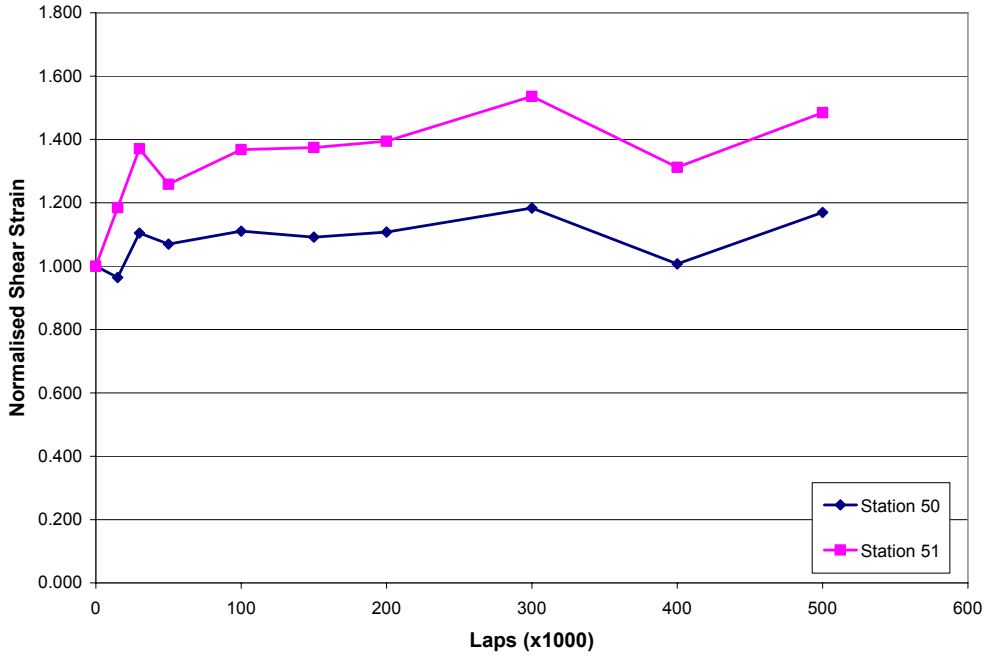

Figure 7.9 First pavement normalised longitudinal shear strain versus loading laps

The life cycle shear strain testing results showed that in both test stations, the overall change in magnitude of both the transverse and longitudinal strains was relatively small.

The transverse shear strains increased to a maximum of 12% over the initial strains (station 51) during the first 30,000 laps and slowly decreased down to a magnitude close to the initial starting strains after 150,000 laps. Following this, the transverse shear strains remained approximately constant until the conclusion of the test. The variation in transverse shear strains during the first 100,000 laps is attributed to the *post construction compaction period* where the basecourse is further compacted and the material slightly realigned due to the application of the wheel load. An illustration of this period within a pavements life is shown in Figure 7.10.

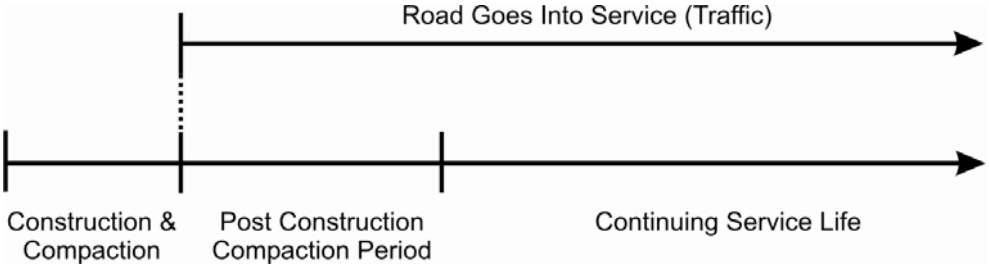

Figure 7.10 Post construction compaction period within a pavement's life

Figure 7.6 and Figure 7.8 show a slight decrease in transverse strain over loading laps. However, this overall change in transverse shear strain is relatively small. For example, the maximum change in magnitude over the pavement test life occurred at station 50 where the shear strains decreased by 150με which is only slightly larger than the noise of the emu system (100με for two pairs). Within pavement analysis, a 150με change in magnitude is almost negligible and therefore the overall trend of the transverse shear strain with respect to loading laps was approximately constant.

Similarly, the longitudinal shear strains increased during the post construction compaction period. The shear strains increased between 11% (Station 50) and 37% (Station 51) during the first 100,000 laps. Following this, the longitudinal shear strains increased at a relatively small rate until the conclusion of the test with an average shear strain increase of 32% over the test life. Again, the fluctuation in longitudinal shear strains during the first 100,000 laps is attributed to the post construction compaction period. The maximum change in magnitude

over the test life occurred at station 51 where the shear strain increased by 935με (48%). The average longitudinal shear strain increase over the pavement life was 662με (32%) and this value is significant enough to conclude that the longitudinal shear strains increased at a low rate as the loading laps increased.

7.3.2 First Pavement Permanent Deformation Measurements

The rut depth (expressed as a VSD, Section 4.1.3) was measured after each strain test at 10 points during the Task 1 test. Table 7.10 shows the maximum rut depths measured after each strain test was conducted. Full transverse rut profiles over loading laps are shown in Appendix B. The permanent deformation over laps graph is shown in Figure 7.11. It should be noted that the variations in the curves are caused by the accuracy limitations of the CAPTIF profilometer (±1mm). The final rut depth values are significantly below the TNZ rut depth failure criteria of 20mm defined in the performance specification for unbound flexible pavements (Transit NZ 1996). Thus, the final state of the pavement was considered to be in good structural condition with respect to permanent deformation and the rut accumulation plots indicate a stable Class A rut progression.

Table 7.10 First pavement rut depths after strain testing

		Laps (x1000)									
	Station	**0**	**15**	**30**	**50**	**100**	**150**	**200**	**300**	**400**	**500**
Station	**50**	0	6	7	8	10	10	12	12	12	13
	51	0	4	4	5	8	8	9	10	10	9
	52	0	5	7	7	7	7	8	9	9	9

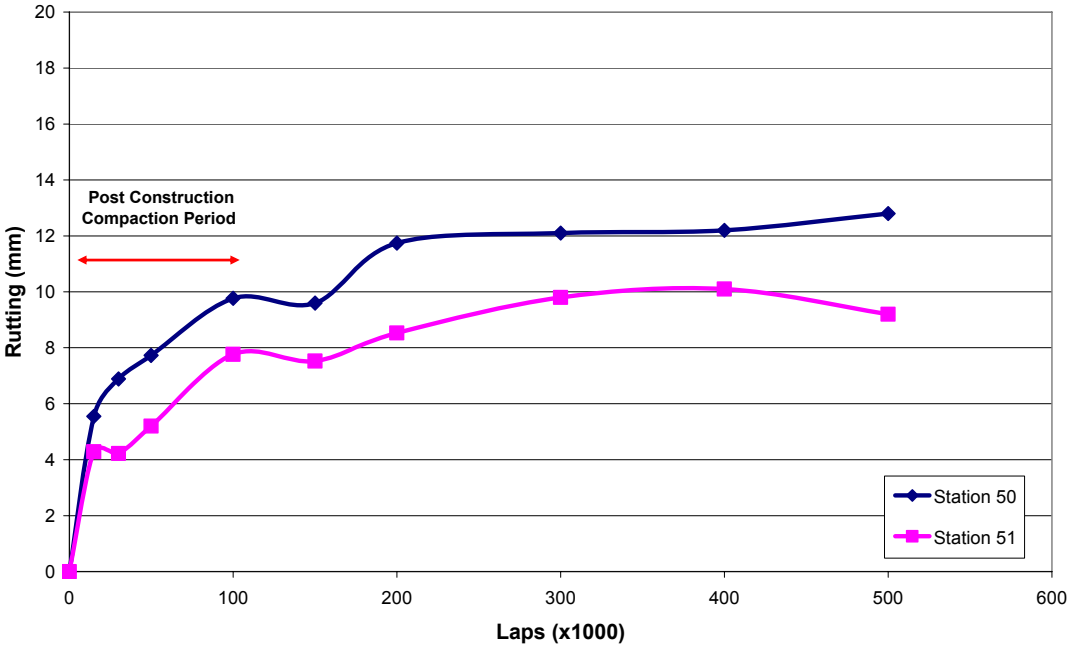

Figure 7.11 First pavement rut depth accumulation over test life

In order to determine in which layers the rutting was manifest, a post mortem trench was excavated at station 50. Using both initial layer profile data during construction and final layer profile measurements from the trench, a cross section of the initial and final layer interfaces was constructed (Figure 7.12). All profile depth measurements are with reference to the tank wall datum. The centre of the dual wheel assembly is shown as a thick dashed line and 200mm movement extremities of the wheel are shown as thin dashed lines.

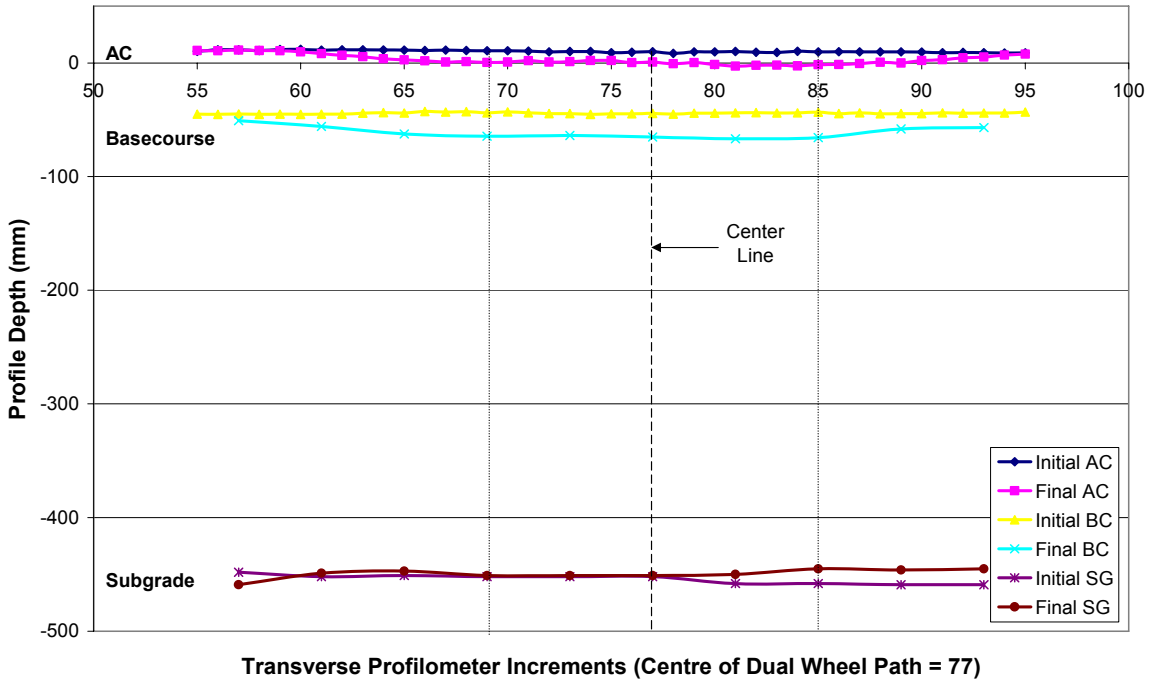

Figure 7.12 Station 50 cross section showing the three initial and final layer interface profiles.

The initial and final AC layer profiles in Figure 7.12 show the permanent deformation measured by the CAPTIF profilometer. The maximum change between these two profiles is 12.8mm as shown in Table 7.10. The initial basecourse profile was measured during construction using the profilometer and can therefore be considered accurate to within ± 1mm. However, the basecourse profile after 500,000 laps, which was determined by subtracting the final cross section thickness of the surface layer (measured from the trench) from the original basecourse profile is not highly accurate. This is due to the difficulty in identifying the layer interfaces and therefore accurately measuring the final surface layer thickness from the test trench. Clearly the final profile is not accurate because it indicates that more deformation has occurred within the basecourse than the total surface rutting. The inaccuracy is caused because the AC and basecourse interface is not easily identifiable due to the aggregate particles bonding to the overlying AC layer. The final subgrade profile is easier to determine than the basecourse because the layer interface is more identifiable. The subgrade transverse profiles show that no permanent deformation occurred in the subgrade. The visible difference between the two subgrade profiles shows that the final profile has risen slightly. However, it is assumed that there was not a volume increase but rather a small migration of material into the lower section of the basecourse which caused the final subgrade profile depth to be measured slightly higher than the true layer interface. It was therefore

determined that there was minimal subgrade rutting. Based on these results it was estimated that 80% of the rutting occurred within the granular basecourse layer due to shear failure and the remaining 20% was due to small amounts of subgrade deformation and compaction of the OGPA. The basecourse failure was concluded to be shear failure because there was a less than a 1% increase in the basecourse density (measured using a nuclear densometer in backscatter mode) at the end of testing compared to the initial density after construction. It was therefore concluded that the basecourse rutting was therefore caused by shear failure and not consolidation.

7.3.3 Second Pavement Shear Strain Measurement

The principal strains measured at 13 points during the Task 1 life cycle testing are shown in Table 7.11. Based on these strains, Mohr's circle of strain was used to calculate the transverse and longitudinal shear strains which are shown in Table 7.12 and Table 7.13 respectively. Similar to the first pavement strain results, normalised shear strains are shown for each station to show each stations percentage change in strain over loading and to show that each station follows a similar trend despite strain magnitude differences caused by local material variation.

Table 7.11 Second pavement principal strains during Task 1 testing

			Laps (x1000)													
	Station	Coil	0	1	2	5	10	20	50	100	170	187	188	203	250	300
Average Strains (Tension -ve)	38	Vertical	401	432	429	479	477	479	528	549	573	589	503	557	528	507
		Transverse	-72	-104	-82	-108	-131	-140	-183	-172	-185	-188	-179	-164	-171	-160
		Longitudinal	-335	-426	-444	-583	-729	-822	-936	-1089	-1160	-1204	-992	-984	-948	-893
	39	Vertical	421	481	482	477	502	509	531	543	560	556	534	541	532	491
		Transverse	-123	-122	-112	-118	-144	-147	-213	-247	-274	-278	-240	-237	-236	-221
		Longitudinal	-445	-483	-530	-564	-592	-627	-717	-817	-848	-865	-803	-788	-684	-800
	40	Vertical	408	456	466	446	465	469	515	539	548	564	493	544	533	513
		Transverse	-53	-75	-52	-72	-81	-93	-117	-116	-98	-131	-96	-119	-121	-105
		Longitudinal	-448	-556	-486	-512	-548	-550	-654	-819	-744	-786	-711	-745	-865	-745

Table 7.12 Second pavement transverse shear strains during Task 1 testing

			Laps (x1000)													
	Station	Value	0	1	2	5	10	20	50	100	170	187	188	203	250	300
Avergage Maximum Transverse Shear Strain	38	Raw Strain	473	536	511	587	608	619	711	721	758	777	682	721	699	667
		Normalised	1.000	1.133	1.080	1.241	1.285	1.309	1.503	1.524	1.603	1.643	1.442	1.524	1.478	1.410
	39	Raw Strain	544	603	594	595	646	656	744	790	834	834	774	778	768	712
		Normalised	1.000	1.108	1.092	1.094	1.188	1.206	1.368	1.452	1.533	1.533	1.423	1.430	1.412	1.309
	40	Raw Strain	461	531	518	518	546	562	632	655	646	695	589	663	654	618
		Normalised	1.000	1.152	1.124	1.124	1.184	1.219	1.371	1.421	1.401	1.508	1.278	1.438	1.419	1.341

Table 7.13 Second pavement longitudinal shear strains during Task 1 testing

			Laps (x1000)													
	Station	Value	0	1	2	5	10	20	50	100	170	187	188	203	250	300
Avergage Maximum Longitudinal Shear Strain	38	Raw Strain	736	858	873	1062	1206	1301	1464	1638	1733	1793	1495	1541	1476	1400
		Normalised	1.000	1.166	1.186	1.443	1.639	1.768	1.989	2.226	2.355	2.436	2.031	2.094	2.005	1.902
	39	Raw Strain	866	964	1012	1041	1094	1136	1248	1360	1408	1421	1337	1329	1216	1291
		Normalised	1.000	1.113	1.169	1.202	1.263	1.312	1.441	1.570	1.626	1.641	1.544	1.535	1.404	1.491
	40	Raw Strain	856	1012	952	958	1013	1019	1169	1358	1292	1350	1204	1289	1398	1258
		Normalised	1.000	1.182	1.112	1.119	1.183	1.190	1.366	1.586	1.509	1.577	1.407	1.506	1.633	1.470

All three of the above tables show that there was a decrease in both the principal strains and shear strains after the one month construction break which occurred between 187,000 laps and 188,000 laps. On average, the transverse shear strains dropped by 90με and the longitudinal shear strains dropped by 176με. A definite explanation for this rapid yet reasonably small reduction was not found although multiple options were investigated including; temperature effects on the instrumentation and dynamic load changes due to the new epoxy asphalt surface on a track section not relevant to this investigation.

It was also considered that a type of pavement relaxation might have occurred after the long break and that this would return to normal after a few hundred load applications. However, because the strain magnitudes continued to remain at slightly lower levels from 188,000 until the end of testing it was concluded that a small electrical shift must have occurred. This was further supported by the fact that CAPTIF coils only 1m away from station 40 and at similar depths and locations to the rosettes did not experience any reduction in strain. For this reason, it has been assumed that a small shift was caused due to unknown electrical reasons. Analysis in later sections shows that following the post construction compaction period, it is the rate of

change not the magnitude of the shear strain that is important. Therefore, plots of the transverse and longitudinal shear strains presented below have been modified so that the strains measured after 187,000 laps have been increased by the difference experienced between 187,000 and 188,000 laps. Thus, the elastic shear strains over time are presented as if the sudden small reduction did not occur. Even if this assumption is wrong, the conclusions drawn later will not be effected because they are based on the rate of change of shear strain and not magnitude. The actual unmodified plots are shown in Appendix D.

Plots of the transverse and longitudinal shear strains over the 300,000 lap test are shown in Figure 7.13 and Figure 7.14 respectively. Normalised plots have not been shown for the second pavement because similar to the first pavement, the plots simply follow the same general trend as presented in the raw shear strain graphs. However, all three traces map closer to each other due to the normalisation with respect to each initial shear strain value.

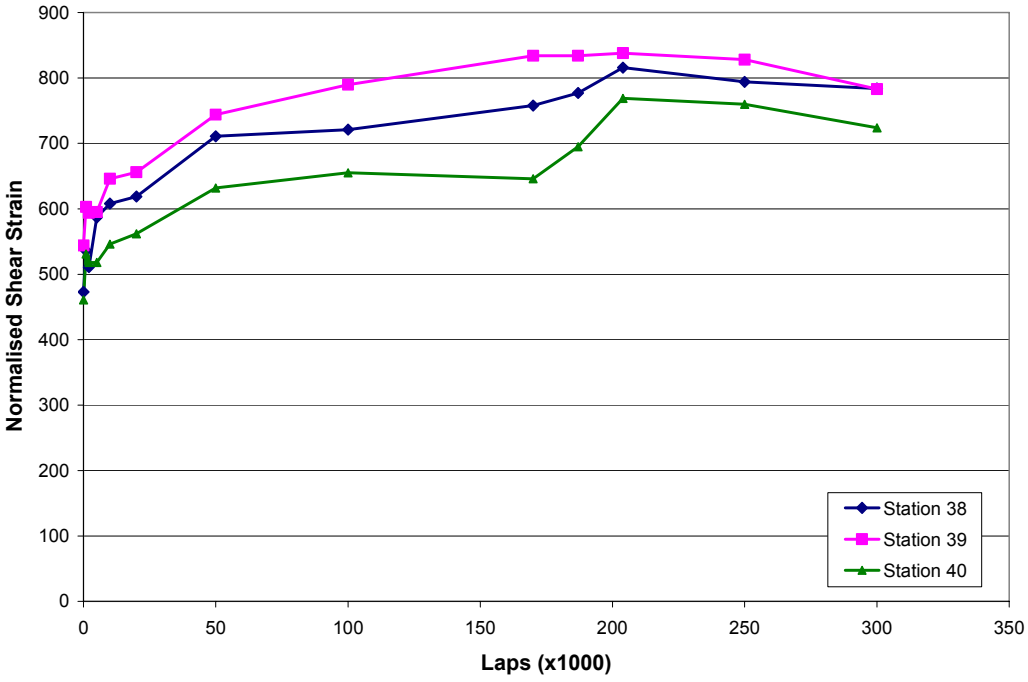

Figure 7.13 Second pavement transverse shear versus loading laps (modified after 187,000 laps)

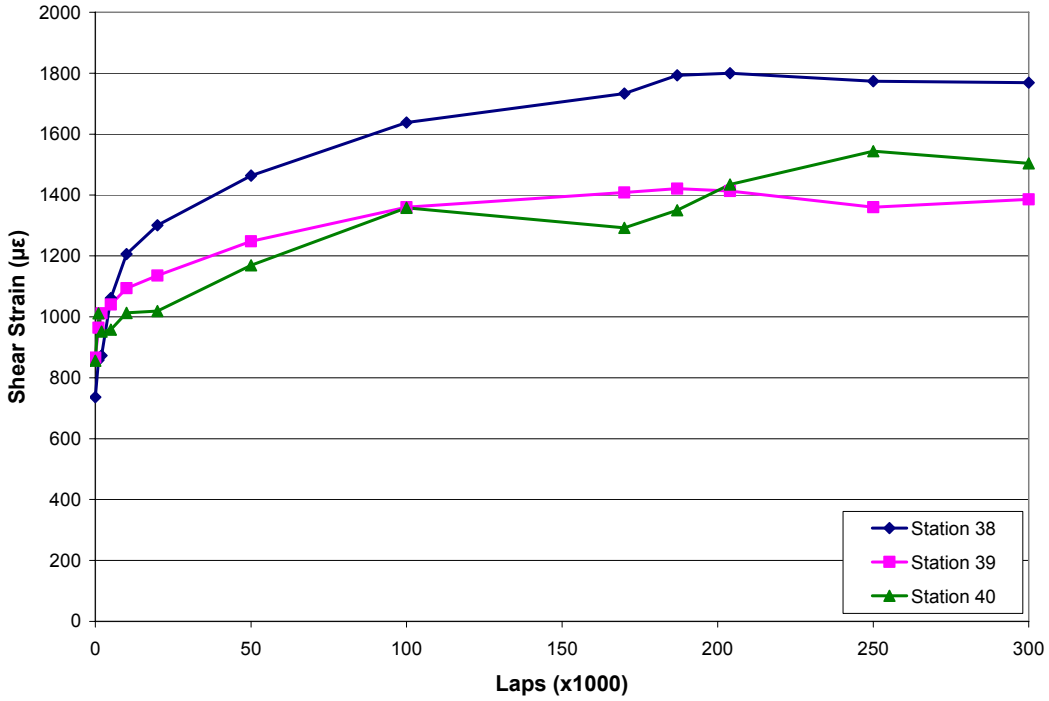

Figure 7.14 Second pavement longitudinal shear strain versus loading laps (modified after 187,000 laps)

The Task 1 testing in Pavement 2 showed that after the post construction compaction phase which was deemed to end at 50,000 laps, there was a relatively small but constant increase in both the transverse and longitudinal shear strain over the remainder of the test. The end of the post construction compaction phase was determined to be at 50,000 laps due to the slowing of development in both shear strain magnitude and rut development.

During the first 50,000 laps, the transverse shear strains initially increased by an average of 47% of the original value. Following this, the shear strains at all three stations increased until 200,000 laps, after which they decreased by a negligible level until the end of testing. The increase in transverse shear strains from 50,000 laps until the end of testing had a maximum increase of 92με (station 40) which is well within the error of the emu system. Thus the transverse strain behaviour after the post construction compaction period is assumed to be constant.

Similarly, the longitudinal shear strain increased rapidly during the first 50,000 laps. The strain increased by an average value of 160% during the post construction compaction phase and a maximum increase of 200% (728 micro-strain) occurred at the station 38. Following this, the average rate of increase in longitudinal shear strains slowed down but continued to

increase at a constant rate until 250,000 laps. After this point, the average shear strain remained constant until the end of testing. Unlike the transverse shear strains, the magnitude change in the longitudinal shear strains after the post construction compaction phase was substantial.

7.3.4 Second Pavement Permanent Deformation Measurements

As with the first pavement, rut depths (expressed as VSD) were measured at the conclusion of each strain measuring period. Table 7.14 shows the measured rut depths and Figure 7.15 shows the permanent deformation accumulation over loading laps with an accuracy of ±1mm. All three sections exhibited similar rutting with the final state being significantly below the 20mm TNZ failure limit. Thus despite constructing a structural base layer that was compacted significantly below recommended field conditions, the pavement did not rut extensively and followed a stable Class A rut progression.

The small but rapid increase in rut depth between 187,000 laps and 204,000 laps has been attributed to the one month construction break and corresponds with the sudden reduction in shear strains. Again, a scientific explanation for this phenomenon could not be determined, however, this tyre of response has occurred in previous CAPTIF pavements where extended non loading periods have occurred (Alabaster 2006).

Table 7.14 Second pavement rut depths after strain testing

		Laps (x1000)											
	Station	0	1	2	5	10	20	50	100	187	203	250	300
Station	38	0	1	2	3	3	4	6	7	8	10	10	10
	39	0	2	2	2	3	3	5	6	7	8	9	8
	40	0	1	1	1	2	2	3	4	4	5	6	6

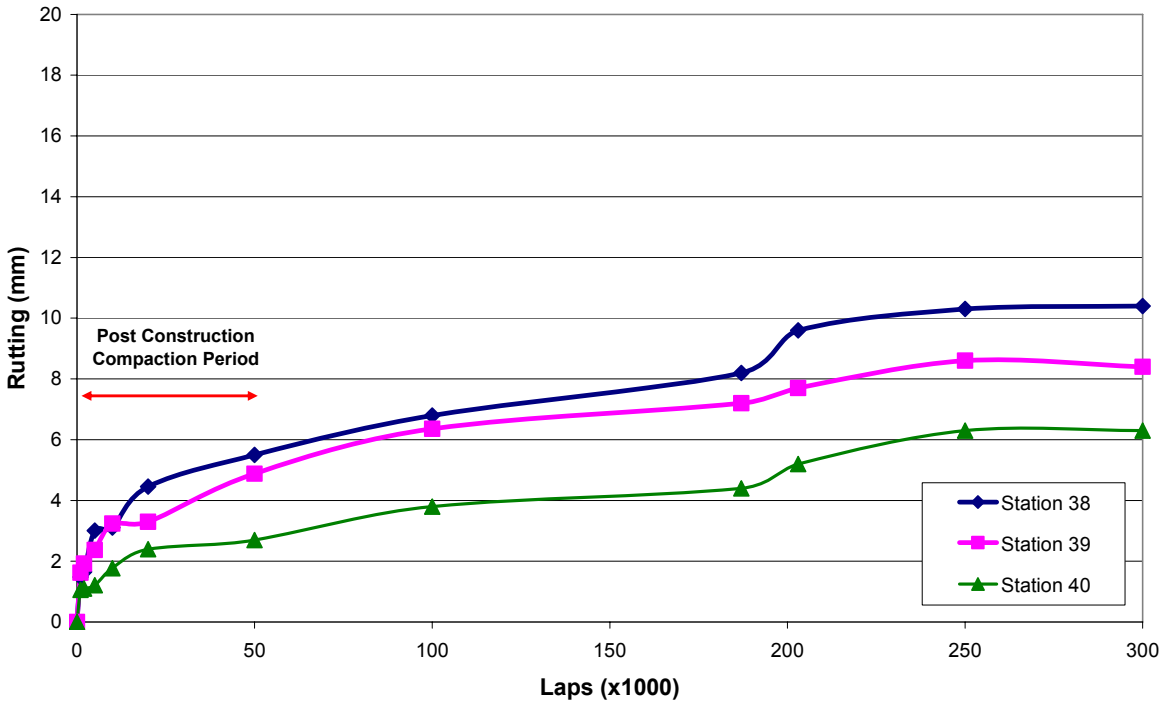

Figure 7.15 Second pavement rut depth accumulation over test life

7.4 Task 1 Testing Comparison between Pavement 1 and Pavement 2

The following section compares the results from both test pavements and focuses on three investigations. Firstly, the two measured shear strains (longitudinal or transverse) were assessed to determine whether one or both should be used in further analysis. Secondly, the shear strains were compared with the vertical compressive strains (which are traditionally the focus in permanent deformation analyses) to determine whether the shear strains are significant. Thirdly, this section compares the shear strain behaviour in both pavements with the accumulated permanent deformation profiles with the aim of analysing the effect of shear strain on rutting.

Throughout this section average rutting and shear strain values are used for each pavement. For example, the longitudinal shear strain for Pavement 2 is defined as the average of the longitudinal shear strains at stations 38, 39 and 40. It has been previously shown that the variations in strains and rut depths between sections in the same pavement are relatively small and this has been attributed to slight localised variations within the pavement due to material, construction differences and noise within the emu system. In addition to this, the student t-tests (Appendix C) prove that the rut profiles and strain measurements for each pavement are

a part of the same population. It can therefore be assumed that average strain and rut values based on measurements from three stations will give a good indication of the overall performance of the pavement under consideration.

7.4.1 Critical Shear Strain Response Parameter

In both pavements, the longitudinal shear strain was substantially larger than the transverse. However, the transverse strains have been presented and analysed in order not to rule out the possibility that this smaller strain has a more dominant effect than the longitudinal shear strain.

When comparing the results from both test pavements it appears that the longitudinal shear strain (which is also the maximum shear strain using a Tresca based criterion, see Chapter 3) is more suitable as a pavement response parameter than the transverse shear strain. Table 7.15 shows the average transverse and longitudinal shear strains at 200,000 laps and 187,000 laps for the first and second pavements respectively. The 200,000/187,000 point was chosen because this was at a point a substantial number of laps after the end of the post construction compaction period. It should also be noted that the choice of second pavement values was the 187,000 laps values (as opposed to 204,000) because these values, which are very close to 200,000 laps, were the last measurements taken before the one month break occurred. Thus the sudden small reduction in strains is not taken into account in this analysis.

The difference in transverse shear strains measured in the two pavements is only 0.5%. This is because both the vertical compressive strain and the transverse tensile strain are similar for both pavements thus creating similar Mohr's circles of strain. Conversely, the longitudinal shear strain is significantly smaller in the second pavement compared to the first. This is due to the larger longitudinal tensile strains in the first pavement creating a Mohr's circle of strain with a larger diameter compared to the second pavement. The difference in longitudinal shear strains between the two pavements also compares well with the difference in permanent deformation after the loading period.

Table 7.15 Average shear strain and rut depths at 200,000 and 187,000 laps for Pavements 1 and 2

	Pavement 1	Pavement 2	% Difference
Transverse Shear Strain	764	768	0.5
Longitudinal Shear Strain	2616	1520	-41.9
Rut Depth (mm)	10.1	6.6	-34.7

Therefore, for further analysis the longitudinal shear strain will be used as the main shear strain response parameter for the following reasons:

- Using a Tresca criterion, the longitudinal shear strain is the maximum shear strain whereas the transverse shear strain is significantly below the maximum shear strain value.
- The longitudinal shear strain appears to be more sensitive between different pavements due to the influence of the principal longitudinal tensile strain.
- The magnitude of the longitudinal shear strain relates well with the magnitude of rutting manifested in the test pavements.

7.4.2 Longitudinal Shear Strains Compared to Vertical Compressive Strains

Generally, vertical compressive strains are the most common basecourse response parameter used to analyse and classify the behaviour of granular layers. For example, repeat load tri-axial testing which is commonly used to classify the behaviour of granular layers under different loading conditions and confining pressures utilises vertical compressive strains to predict the rutting behaviour of materials. In addition to this, due to the large amount of field measured vertical compressive strain data and the lack of measured shear strain data, vertical compressive strains are commonly used in pavement modelling to verify granular layer models. A comparison between vertical compressive strain and longitudinal shear strain data from this project was required to determine whether shear strains provide any additional data for explaining the degradation of basecourse layers and how these shear strains compare with the more common vertical strains.

Table 7.16 shows a comparison of the average vertical compressive and longitudinal shear strains at 200,000 and 187,000 laps for the first and second pavements respectively. There is only a 4.7% difference between the two vertical compressive strains which can be considered negligible. However, the 42% magnitude difference in longitudinal shear strain compares well with the 35% difference in rut depth between Pavements 1 and 2. This compares well with

observations made by Steven (2005) based on substantial amounts of CAPTIF data taken from multiple different projects. Steven (2005) observed that when pavements exhibited rutting behaviour of either Class A or Class B, the resilient vertical strain was constant over the duration of the test (ignoring the initial "bedding in" cycles). (Steven 2005)

Table 7.16 Average strain magnitude comparisons between test Pavements 1 and 2 at 200,000 and 187,000 laps respectively

	Pavement 1	Pavement 2	% Difference
Vertical Compressive Strain	598	570	-4.7
Longitudinal Shear Strain	2616	1520	-41.9
Rut Depth (mm)	10.1	6.6	-34.7

In addition to this, Table 7.17 shows that in both test pavements the longitudinal shear strain was more sensitive than the vertical compressive strain over the full test life. Also, the longitudinal shear strain followed a consistent trend of increasing as the rut depth increased, however the vertical compressive strain decreased in the first pavement and increased in the second pavement.

Table 7.17 Average changes in strain over test life

	Strain at beginning of test	Strain at end of testing	% Change
Pavement 1 Vertical Compressive	701	609	-13.1
Pavement 1 Longitudinal Shear	2110	2774	31.5
Pavement 2 Vertical Compressive	410	574	40.0
Pavement 2 Longitudinal Shear	820	1554	89.5

Based on these observations, the relationship between the magnitude of the longitudinal shear strain and the degree of rutting is better than the vertical compressive strain, and the longitudinal shear strain is more sensitive than the vertical strain over the full test life. For these reasons the shear strain seems to provide a greater insight into the structural changes occurring within the granular layers and thus the initial hypothesis of investigating shear strains as opposed to vertical compressive strains is verified.

7.4.3 Shear Strain and Rut Development Comparison in Pavement 1 and 2

Up to this point a system has been developed to calculate in-situ shear strains in granular layers based on measured principal strains. In two pavements, shear strains have been measured over time along with accumulated rut profiles. It has been found that of the two shear strains measured, the longitudinal shear strains are the most appropriate to use as a pavement response parameter for the remainder of the analysis. In addition, the longitudinal shear strains have been compared with the vertical compressive strains and it was concluded that the shear strains compare better with the measured pavement rutting than vertical strains (which are traditionally used).

The following sub-section compares the magnitude of longitudinal shear strains, the development of shear strains over loading laps and the degree of rutting manifested in the two pavements in order to draw conclusions on the relationship between shear strain and permanent deformation in unbound pavements.

Figure 7.16 and Figure 7.17 show the development of the average shear strain and rutting in Pavements 1 and 2. The strain data is shown on a scale with an upper limit of 5000 which corresponds to the failure magnitudes measured during the preconditioning of Pavement 1. The rut data is shown on a scale with an upper limit of 20mm which is the TNZ intervention level for permanent deformation (Transit NZ 1996).

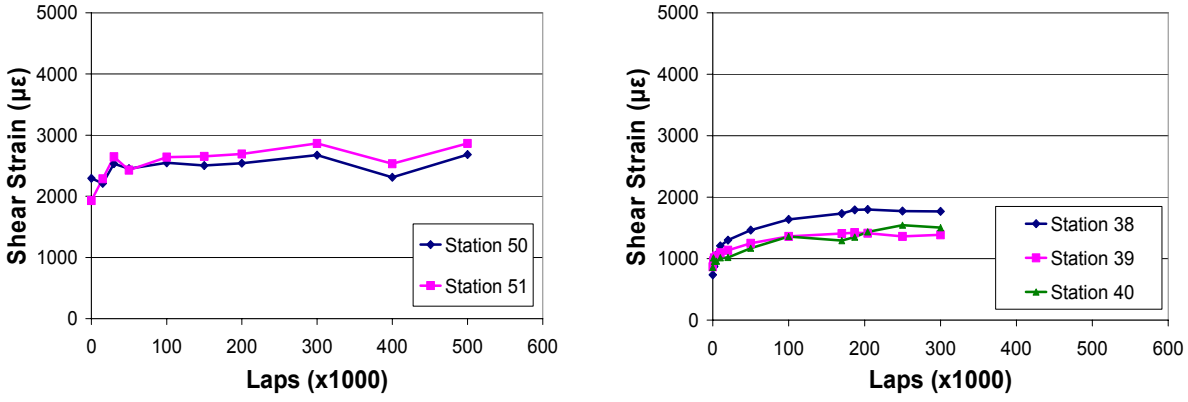

Figure 7.16 Longitudinal shear strain development in pavements 1 (left) and 2 (right)

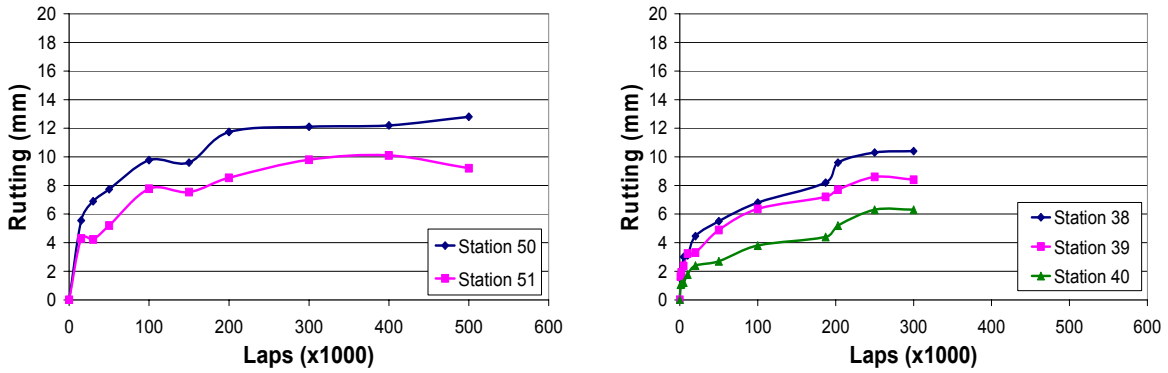

Figure 7.17 Rut depth development in pavements 1 (left) and 2 (right)

The above figures show that the shear strain development follows the rut accumulation whereby there is rapid increase and fluctuation in shear strain during the post construction compaction phase corresponding with a rapid increase in rut depth. After this bedding in phase, the strains plateau and only increase slightly which corresponds well with the plateau in rut accumulation.

Figure 7.18 shows the relationship between longitudinal shear strain and rut depth for Pavements 1 and 2, with the post construction compaction periods shown. The analysis that follows in this chapter is focused on the two periods in the pavements' lives (during the post construction compaction period and after the post construction compaction period has finished) because the relationship between longitudinal shear strain and rut depth is different in each period. This is further analysed and discussed in this sub-section.

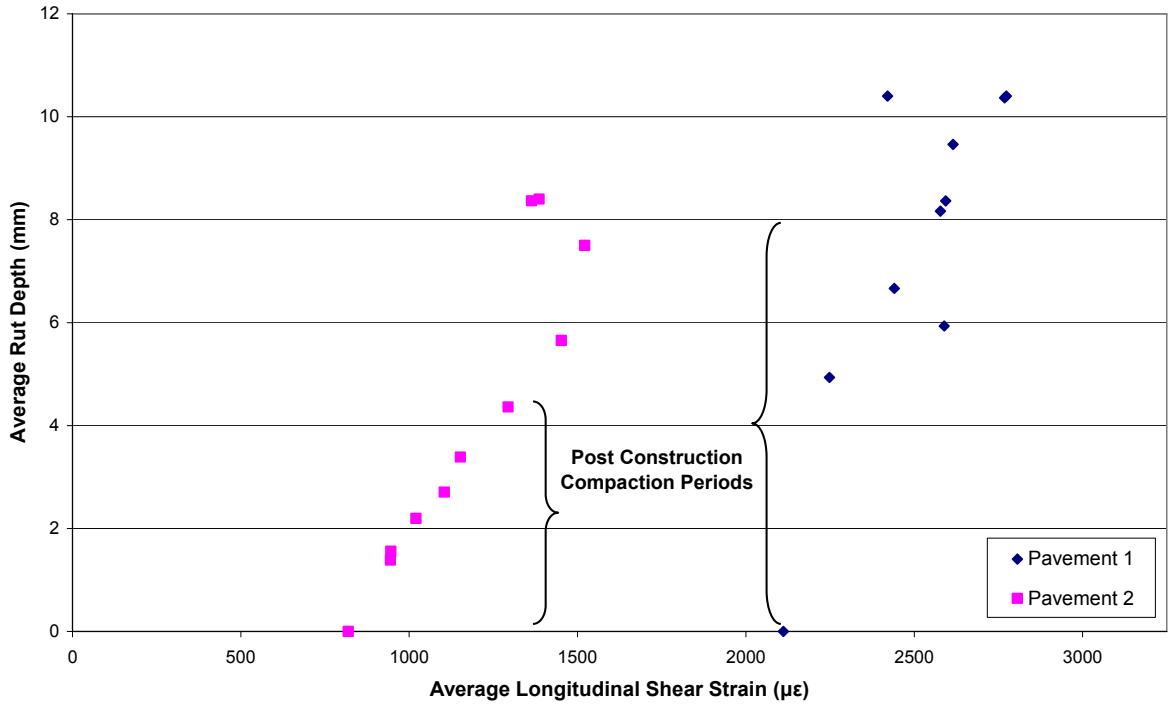

Figure 7.18 Average shear strain versus average rut depth for Pavement 1 and Pavement 2

The magnitude of the shear strains in each pavement correspond with the initial increase in rut depth during the post construction compaction period. Table 7.18 shows that the 48% smaller shear strain magnitude in Pavement 2 also corresponds with 50% smaller rut depth after the post construction compaction phase when compared with Pavement 1. In addition to these results, the pre conditioning failure results from Pavement 1 also support this conclusion whereby an average longitudinal shear strain of 5368 correspond to an average rut depth of 17mm. Therefore, an increase from 2594με to 5368με (107%) in Pavement 1 relates to an increase in rut depth from 8.8mm to 17.3mm (97%) further implying a strong relationship between initial shear strain magnitudes and early rut depth development. Using these three shear strains and rut depth measurements, Figure 7.19 shows that a linear relationship exists between shear strain magnitude at the end of the post construction compaction period and rut depth at the end of this period. This relationship has a coefficient of determination (R^2) of 0.999 indicating a strong linear relationship exists based on the measured data.

Table 7.18 Average shear strain and rut depth at end of post construction compaction period

	Pavement 1	Pavement 2	% Difference
Shear Strain	2594	1340	48
Rut Depth	8.8	4.4	50

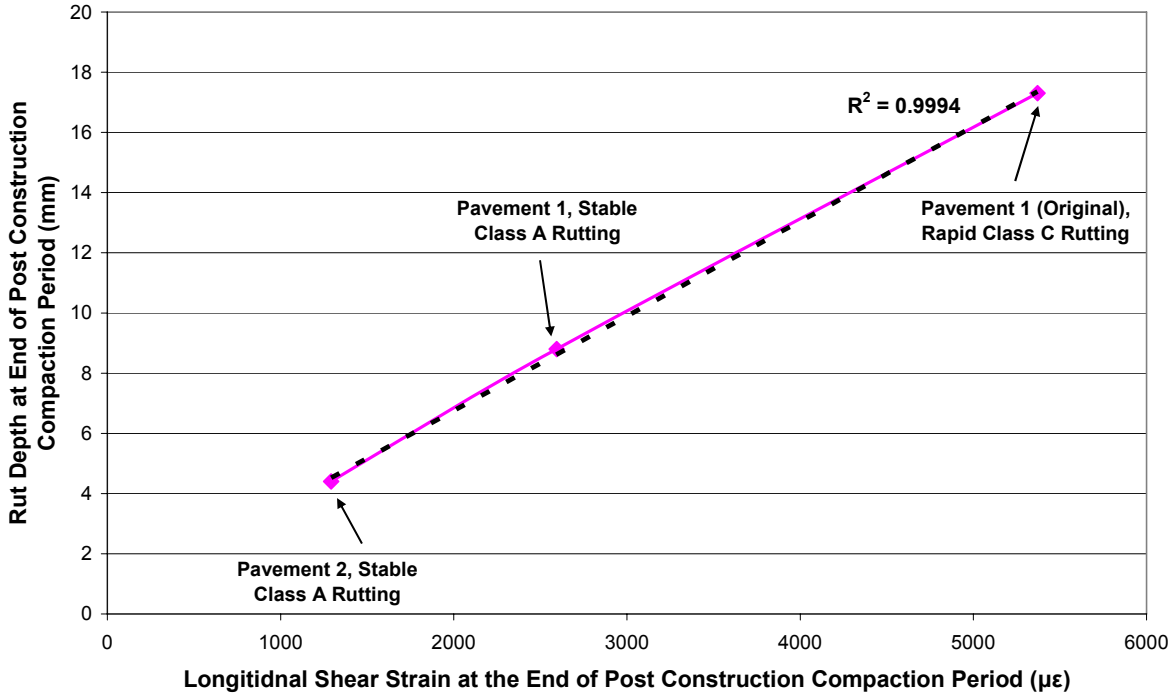

Figure 7.19 Shear strain magnitude versus rut depth at end of post construction compaction period

The length of the post construction compaction period in each pavement is different due to the strength of each pavement. In the case of the first pavement during the chipseal preconditioning period the length of the post construction compaction period was approximately 8000 laps. The strengthened first pavement was deemed to have a post construction compaction period of 100,000 laps and the second pavement had a period of 50,000 laps. This is confirmed by Steven (2005) who states that the steady state phase (which begins after the post construction compaction period) usually starts within the first 100,000 laps in CAPTIF tests (Steven 2005). The difference in the lengths of the post construction compaction periods (where the majority of the rutting is formed) does not weaken the relationship. It simply means that the linear relationship cannot be used to estimate the number of laps that the post construction compaction period will last for. The implications of this are discussed in Chapter 8.

Following this, the changes in shear strain magnitude from the end of the post construction compaction phase until the end of testing correspond well with the changes in rut depth accumulation after the post construction compaction period. Table 7.19 and Table 7.20 show that the percentage increase in rut depth in both pavements is approximately in proportion to the percentage change in shear strain. Two phases were identified after the post construction compaction period. The first development phase involved a slow but constant increase in both rut depth and shear strain. This phase was deemed to end after 300,000 laps on the first pavements and 250,000 laps on the second pavement after the rut accumulation reached a plateau. The second phase involved a constant rut depth and minimal change in shear strain, this phase continued in both pavements until the end of testing.

Table 7.19 Average changes in shear strain and rut depth from the end of the post construction compaction phase until the end of phase 1 development.

		End of initial post construction period	300000/ 250000 laps	% Change	Proportion
Pavement 1	Shear Strain	2594	2768	7	3.7
	Rut Depth (mm)	8.8	11	25	
Pavement 2	Shear Strain	1292	1560	21	4.4
	Rut Depth (mm)	4.4	8.4	91	

Table 7.20 Average changes in shear strain and rut depth from the end of phase 1 development until the end of testing (phase 2 development)

		300000/ 250000 laps	End of Test	% Change	Proportion
Pavement 1	Shear Strain	2768	2774	0.2	0.0
	Rut Depth (mm)	11	11	0.0	
Pavement 2	Shear Strain	1560	1554	-0.4	0.0
	Rut Depth (mm)	8.4	8.4	0.0	

Therefore in conclusion, the above results indicate that the magnitude of the initial shear strain appears to be directly related to the increase in rut depth during the post construction compaction phase. Further to this, the change in shear strain magnitude following the post

construction compaction phase corresponds to the increase in rut depth after the post construction compaction deformation has occurred.

The only investigation that was not possible during the project was to monitor the change in shear strain during a Class B pavement failure (Section 4.2.2). This type of failure was expected to occur within the first 200,000 laps on the second pavement however this did not eventuate. The second pavement was designed to induce shear failure in a sub-standard basecourse layer. However, despite all efforts to construct a poorly compacted layer, the pavement performed better than the first, well built pavement. Various hypotheses as to why the second pavement performed so well were proposed and tested;

1. Although the basecourse was constructed to an average density of 93% of maximum dry density (NZS:4402 1986), which is significantly below the average construction standards of 98% (Transit NZ 1997), it was suggested that the basecourse may have quickly compacted within the wheel path soon after the wheel loads began to be applied. A comparison of nuclear density measurements prior to testing and after 200,000 laps showed that the pavement density within the test section decreased by 1%. This value was determined from nine measurements within the test section and considering the error typical of the nuclear density gauge it can be concluded that no densification occurred within the test section.
2. Although dynamic cone penetrometer results indicated a very similar subgrade in both pavements, the subgrade in the second pavement may have been weaker and this less stiff subgrade may have absorbed more of the load thus reducing the strain in the second pavement basecourse. A comparison of the strains at the top of the subgrade in both pavements showed that the vertical compressive strains had decreased from 2303με ion the first pavement to 1138με in the second test pavement. Thus, the basecourse in the second pavement was distributing the load more efficiently than the first pavement.

Therefore, the unexpected performance of the second pavement could only be attributed to the additional 70mm of basecourse depth. CAPTIF research has also concluded that the low moisture content in the second pavement had an unexpectedly large effect and that the basecourse moisture content appeared to contribute substantially more to the performance of granular layers than the compaction effort and in-situ density. Thus the effects of the

additional depth along with the low moisture content outweighed the effect of constructing a sub-standard pavement base.

7.5 First Pavement Task 2 Testing

The following section presents the results from the variable wheel load investigation and the load location investigation that was undertaken at 300,000 laps on the first pavement. Refer to Section 4.2.2 for details on the testing regime. The graphs in this section present only the longitudinal shear strain because it has been concluded in Section 7.4.1 that these strains are the most appropriate shear strain to use as a pavement response parameter.

7.5.1 Task 2A – Single Wheel with Varied Load Location

The principal strains measured when the 23kN single tyre (220mm tyre width) was located at different points over the centroid of the coil pairs are shown in Table 7.21. Based on these principal strains, the transverse and longitudinal shear strains were calculated (Table 7.22) and shown in Figure 7.20.

Table 7.21 Principal strains from single tyre at different locations over coils

			Wheel Location Over Coils			
	Station	Coil	Inner Edge	Inner Quarter	Center	Outer Edge
			Principal Strains (με)			
Strain of Interest	50	Vertical	726	781	764	688
		Transverse	-374	-368	-337	-309
		Longitudinal	-1015	-1067	-1106	-1096
	51	Vertical	462	505	495	405
		Transverse	-157	-165	-184	-177
		Longitudinal	-1188	-1297	-1295	-1244
	52	Vertical	495	517	531	449
		Transverse	-216	-212	-266	-228
		Longitudinal	-434	-451	-459	-495

Table 7.22 Calculated shear strains from single tyre at different locations over coils

Station	Strain	Wheel Location Over Coils			
		Inner Edge	Inner Quarter	Center	Outer Edge
		Shear Strains (με)			
50	Transverse	1100	1149	1101	997
	Longitudinal	1741	1848	1870	1784
51	Transverse	619	670	679	582
	Longitudinal	1650	1802	1790	1649
52	Transverse	711	729	797	677
	Longitudinal	929	968	990	944

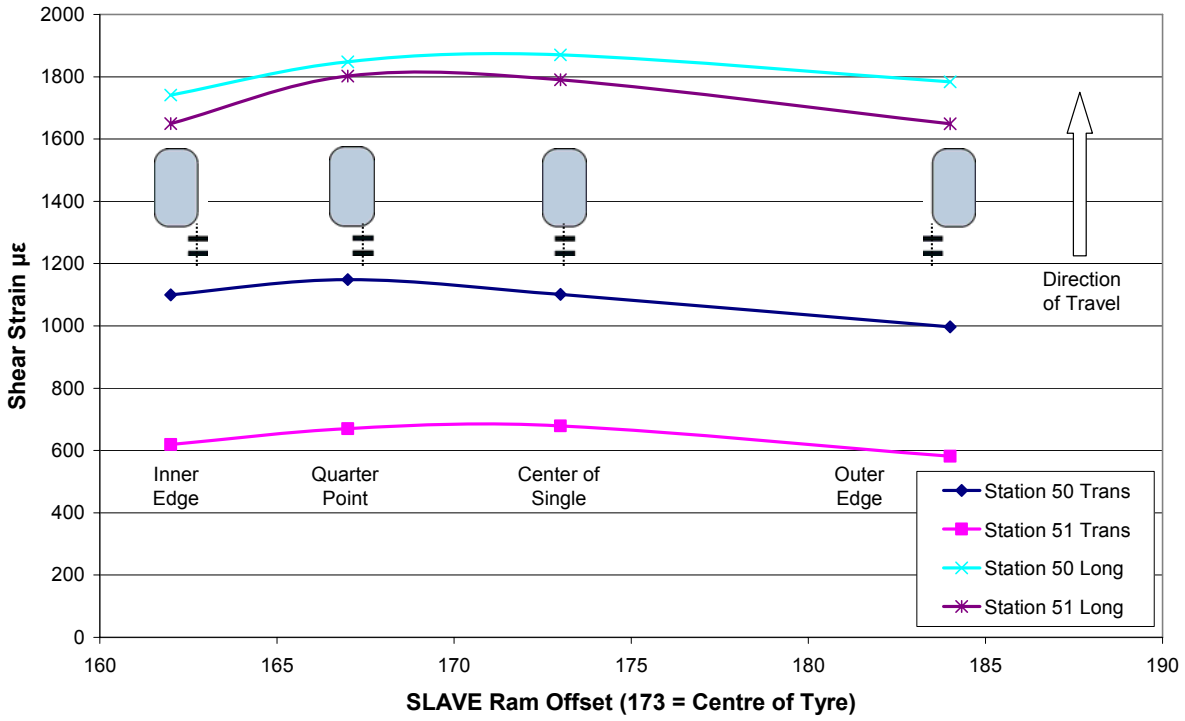

Figure 7.20 Transverse and Longitudinal Shear Strains versus Tyre Location of Coils

Figure 7.20 shows that over both test stations, the transverse and the longitudinal shear strains did not vary much as the single tyre is moved laterally further away from the centroid of the rosette. Generally, both the transverse and longitudinal shear strains decreased slightly as the tyre was moved to the left and right of the centre of the rosette. However, the magnitude change never exceeded 160με and in some cases (for example station 50) the magnitude of the shear strain remained the same at the edge of the tyre and it was at the centre. Therefore under a single 23kN wheel load, both the transverse and the longitudinal shear strains at a

point of interest remain approximately constant independent of how much tyre area covers the point of interest (assuming that at least the edge of a tyre is positioned over the centroid of the point of interest).

7.5.2 Task 2C – Dual Wheel Load with Varied Load Location

The principal strains measured when the 40kN dual wheel assembly was located at different points over the centroid of the coil pairs are shown in Table 7.23. Based on these principal strains, the transverse and longitudinal shear strains were calculated (Table 7.24) and shown in Figure 7.21.

Table 7.23 Principal strains from dual wheel at different locations over coils

		Wheel Location Over Coils					
Station	**Coil**	**360mm Away**	**240mm Away**	**120mm Away**	**Outside Edge**	**Inside Edge**	**Center of Assembly**
		Principal Strains (με)					
50	Vertical	101	129	323	629	809	787
	Transverse	-48	-51	-95	-289	-196	-178
	Longitudinal	-239	-384	-647	-987	-1724	-1716
51	Vertical	102	109	194	442	570	534
	Transverse	-34	-40	-37	-117	-92	-91
	Longitudinal	-240	-408	-725	-1194	-2119	-2119
52	Vertical	86	105	165	360	550	523
	Transverse	-27	-37	-94	-164	-179	-152
	Longitudinal	-151	-254	-385	-551	-737	-753

Table 7.24 Calculated shear strains from dual wheel at different locations over coils

		Wheel Location Over Coils					
Station	**Strain**	**360mm Away**	**240mm Away**	**120mm Away**	**Outside Edge**	**Inside Edge**	**Center of Assembly**
		Shear Strains (με)					
50	Transverse	149	180	418	918	1005	965
	Longitudinal	340	513	970	1616	2533	2503
51	Transverse	136	149	231	559	662	625
	Longitudinal	342	517	919	1636	2689	2653
52	Transverse	113	142	259	524	729	675
	Longitudinal	237	359	550	911	1287	1276

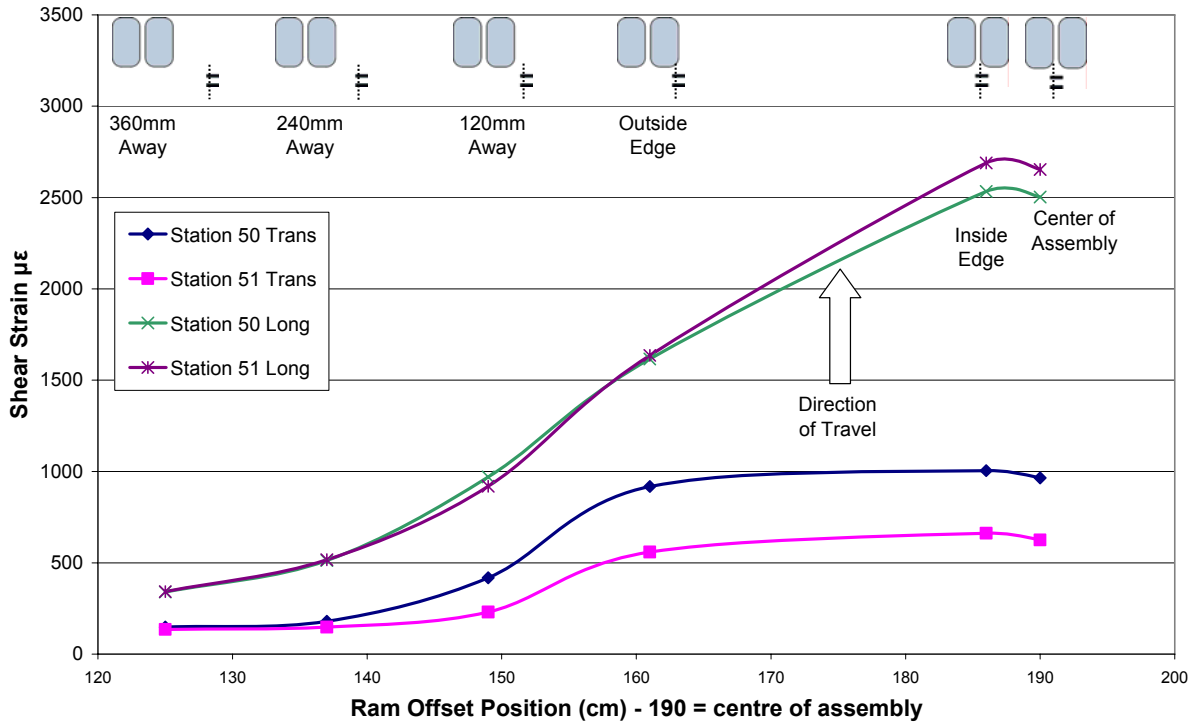

Figure 7.21 Transverse and longitudinal shear strains versus dual wheel location of coils (40kN Load)

Figure 7.21 shows that a dual wheel's location over a point of interest had a substantially greater impact on the magnitude of the shear strain at a point of interest than a single wheel load. The figure shows that once the dual wheel assembly had been moved to a positive where only the outside edge of one tyre was located over the centroid of the coils, the shear strain dropped by approximately 40% of the maximum value. The shear strains reached a negligible magnitude once the outside edge of the wheel assembly was 240mm away from the coil's centroid.

7.5.3 Task 2B – Dual Wheel with Varied Load

The principal strains measured with varying dual wheel loads centred directly over the centroid of the rosette are shown in Table 7.25 and the calculated longitudinal and transverse shear strains are shown in Table 7.26.

Table 7.25 Principal strains under varying dual wheel assembly loads

			Dual Wheel Load (kN)			
	Station	Coil	23	30	40	50
			Principal Strains (με)			
Strain of Interest	50	Vertical	686	787	791	855
		Transverse	-115	-182	-184	-286
		Longitudinal	-997	-1592	-1749	-1918
	51	Vertical	428	449	488	530
		Transverse	-56	-88	-66	-134
		Longitudinal	-1023	-1913	-2203	-2518
	52	Vertical	426	498	516	586
		Transverse	-56	-132	-132	-201
		Longitudinal	-341	-597	-733	-867

Table 7.26 Calculated shear strains under varying dual wheel loads

		Dual Wheel Load (kN)			
Station	Strain	23	30	40	50
		Shear Strains (με)			
50	Transverse	801	969	975	1141
	Longitudinal	1683	2379	2540	2773
51	Transverse	484	537	554	664
	Longitudinal	1451	2362	2691	3048
52	Transverse	482	630	648	787
	Longitudinal	767	1095	1249	1453

Figure 7.22, which shows the relationship between the longitudinal shear strain and load, indicates an approximately linear relationship exists, whereby an increase in dual wheel load causes an increase in shear strain. Stations 50 and 51 had linear correlation coefficients of 0.92 and 0.95 respectively indicating that the data had a reasonably good fit to a linear trend line. The 100με error bars shown for Station 50 indicate that a perfect linear relationship could fit within the error of emu system.

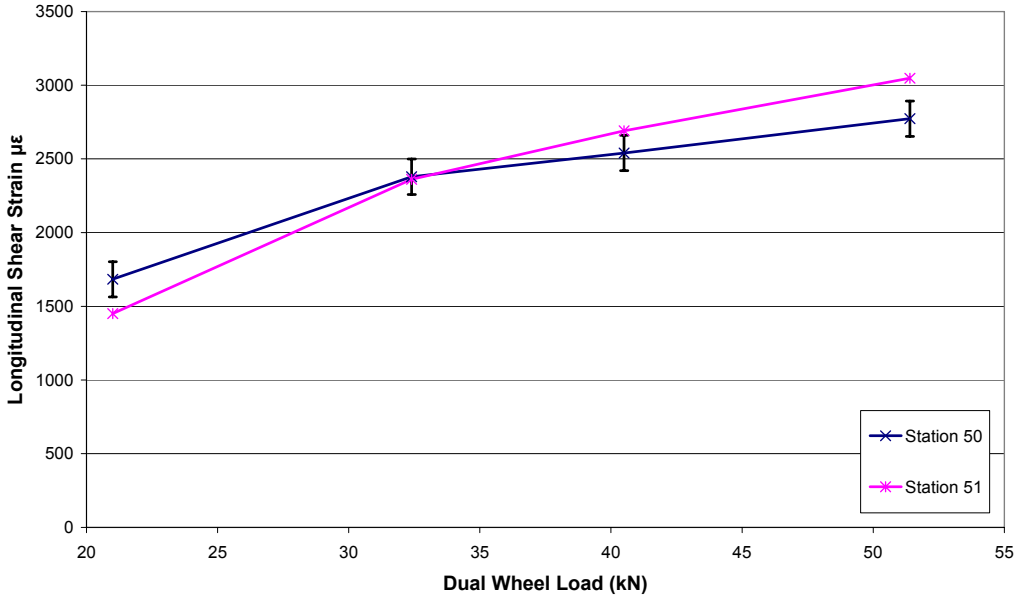

Figure 7.22 Longitudinal shear strains versus dual wheel assembly load

Again the variation in shear strain magnitudes between the two stations can be assumed to be due to variations in the pavement materials and the different particle to particle interlock forces due to construction. This can be proven once more by comparing the vertical compressive strains in Table 7.25 to the Prima FWD modulus at each station as previous mentioned in Section 7.3.1.

These results show that the system could be implemented in the field for the following objectives.

1. The coils could be used as a low cost and reasonably accurate alternative to a weigh bridge. So long as the strain magnitudes were calibrated with respect to some initially known axle loads, a linear relationship for shear strain versus half axle load could be developed. The coils could then be used to infer the shear strains from any dual wheel assembly and based on the linear relationship, the axle load could be determined. Likewise, additional relationships could be determined for tandem and tridem assemblies.
2. If a specific linear relationship is known for a particular pavement, the road user charges due to damage of the pavement from heavy vehicles could be determined based on the vehicle's consumption of the pavement. For example, heavy vehicles would be charged more on low strength low volume pavements and conversely charged less on high strength pavements.

7.6 Results Summary

The strain and rut measurements taken over the course of two test pavements that have been presented above lead to the following conclusions:

- The rosette system that was designed to measure in-situ shear strains worked well in both test pavements and all the coil pairs operated correctly throughout testing.
- The longitudinal shear strain is the more appropriate shear strain to use as a shear strain pavement response parameter.
- The longitudinal shear strain corresponded with measured rut depth better than the traditionally-used vertical compressive strain, thus verifying the importance of shear strains in granular layers.
- The initial magnitude of the shear strain related well to the initial rut development during the post construction compaction phase of the pavements' lives.
- The change in magnitude of shear strain from the end of the post construction compaction period until the conclusion of the test life corresponded well with the change in rut development during this same period.
- There was an almost linear relationship between shear strain and applied wheel load and therefore as long as a specific relationship is known for a pavement, axle loads of vehicles can be estimated based on measured basecourse shear strains. In addition to this, offset curves can be developed for specific pavements to estimate the applied load if a wheel assembly is not applied directly over the coil stack.

The next chapter will relate these results to the New Zealand transportation sector and discuss the various implications of utilising this strain measuring system within the field.

CHAPTER 8

DISCUSSION AND RECOMMENDATONS

The following chapter discusses the results presented in the previous chapter and shows how the emu strain measuring system can be applied in the field in order to utilise in-situ basecourse shear strain measurements to predict permanent deformation in unbound flexible pavements and to estimate pavement consumption by heavy vehicles. Additional observations that were made throughout testing are also discussed for the benefit of further research.

This section focuses on longitudinal shear strains because it was previously shown in Chapter 7 that the longitudinal shear strain is the maximum shear strain and also has a better correlation with rut development than the significantly smaller transverse shear strain.

8.1 Pavement Rut Progression Estimation Based on Shear Strain Measurements

The following section discusses how the emu coil strain measurement system and induction coils could be utilised in the field to estimate both the rut development during the post construction compaction period and the rut progression over the pavement life, based on longitudinal shear strain measurements.

8.1.1 Rut Depth Estimation at End of Post Construction Compaction Period

In the previous chapter it was shown that the magnitude of the longitudinal shear strain at the end of the post construction compaction period is proportional to the degree of rutting expected at the end of the same period. The shear strain magnitude at the end of the post construction compaction period was shown to have a linear relationship with the rut depth at the end of this period. The relationship had a linear coefficient of determination (R^2) of 0.999. The strains at the end of the post construction compaction period were used in this analysis because it was considered appropriate to use strain measurements that were taken at the same time as the rut depth measurements.

However, if the magnitude of the longitudinal shear strains in the field are to be used to estimate the rut depth at the end of the post construction compaction period, then shear strains measured soon after construction (as opposed to strains measured at the end of the post

construction compaction period) will need to be used. Figure 8.1 shows the relationship between initial shear strain magnitude (measured within the first 100 laps) and the rut depth measured at the end of the post construction compaction period. The three data points are from Pavement 1 prior to pre-conditioning failure (N<1000 laps), Pavement 1 after the structural overlay (N<100 Laps) and Pavement 2 (N<100 Laps). The plot shows that a strong linear relationship (R^2 = 0.999) still exists when the initial shear strain values are used instead of the strain values at the end of the post construction compaction period.

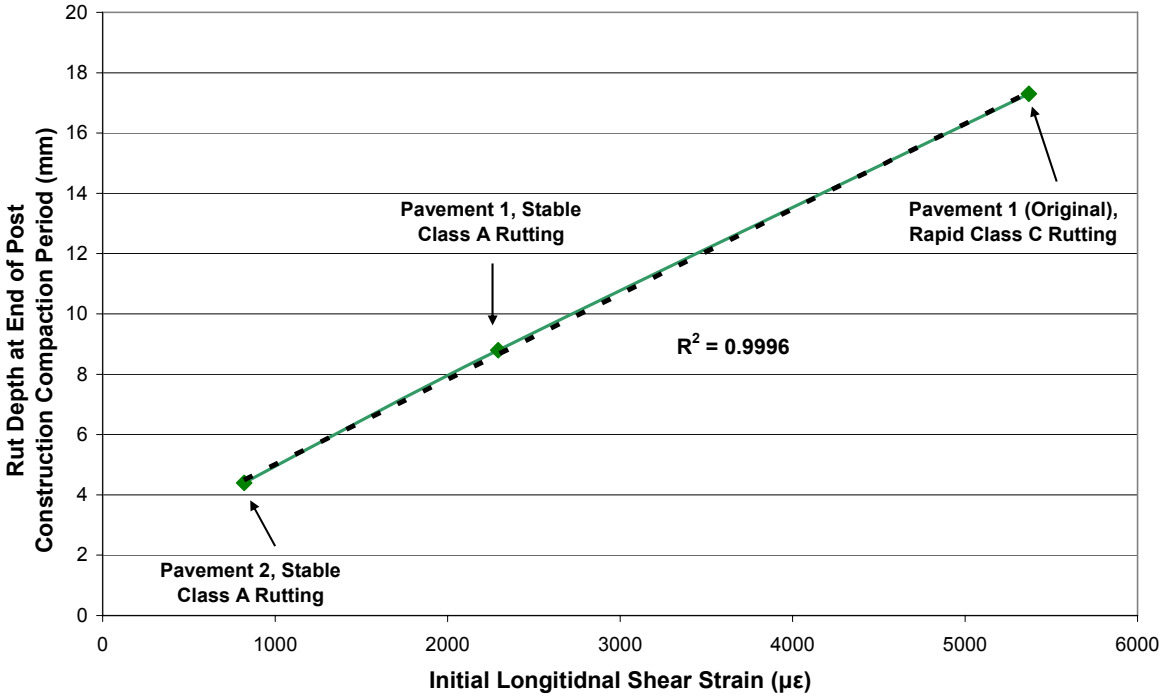

Figure 8.1 Initial longitudinal shear strain magnitude versus rut depth at end of post construction compaction period

The potential therefore exists for induction coils to be used to estimate the rut depth after the post construction compaction period using measured shear strains. This is a very beneficial tool because previously it has been very difficult to estimate this significant portion of the total rutting. Researchers such as Steven (2005) have focused their unbound flexible pavement rut depth modelling work on the development of permanent deformation after the post construction compaction period because of the "difficulty in determining the initial post construction compaction of a pavement" (Steven 2005). Due to the general behaviour of Class A and B rut development, the rut depth at the end of this period typically makes up a large proportion of the total rut depth expected throughout the pavement life (assuming major rut

failure does not occur). Coils could be installed either during the construction of a new pavement or after rehabilitation has occurred (for example a granular overlay). Field testing would also only require two coil pairs for each rosette, namely a vertical pair and a longitudinal pair, since it has been shown that the longitudinal shear strain is more sensitive than the transverse and thus a better pavement response indicator. The installation of two pairs instead of three would obviously save time through calibration, installation and testing. Shear strain measurements could then be taken using a vehicle with a 40kN dual wheel assembly (i.e. a standard axle) and the magnitude of the shear strain could be used to estimate the rut depth expected at the end of the post construction compaction period.

However, as mentioned in Section 7.4.3 the linear relationship uses the shear strain magnitude to estimate the rut depth at the end of the post construction compaction period but the length of this period cannot be determined. For example, given a longitudinal shear strain of 3000με the rut depth at the end of the post construction compaction period could be determined to be approximately 10.5mm using Figure 8.1 but the number of load applications required to cause this rut depth is unknown. Based on the two pavements tested and Stevens' previous observations it can be reasonably assumed that the majority of the rutting will occur within the first 50,000 to 100,000 laps however this may vary for different pavement designs.

This system could be implemented immediately in unbound flexible pavements constructed from similar basecourse aggregate (Canterbury Greywacke M/4 AP40). However, it is unclear how sensitive basecourse shear strains are to material type. Therefore further research would need to be conducted in order to investigate whether the initial strain to rut depth relationship presented above is applicable to other unbound pavements with different base materials or whether calibration coefficients are required to accommodate different material types. This research would involve full scale pavement tests either at an accelerated testing facility such as CAPTIF or on actual field pavements with test vehicles with standard axle loads (8.2 tonne). If the material type proves to have a large influence on the magnitude of the basecourse shear strains, then a laboratory based test will be required to calculate a shift factor to adjust the shear strain to permanent deformation relationship for a specific material.

8.1.2 Rut Development from End of Post Construction Compaction Period Onwards

In addition to estimating the degree of rutting expected after the post construction compaction period, the induction coils and emu system could be used within the field to estimate rut development rates throughout the pavement life after the post construction compaction period has ended. It has been shown that there is a good relationship between the change in longitudinal shear strain magnitude and the change in rut depth. The system could therefore be used to periodically measure the shear strain magnitudes under a standard axle load and based on the rate of strain change, the rate of rut depth development can be estimated. The system could be used as an intervention estimation tool. This would involve determining the rate of strain change from in-situ coils (after the post construction compaction period) and consequently determining the estimated rate of rut depth change. Based on the known rut depth at the end of the post construction compaction period (which would be measured on site) the estimated rate of rut development could be used to calculate the approximate time period until the pavement reaches a condition where maintenance intervention would be required. The change in rut depth rate could be systemically re-calculated throughout the pavement life to re-evaluate the estimated failure time. This tool could be used independently or utilised with pavement deterioration models to improve maintenance schedules and the timing of rehabilitation work.

The research conducted at CAPTIF showed that there was an approximately 4:1 ratio between the percentage change in rut depth and the percentage change in shear strain. For example, a 21% increase in the magnitude of shear strains (Pavement 2) resulted in a 91% increase in the rut depth. However, again further research is required to determine the effects of material type and moisture content on this relationship.

8.1.3 Non-Destructive Layer Analysis after Failure

The system could also be used to non-destructively estimate in which pavement layers failure is occurring. For example, if a thin surfaced unbound flexible pavement is experiencing a consistent increase in rut depth after the post construction compaction period yet the change in basecourse shear strain is negligible, this would indicate that low subgrade strength may be the main contributor to failure. The same premise can be used with the strain magnitude relationship. For example, if a pavement undergoes severe rutting soon after construction yet the magnitude of the basecourse shear strains is at a reasonable level (for example below

3500με as a conservative estimate based on Figure 8.1) this would again indicate accelerated subgrade failure.

8.2 Low Cost Weigh Bridge and Pavement Consumption Tool

Task 2 testing in the first pavement showed that a linear relationship existed between wheel load and shear strain. Based on this relationship, the induction coil and emu system could be used in the field to function as a low cost alternative to a weigh bridge. The following describes the steps required for such a system to be implemented.

1. Rosettes would be installed in the basecourse of a new or existing pavement. The transverse pair is not a necessity as mentioned previously.
2. Site specific load to shear strain relationships must be developed for each axle type expected. For example, a minimum of four different weight dual wheel axles would be required to determine the dual wheel load to shear strain relationship. This relationship would be constructed by applying a series of different known vehicle loads over the coils and calculating the maximum strain magnitude from the voltage traces for each load. This would require the loads to be applied directly over the coils to ensure that the maximum shear strain is measured. A relationship would need to be created for both single and dual wheel assemblies.

Task 2 testing also showed that there is a significant reduction in longitudinal shear strain magnitude as the dual wheel assembly shifts laterally over the centroid of the coil stack. This reduction is not so critical for single wheels. Based on Figure 7.21 it was concluded that 50mm of lateral dual wheel travel either side of a rosette centroid is the maximum allowable variation where one rosette can be used to calculate the maximum shear strain with a reasonable degree of accuracy. This becomes a problem in field testing because the centre line of a vehicle's wheel assembly will not follow an exact predetermined path. In order to solve this problem, multiple rosettes must be installed adjacent to each other and all coils must be operating simultaneously. Using this method, the maximum shear strain can be determined by using the largest measured voltage from a set of multiple rosettes. Using the 50mm of allowable variation either side of the coil centroid, rosettes should be installed with a maximum horizontal separation distance of 100mm between the centroids of the rosettes.

Since it has been shown that the magnitude of longitudinal shear strain within the basecourse is related to the degree of rutting expected within the pavement, this system also has the potential to be used as a road consumption assessment tool. A road controlling authority (RCA) or interested party could measure the pavement strains induced by different vehicles and determine road user charges based upon the vehicles consumption of the road asset as opposed to purely weight and tyre configurations. This application would obviously involve substantial development, but the idea is presented for consideration as further road reform is considered in New Zealand.

8.3 General Observations

The following section presents some of the general observations that were made during the investigation that were unknown prior to testing. The purpose of this section is to outline some of the more important phenomena that affected the results of the investigation and also to present the information for consideration in future research.

1. In both pavements, the magnitude of the longitudinal tensile strain was significantly larger than expected by pavement engineers or predicted by modelling software. The measured longitudinal tensile strains were between two and four times the magnitude of the strains predicted by both finite element models and linear elastic models. Discussions with New Zealand pavement industry researchers and pavement designers confirmed that longitudinal tensile strains exceeding the magnitude of vertical compressive strains were not expected. It is clear that when the longitudinal tensile strains reach these magnitudes they become the dominant factor in the magnitude of the shear strain. The research identified the dominance of the longitudinal strain within unbound layers and the two major outcomes of this observation are:
    a. The consideration of shear strain as pavement performance parameter as opposed to the traditional vertical compressive strain.
    b. The further development and implementation of stabilised granular layers in order to increase tensile strength and consequently reduce shear strain within the basecourse.

    It has been assumed that the dominance of the longitudinal tensile strain compared with both the vertical compressive and the transverse tensile is due to the anisotropic nature of

granular layers. Several researches have reported that anisotropy in granular pavements is caused not only by the stress distributions during loading but also by construction. Kim et al. (2005) and Masad et el. (2006) state that during deposition granular materials tend to align themselves with the maximum dimension in the horizontal longitudinal direction. In addition to this, compaction equipment generally orientates the aggregate in the longitudinal direction and rarely travels in the transverse direction. The particles are thus further orientated towards the direction of travel. It has therefore been concluded that the longitudinal orientation of the material particles caused by gravity during deposition and construction techniques may have contributed to the dominant magnitude of the longitudinal tensile strains. Further research could be conducted in this area to determine whether deposition and compaction of the aggregate in the transverse direction reduces the magnitude of the longitudinal strain and increases the size of the transverse tensile strains.

2. The AC patch over station 52 in the first pavement showed the large impact that a thin dense mix AC layer (in addition to the surface layer) can have on the longitudinal tensile strain and consequently the longitudinal shear strain. The AC patch caused a 40% reduction in the magnitude of the longitudinal shear strain but had minimal effect on the vertical and transverse principal strains. Therefore, in addition to basecourse stabilisation, a thicker AC surface course could be used to minimise longitudinal tensile strains and the consequent shear strain.

3. The initial preconditioning period in the first pavement showed that Class C rapid failure can occur very quickly (8000 laps), however the Class B failure that was a desired outcome in both pavements did not occur. It is unknown whether either of the two test pavements would have undergone Class B failure if the test was allowed to continue for an additional one or two million laps. However, commercial time restrictions limited the test lengths and therefore further research could be undertaken to monitor the shear strain changes and rut development over a significantly longer loading period. This may give further insight into the relationship between shear strains and rut progression during a failure period.

4. The one month non-loading period due to the construction works from Station 1 to Station 26 had a noticeable effect on the rut accumulation profiles for the whole track and the

measured strains at the stations relevant to this investigation. The reasonably small but rapid increase in rut depth after loading resumed has also occurred in other accelerated test pavements at CAPTIF. However, significant research has not been conducted to explain this situation. Basic steps were taken within this project to try to explain the changes such as comparing the dynamic loading traces before and after construction to see whether the loads were being applied differently after a new AC surface was applied. However, no explanation could be developed. In addition to this, the small reduction in principal strains (and consequently shear strains) after loading resumed could not be explained. Although it was assumed that this was an electrical shift (since other CAPTIF coils within very close proximity did not change), coil testing such as comparing the standard pair static voltages and the in-situ static voltages before and after the break did not reveal a reason for the change. The effects of large loading breaks on pavement response and performance could be further investigated.

5. Minor changes in basecourse moisture content (0.5%) have a greater effect on the performance of a pavement than basecourse depth or density. The 0.5% reduction in moisture content in the second pavement resulted in elastic strains and plastic strains approximately half that of the first pavement even though it was compacted to a significantly lesser degree.

CHAPTER 9

CONCLUSIONS

9.1 Conclusions

A laboratory investigation was conducted to determine a feasible method of measuring in-situ basecourse shear strains. Based on this investigation a rosette configuration consisting of three sets of co-axial pairs measuring principal strains was decided to be the most appropriate method of measuring shear strains in granular layers. The assumption that the measured strains are approximately equal to the principal strains at the instant that the tyre was over them was verified using finite element modelling, and the accuracy and repeatability of the system was confirmed with multiple test sections measuring similar strain magnitudes in all cases.

Shear strain results were measured for an unbound flexible pavement that failed quickly due to basecourse shear. It was observed that shear strains with magnitudes of approximately 5000με resulted in failure due to permanent deformation within 8,000 ESA laps (where one laps equals two load applications).

Two unbound flexible test pavements were tested to 500,000 laps and 300,000 laps respectively. Shear strains and rut depths were measured at three consecutive test stations at various intervals throughout the test lives. The following conclusions are drawn based on the Task 1 life cycle testing:

- In both pavements, the longitudinal shear strains were significantly larger and more sensitive to load than the transverse shear strains and therefore the longitudinal strain (which is also the maximum shear strain using a Tresca criterion) was determined to be the most appropriate shear strain to be used in further analysis.
- In both pavements, the longitudinal shear strain correlated well to the measured rut depth better than the traditionally used vertical compressive strain thus reinforcing the possibility that shear strain may be directly related to basecourse rutting.
- The test pavements showed that the initial magnitude of the shear strains during the first 100 laps of loading correlated well to the depth of rutting expected at the end of the post construction compaction period. Based on this observation it has been suggested that if

further research confirms this conclusion, rosettes could be used to estimate rut depth after the post construction compaction period in new or rehabilitated pavements. This rut depth often makes up a large majority of the total rutting expected until intervention levels are reached and therefore this could be a very beneficial tool for pavement management purposes.

- It was also shown in both pavement tests that there is a good relationship between the change in magnitude of shear strain from the end of the post construction compaction phase until the conclusion of the test life and the change in rut development during this same period. Similarly, if this relationship is further proved with future testing, it could be used to estimate rut depth development over time after the post construction compaction period. This could consequently be used to predict the amount of time until intervention levels are reached and thus utilised within maintenance schedule planning.
- The magnitudes of the measured basecourse shear strains can be used as a method of non-destructive layer analysis after failure. Large strains would indicate a high likelihood of basecourse failure whilst small shear strains (below 3500με) would indicate that subgrade deformation is more likely.

Task 2 testing on the first pavement showed that there was a close linear relationship between the vehicle load and the induced shear strain. In addition to this, wheel offset testing showed that 50mm is the maximum amount of lateral wheel movement that would result in similar shear strain measurements at one point. Based on these tests it has been concluded that a series of adjacent rosettes with 100mm lateral separation spacing could be used to measure vehicle axle loads based on the maximum shear strain measured. Alternatively the system could be utilised to charge a vehicle based on its consumption of the pavement asset (using shear strain) as opposed to its gross weight.

All three of the objectives outlined at the beginning of the investigation were achieved and the only unsuccessful aspect of the investigation was the inability to induce failure in the second pavement despite constructing a substantially substandard basecourse layer.

9.2 Further Research

This investigation has highlighted a number of areas where further research could be conducted. These areas include:

1. The magnitude of the longitudinal strains measured is significantly larger than that expected by New Zealand pavement experts, and by both finite element and linear elastic models. Within the modelling side of pavement analysis, further work could be undertaken to more accurately predict these large strains and the consequent effect of large tensile strains in an unbound material with minimal tensile strength. This would involve determining factors to model the anisotropic nature of granular materials.
2. Shear strains could be incorporated as an additional parameter into already proposed permanent deformation models such as those presented by Steven (2005). Using vertical compressive strain as a parameter should not be rejected totally, but rather investigation into the benefits of including shear strain as an additional parameter could be considered.
3. Investigating the relationship between shear strain and rut development during a steady Class B failure in a weak pavement. This would involve constructing a pavement where the compaction density is lower than normal construction standards and more importantly, the moisture content is greater than normal standards.
4. The relationship between shear strain magnitude and rut depth at the end of the post construction compaction period needs to be investigated for different material types. If significant differences occur, a laboratory based test is needed to characterise materials in order that shift factors can be developed to change the strain to rut depth relationship for different materials.
5. The relationship between the change in shear strain and the change in rut depth after the post construction compaction period should also be further investigated for different unbound materials. Similar to point 2 above, a laboratory test may be needed to shift a well established relationship for different materials.
6. It has previously been suggested that the dominant size of the longitudinal tensile strain compared to the vertical compressive and transverse tensile strain could be caused by the increased anisotropy of the material during construction. Research could be conducted either in an accelerated testing facility or in the field to investigate the impact of compaction direction on the in-situ strain magnitude. For example, a test section where the aggregate is compacted in the transverse direction (as opposed to the direction of travel) could be compared to a control section to determine whether compaction equipment has an effect on the in-situ strains.

7. The effect of large breaks in loading on both pavements' structural response and performance could be investigated, and the concept and mechanism of pavement relaxation and the subsequent rapid rutting after loading resumes could be studied.

REFERENCES

AASHTO. (2004). "Guide for Mechanistic-Empirical Design of New and Rehabilitated Pavement Structure." N.C.H.R.P., ed., AASHTO.

Alabaster, D. (2006). "Peer Communication, Rut Progression in CAPTIF Pavements."

Alabaster, D., Steven, B., and Fussell, A. (2006). "Fatigue Design Criteria for Low Noise Surfacings." *Land Transport New Zealand Research Report*, Pending Review.

AUSTROADS. (2004). "Pavement Design - A Guide to the Structural Design of Road Pavements." Pavement Technology Series, ARRB, ed., AUSTROADS.

Chen, W., and Saleed, A. (1994). *Constitutive Equations for Engineering Materials*, Elsevier.

Das, M. B. (2002). *Principles of Geotechnical Engineering*, Brooks/Cole.

Dawson, A. R. (1997). "Rutting in unsurfaced roads - materials and structure interaction effects." *International symposium on Thin Pavements, Surface Treatments and Unbound Roads*, 101 - 108.

Dawson, A. R. "ENTR 602 Unsealed Roads (2002)." *University of Canterbury Department of Transportation Course Notes*.

Douglas, R. A. (1997). "Unbound roads trafficked by heavily loaded tyres with low inflation pressure." *Proceedings of the Institution of Civil Engineers, Transport*, 123(3), 163-173.

Gonzalez, A., Adnan, A., and Saleh, M. (2004). "Evaluating Non-Linear Elastic Models for Unbound Granular Materials in an Accelerated Testing Facility." *Transportation Research Record*, Abstract Accepted - Currently in Review.

Hayward, B. J. (2004). "The Accuracy and Feasibility of Using Free Floating Induction Coils to Measure Vertical Compressive Strains in Unbound Flexible Pavements," 3rd Professional Project, University of Canterbury, Christchurch.

Jameson, G. W. (2003). "Technical Basis of the 2003 Austroads Pavement Design Guide (Flexible Pavements)." *AP-T33/04 ARRB Transport Research*.

Janoo, V., Irwin, L., and Knuth, K. (2000). "Use of Inductive Coils to measure Dynamic and Permanent Pavement Strains." US Army Cold Regions Research, New Hampshire.

Masad, S., Little, D., and Eyad, M. (2006). "Analysis of Flexible Pavement Response and Performance Using Isotropic and Anisotropic Material Properties." *ASCE Journal of Transportation Engineering*, April 2006, 342-349.

NZS:4402. (1986). "Determination of the Dry Density/Water Content Relationship." Methods of Testing Soils for Civil Engineering Purposes - Test 4.1.1, New Zealand Standards, 1-5.

Parry, R. H. G. (1995). *Mohr Circles, Stress Paths and Geotechnics*, E & FN Spon.

Paterson, W. D. O. (1972). "The Measurement of Pavement Deformations Using Induction Coils." *New Zealand Road Research Unit*(RRU Bulletin 13), 1-30.

Pidwerbesky, B. D. (1996). "Fundamental behaviour of unbound granular pavements subjected to various loading conditions and accelerated trafficking : PhD Thesis," PhD, University of Canterbury, Christchurch.

Pidwerbesky, B. D. (2005). "Peer Communication, New Zealand Basecourse Failures."

Steven, B. D. (2005). "The Development and Verification of a Pavement Response and Performance Model for Unbound Granular Pavements: PhD Thesis," University of Canterbury.

Theyse, H. (2004). "Empirical Shear Strength Models for Unbound Road-Building Materials." *6th International Symposium on Pavements Unbound (UNBAR 6)*, 6, 199-208.

Theyse, H., de Beer H, and F, R. "Overview of the South African Mechanistic Pavement Design Analysis Method." *75th Annual Transportation Research Board Meeting*, Washington D.C.

Timoshenko, S. (1953). *History of Strength of Materials*, McGraw-Hill.

Transit NZ. (1996). "State Highway Asset Management Manual." Wellington.

Transit NZ. (1997). "TNZ B/2: Specification for Construction of Unbound Granular Pavement Layers." Wellington.

Transit NZ. (2000). "New Zealand Supplement to Austroads Pavement Design Guide." A Guide to the Structural Design of Road Pavements, TNZ, Wellington.

Transit NZ. (2004). "TNZ M6: Specification for Sealing Chip." Wellington.

Transit NZ. (2005). "TNZ M/4 Specification for Basecourse Aggregate." Wellington.

Vuong, B. T. (2004). "Incorporation of laboratory performance tests into performance-based specifications for unbound granular materials." *Road and Transport Research (ARRB)*, 13(13), 3-23.

APPENDIX A
VOLTAGE TRACES FROM FIRST AND SECOND PAVEMENTS

This Appendix shows voltage traces from station 50 and 38 in test pavement 1 and 2 respectively. For each test pavement, vertical, transverse and longitudinal traces are shown for the first strain measurements at 0 laps and for the final strain measurements at 500,000 and 300,000 laps respectively.

A.1 First Pavement Voltage Traces

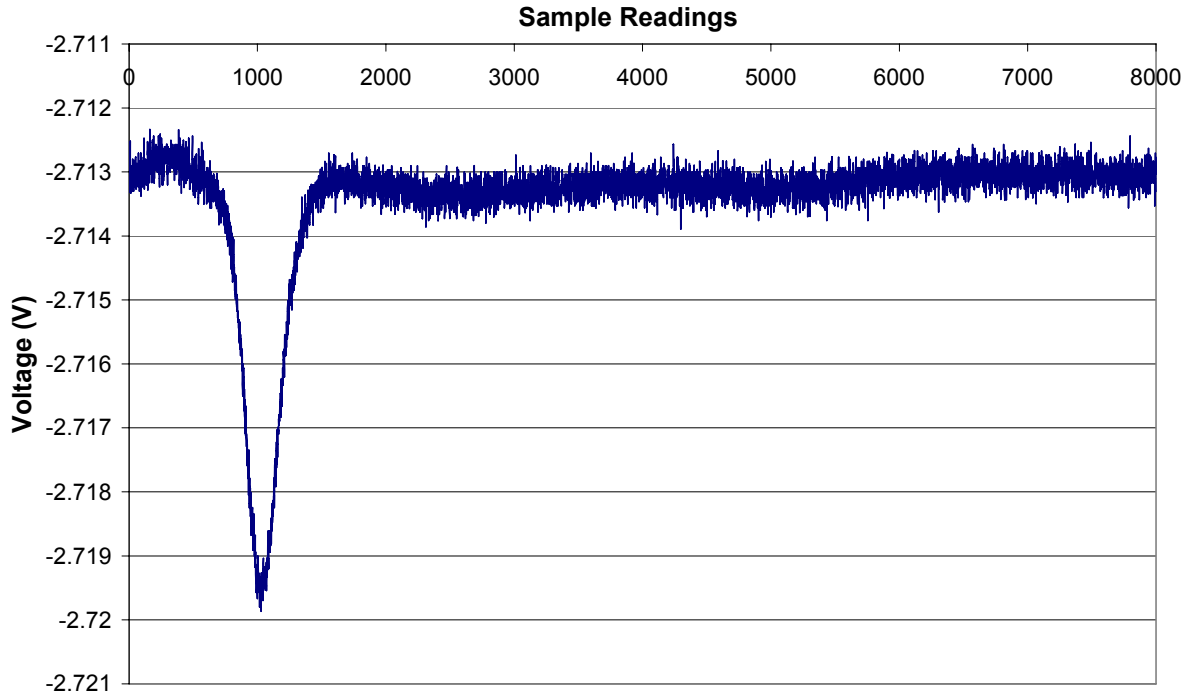

Figure A. 1 Pavement 1 vertical voltage trace 0 laps

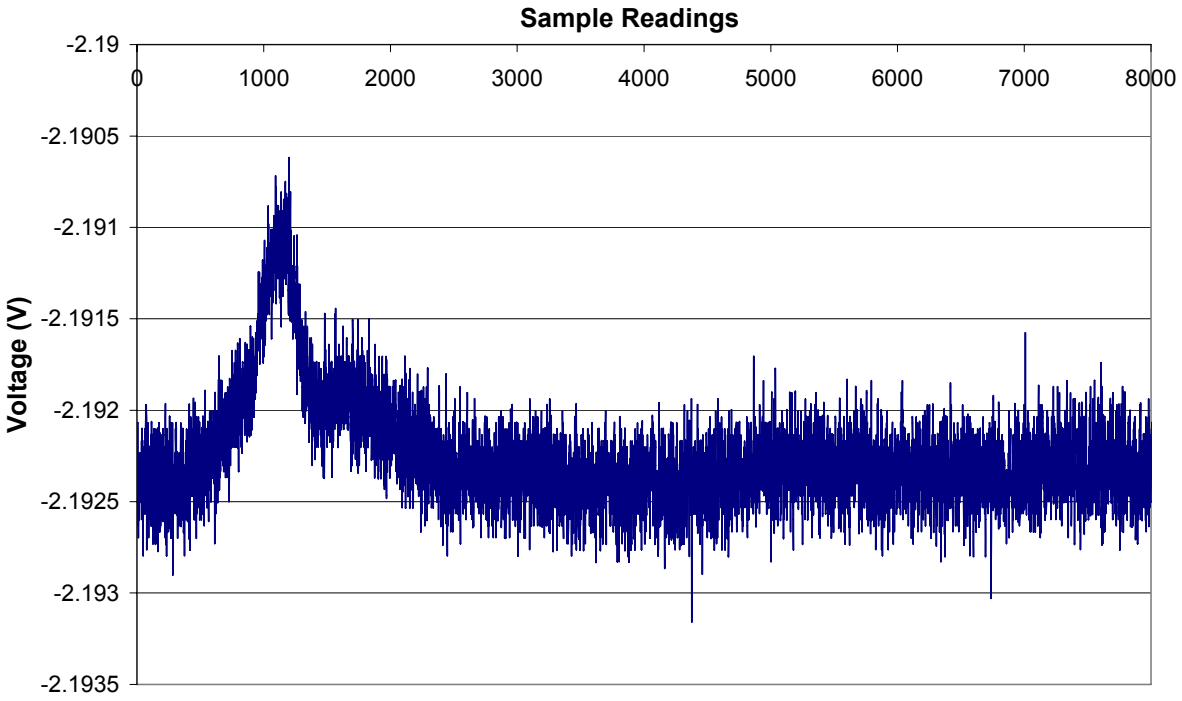

Figure A. 2 Pavement 1 transverse voltage trace 0 laps

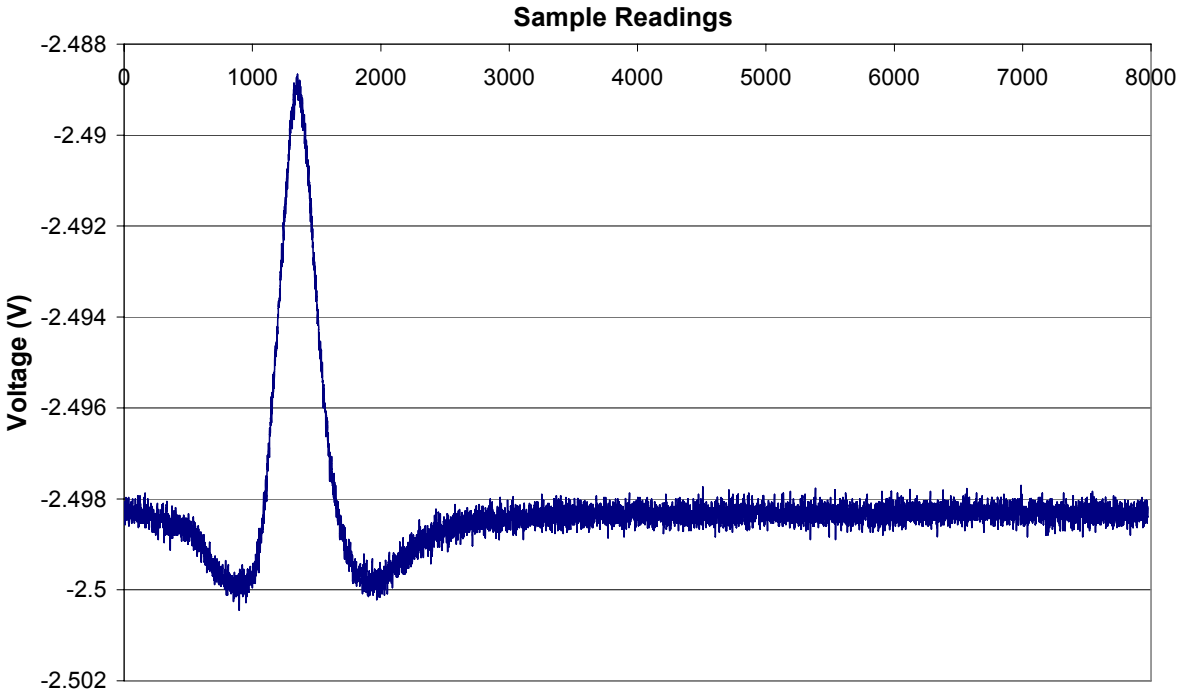

Figure A. 3 Pavement 1 longitudinal voltage trace 0 laps

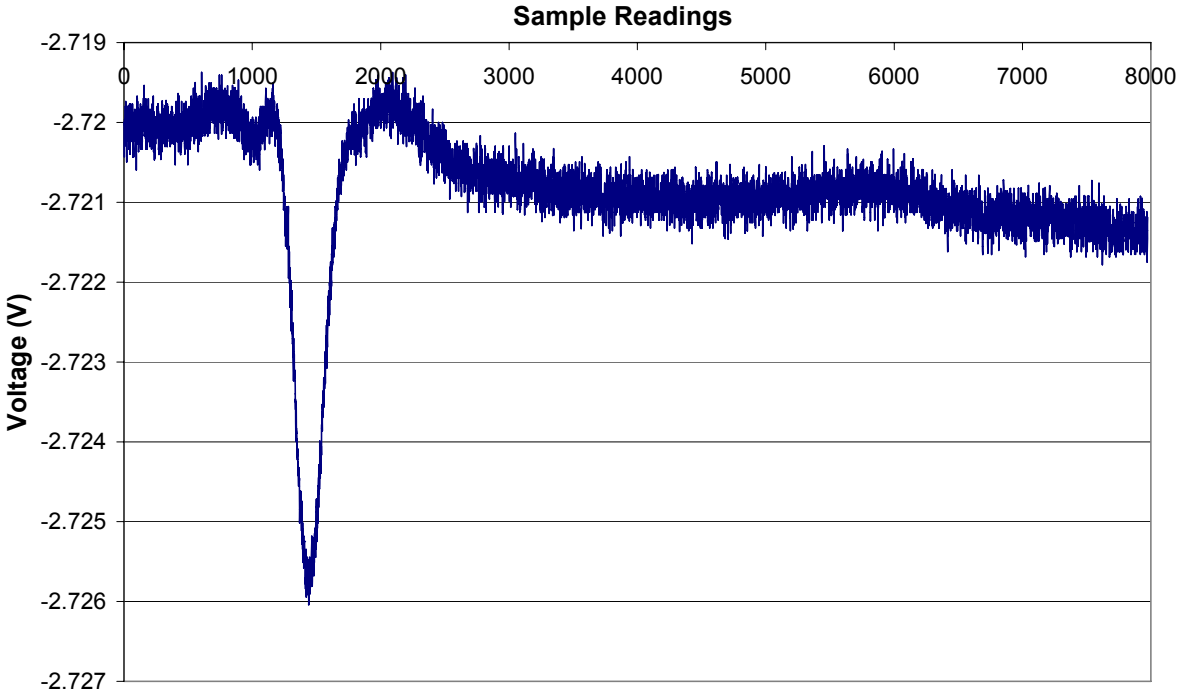

Figure A. 4 Pavement 1 vertical voltage trace 500,000 laps

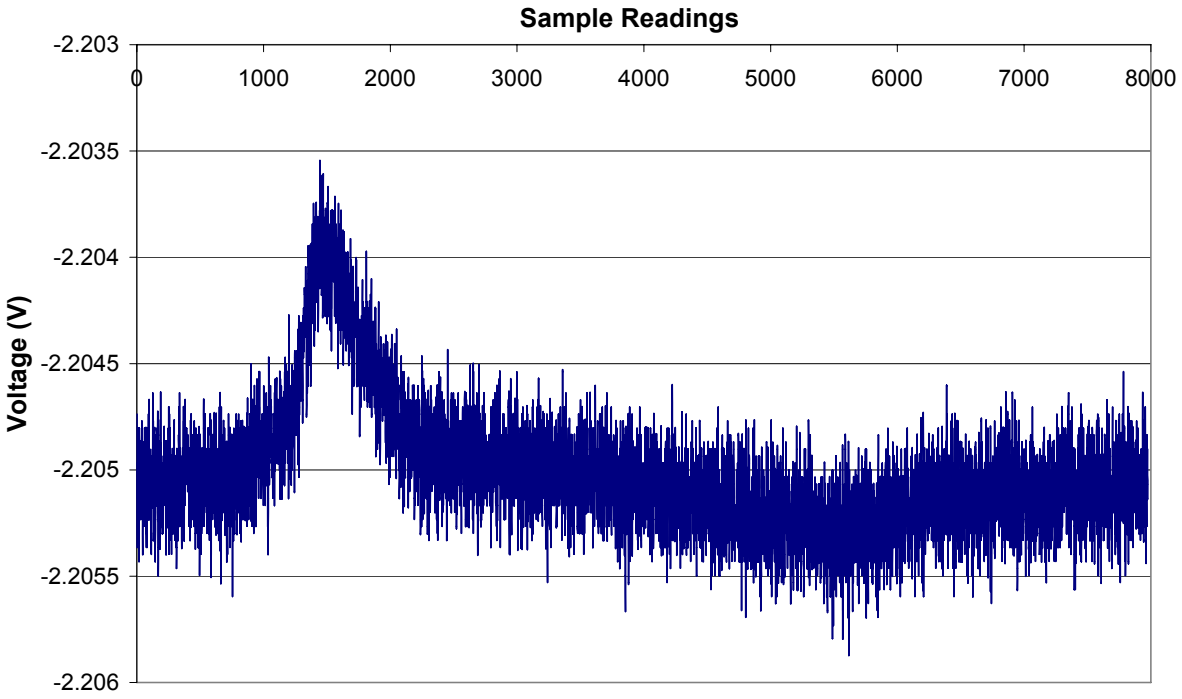

Figure A. 5 Pavement 1 transverse voltage trace 500,000 laps

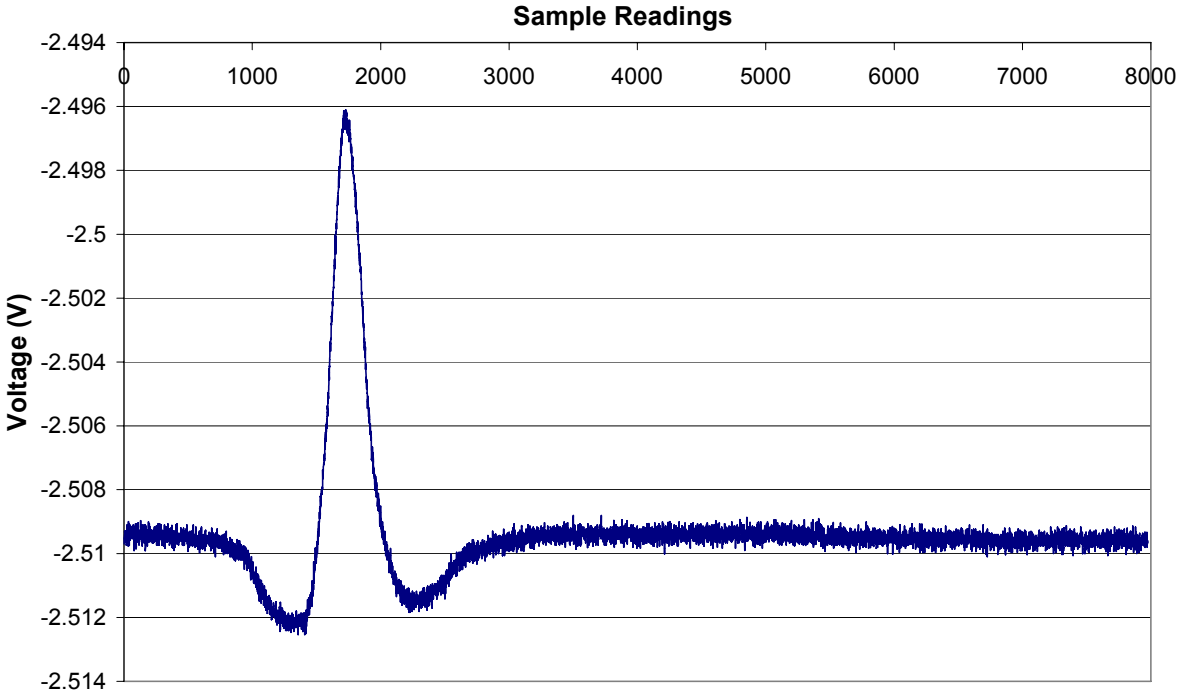

Figure A. 6 Pavement 1 longitudinal voltage trace 500,000 laps

A.2 Second Pavement Voltage Traces

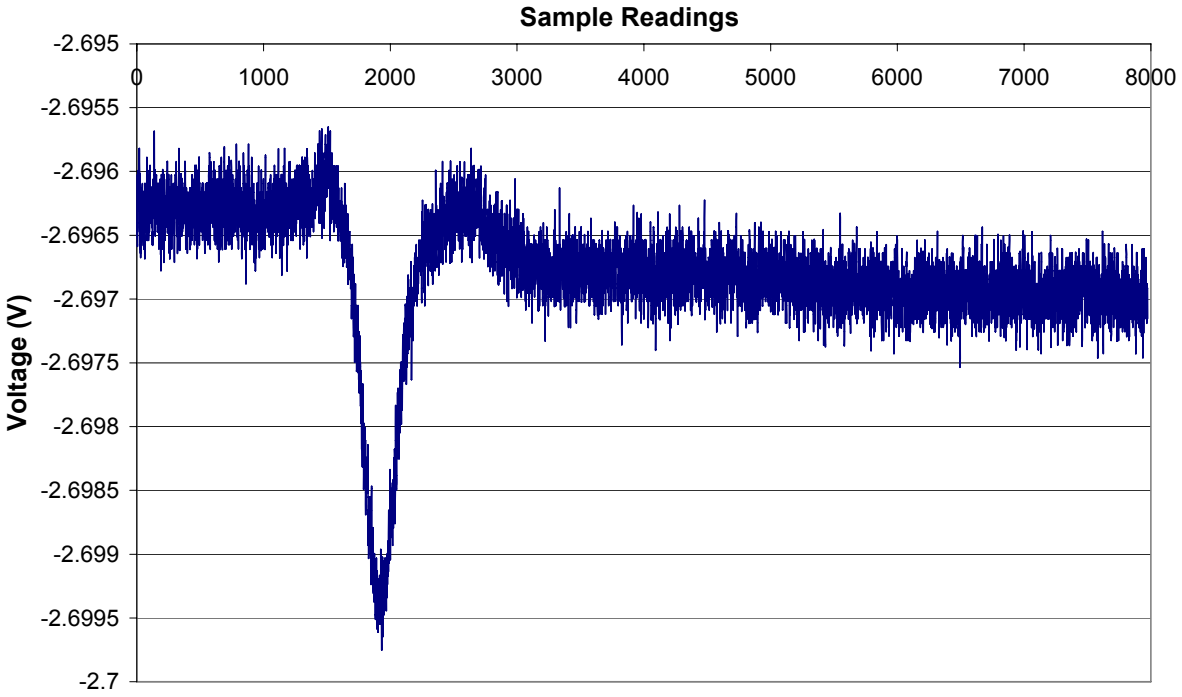

Figure A. 7 Pavement 2 vertical voltage trace 0 laps

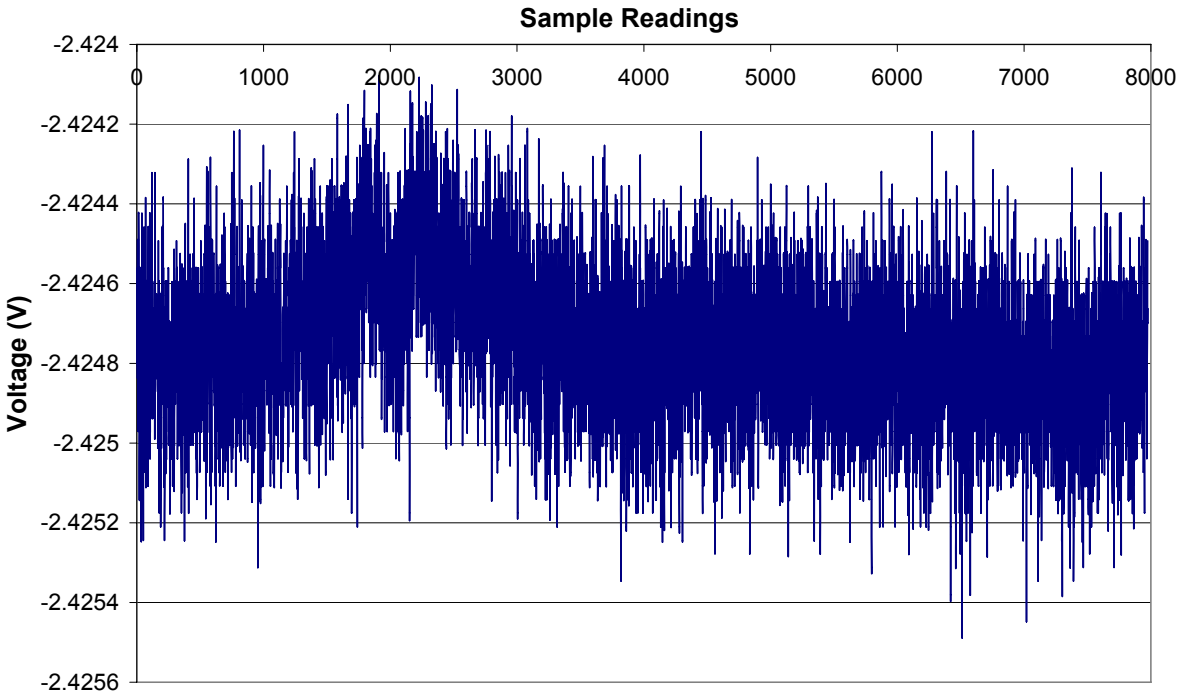

Figure A. 8 Pavement 2 transverse voltage trace 0 laps

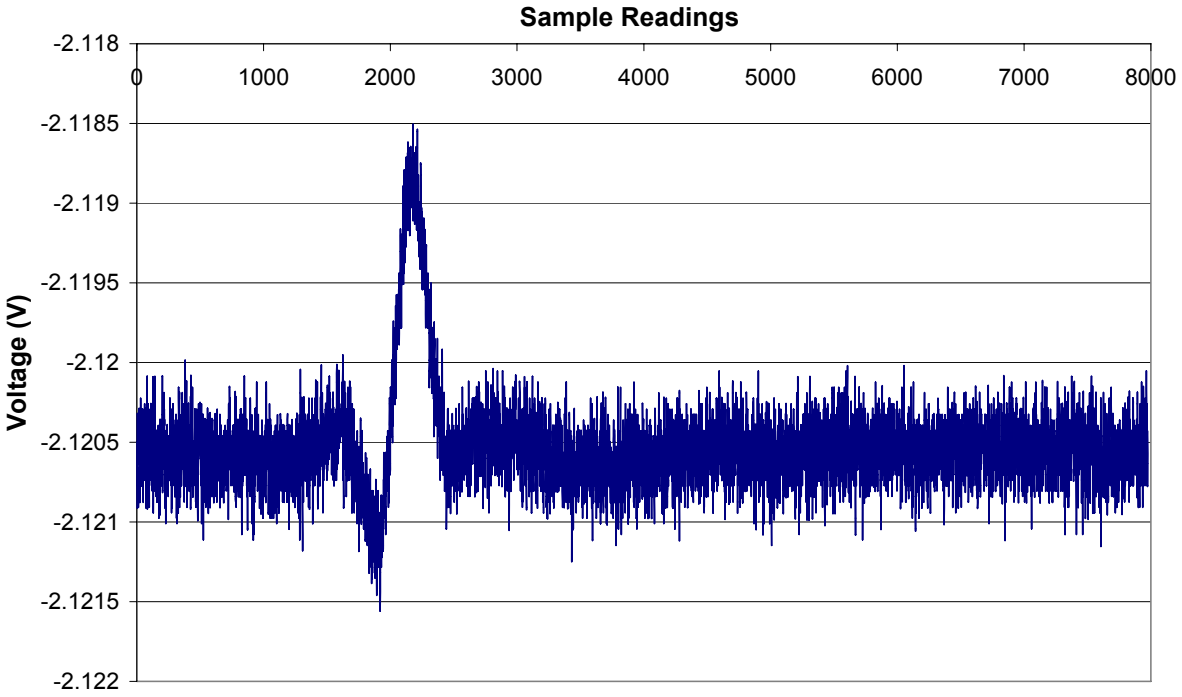

Figure A. 9 Pavement 2 longitudinal voltage trace 0 laps

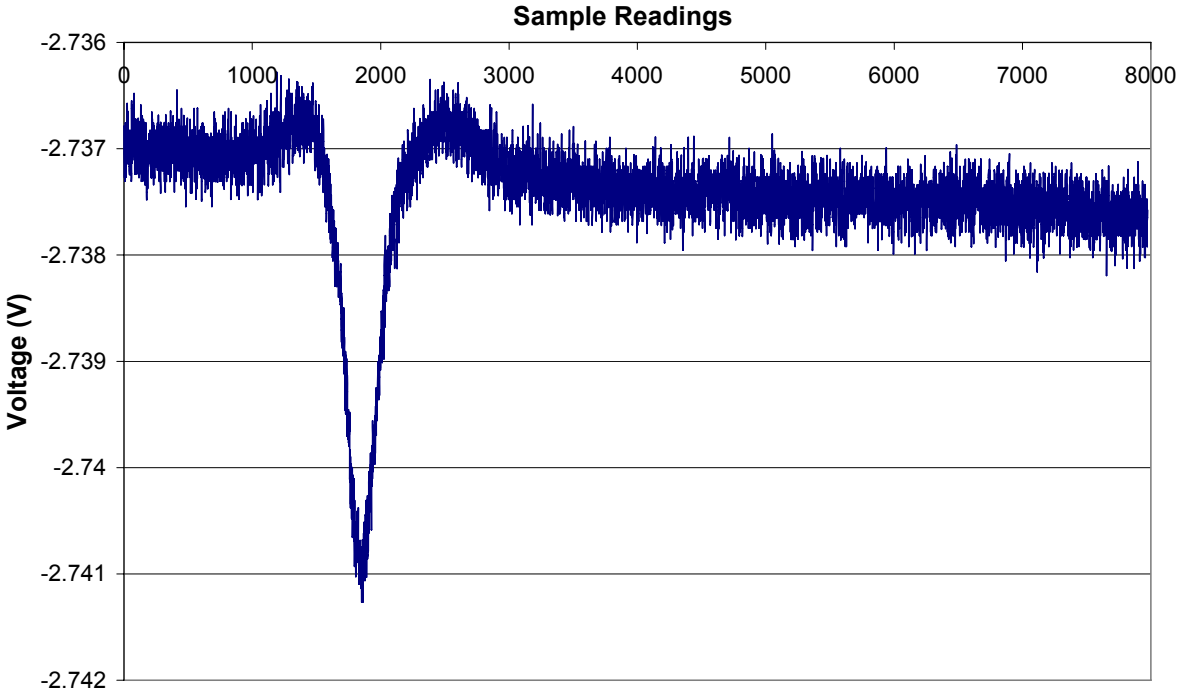

Figure A. 10 Pavement 2 vertical voltage trace 300,000 laps

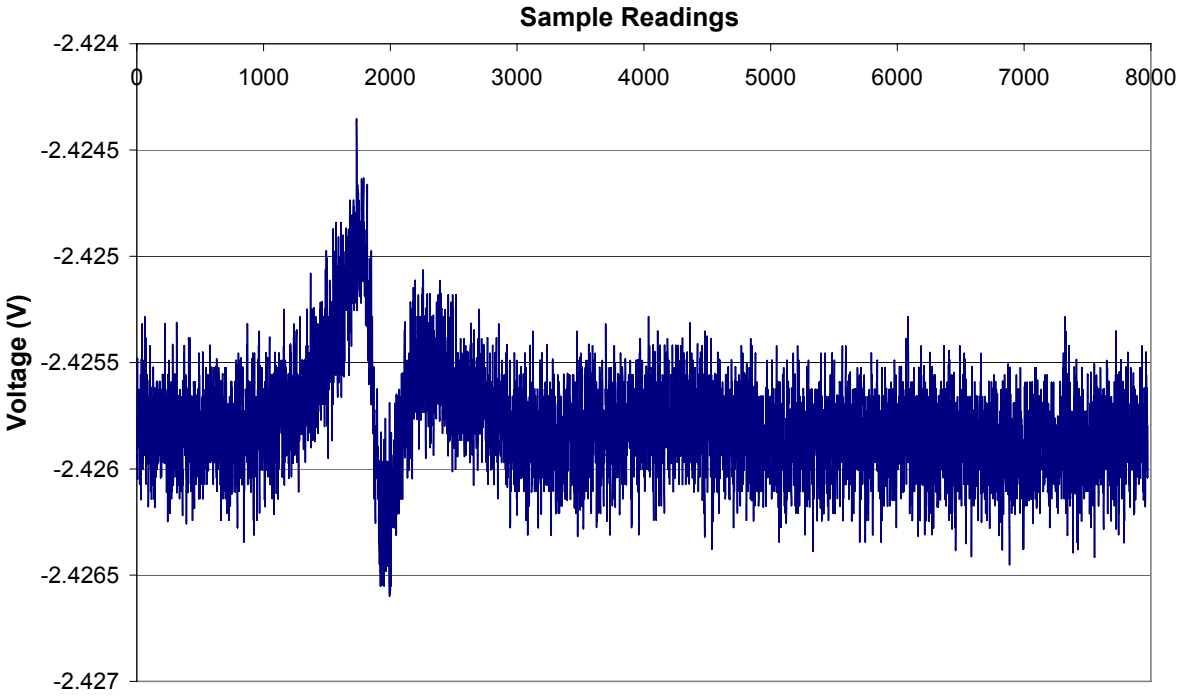

Figure A. 11 Pavement 2 transverse voltage trace 300,000 laps

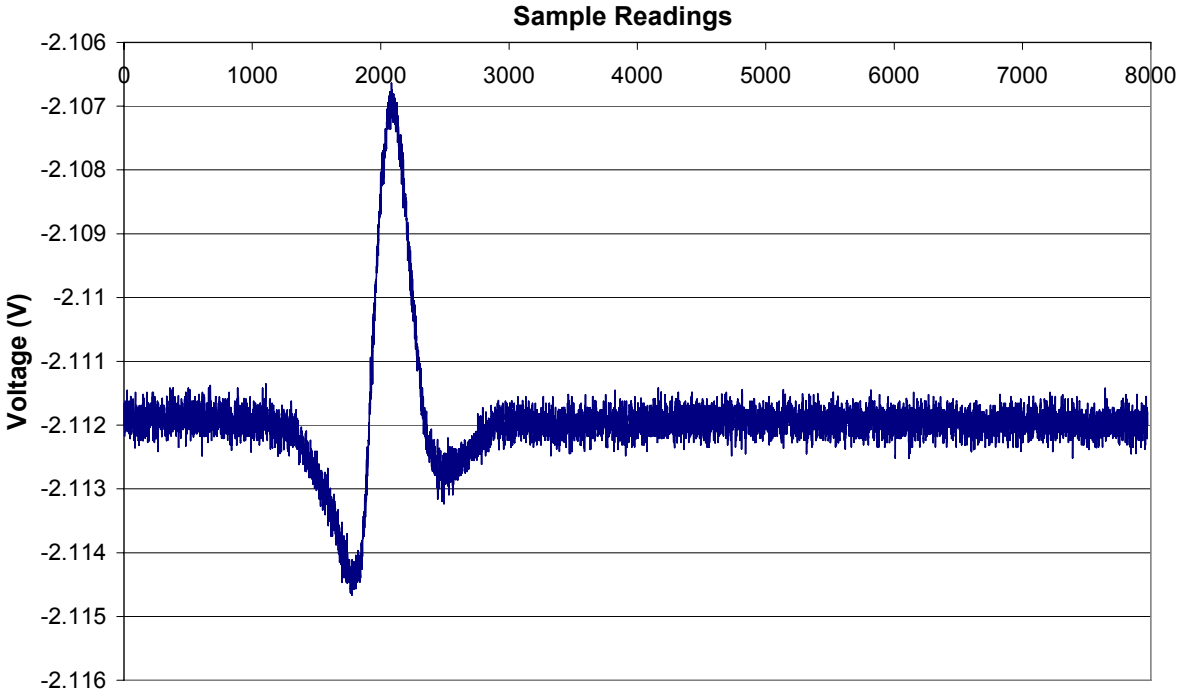

Figure A. 12 Pavement 2 longitudinal voltage trance 300,000 laps

APPENDIX B
TRANSVERSE RUT PROFILES OVER LOADING LAPS

This appendix shows the full transverse rut profiles measured at each station at the beginning and conclusion of Task 1 testing for the first and second pavements. The x axis scale has units based on the profilometer reading number between 1 and 140. Profilometer number 77 coincides with the centre of the dual wheel assembly. The y axis has units of mm based on the LVDT displacement.

B.1 First Pavement Transverse Rut Profile Development

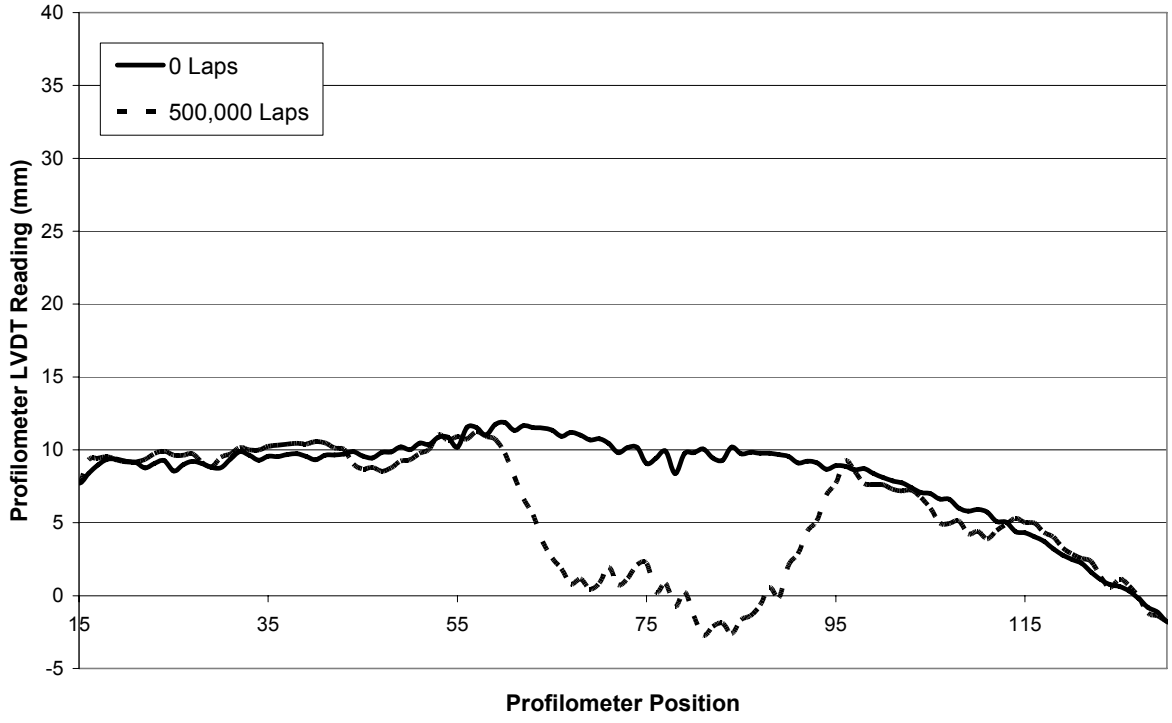

Figure B. 1 Station 50 transverse rut profile development

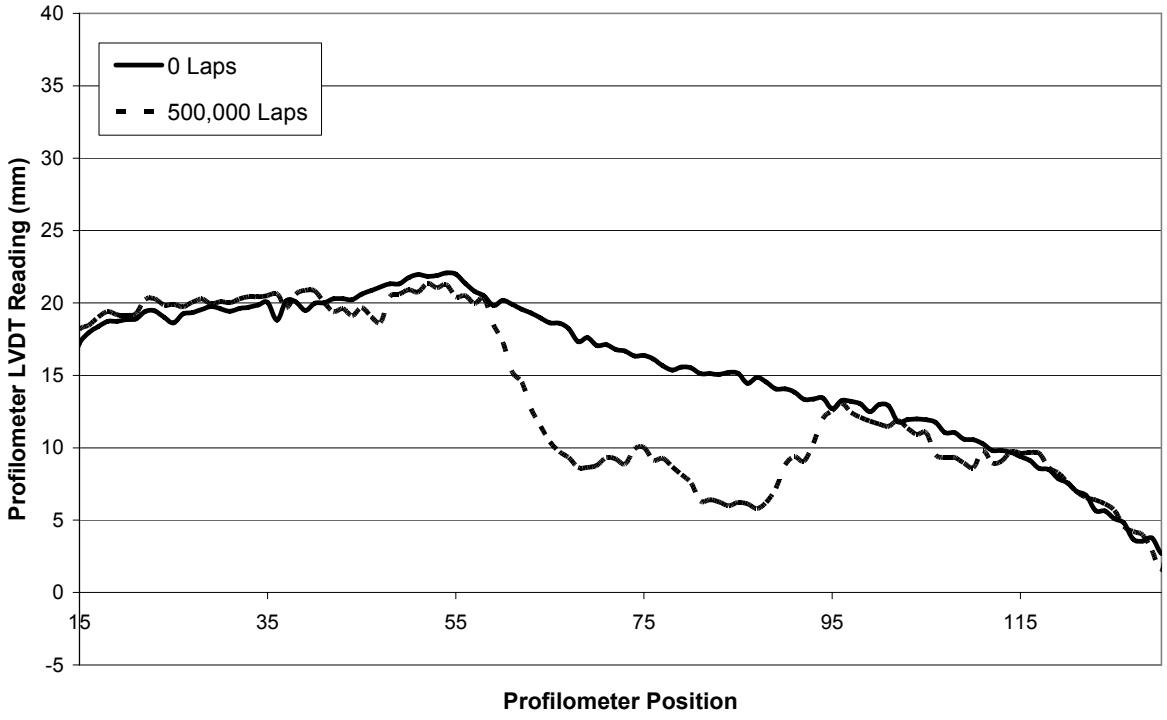

Figure B. 2 Station 51 transverse rut profile development

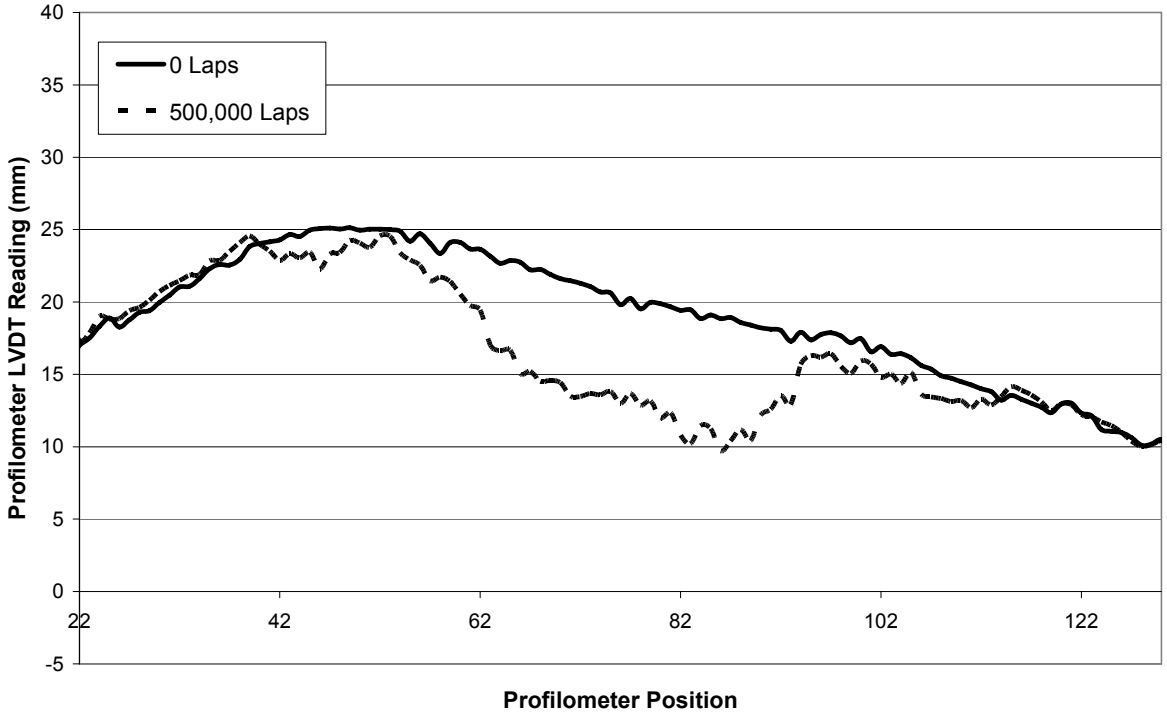

Figure B. 3 Station 52 transverse rut profile development

B.2 Second Pavement Transverse Rut Profile Development

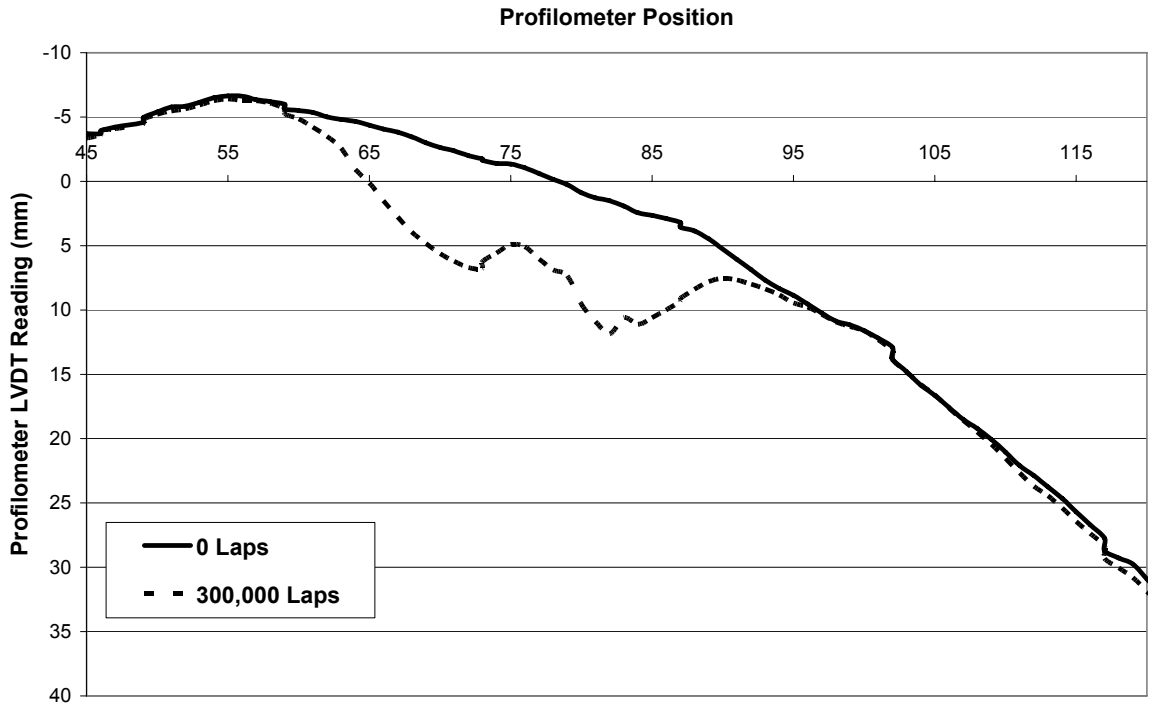

Figure B. 4 station 38 transverse rut profile development

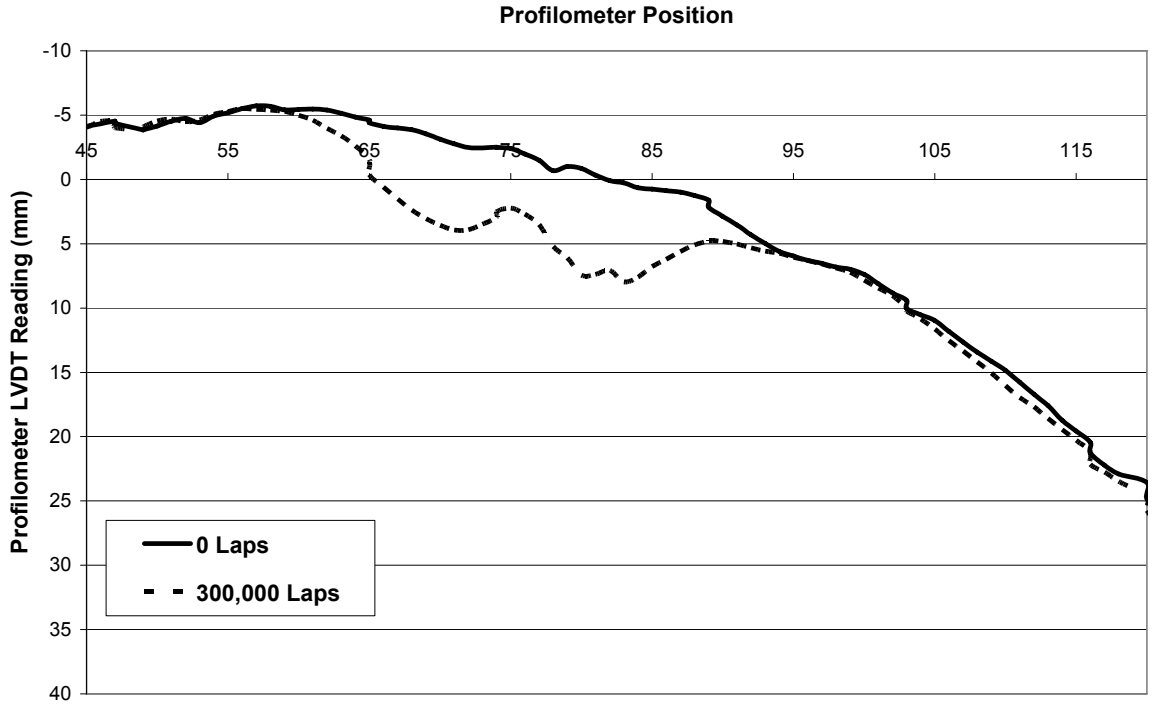

Figure B. 5 Station 39 transverse rut profile development

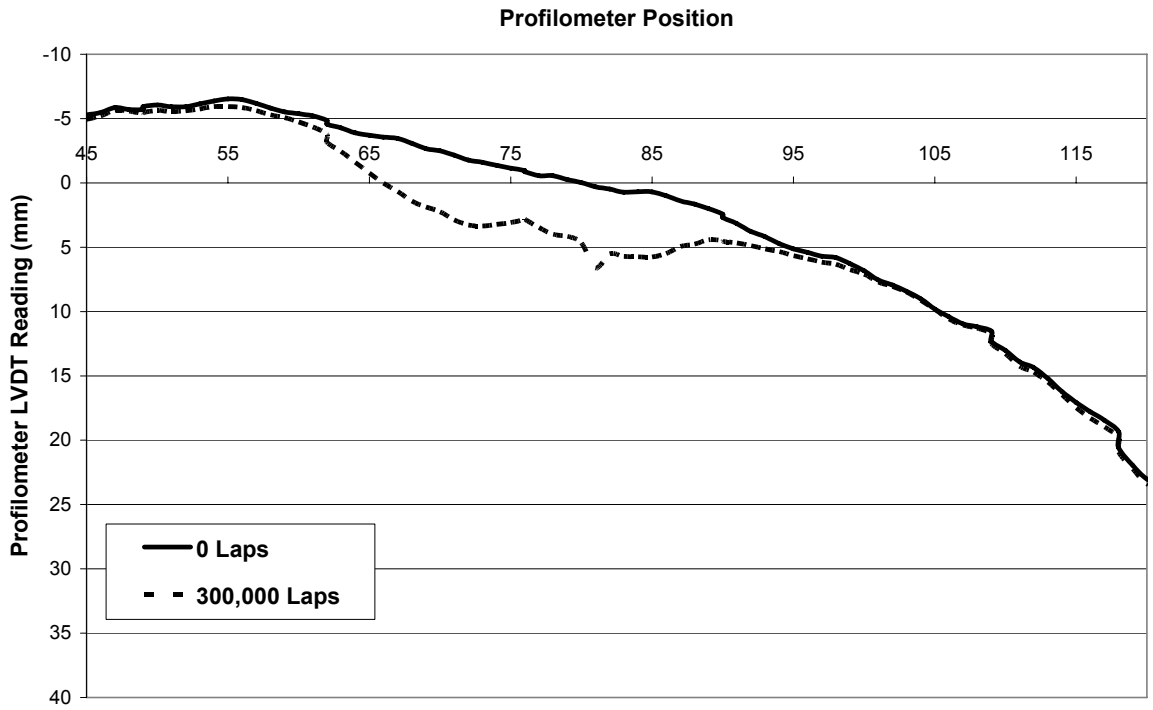

Figure B. 6 Station 40 transverse rut profile development

APPENDIX C
STUDENT T-TESTS

This appendix shows the calculations conducted on the first pavement longitudinal shear strain and rut depth data. In general, this data had a greater variance that the second pavement's data and there was a noticeably large variation in the strain data at station 52 compared with stations 50 and 51. This variation was attributed to the AC patch constructed over this station, however, statistical testing was conducted to prove that the strain data at this station was from a different population, and the station 52 data could justifiably be excluded from the analysis. All analysis was conducted with a degree of confidence of 95%.

Each analysis involved three student t-tests comparing two stations in each test. Initially an F statistic (F stat) was calculated for each test and the calculated F stat was compared to the critical value determined from statistical tables using 95% confidence. In both the strain and rut analysis, the F stat values were less than the critical F value (tabulated) and thus the pooled variance could be used in the t-tests.

The pooled variance was calculated for each set of two stations and this was in turn used to calculate the t statistic (t stat) for each pair. The t stat was compared to a critical value determined from statistical tables with a degree of confidence of 95%. If the t stat was less than the critical value, this indicated that the two sets of data were statically from the same population.

The testing showed that the shear strains from station 50 and station 51 were from the same population since the t stat of 1.82 was less than the critical value of 2.31. The analysis also proved that the low strain values at station 52 were not from the same population as station 50 and 51. This gave statistical weight to excluding the station 52 data from analysis due to the AC patch over this section.

In addition to this, because the t-tests showed that the shear strain and rut depth measurements at station 50 and 51 were from the same population, it was considered acceptable to use average values from this population to produce average strain and rut values from the overall pavement. These values were used in sensitivity analysis in Chapter 7.

C.1 Student T-Test on Longitudinal Shear Strain Measurements

Laps	50 (x)	51 (y)	52 (z)
100	2547	2640	1325
150	2503	2653	1276
200	2540	2691	1249
300	2713	2964	1338
400	2310	2532	1053
500	2682	2865	1279
Average	2549	2724	1253
Variance	20781	25506	10726

Number of Samples (n)	6

F stat		
	Var x/y	1.23
	Var y/z	2.38
	Var x/z	1.94

Since F stat are less than critical value from Fvalue table….use pool variance t test. **F value = 5**.

Pool Var xy	27772.52
Pool Var yz	21739.22
Pool Var xz	18904.34

T stat			
	Tstat (xy)	1.82	**Same Set**
	Tstat (yz)	17.28	**Not Same**
	Tstat (xz)	16.32	**Not Same**

If T stat is less than critical T value from table then reults are from same population. **T value = 2.31**

Conclusion

Strain data from station 50 and 51 are statistically from the same population (95% probability). Station 52 (z) strains are statistically not from the same population. This is probably due to the AC patch.

Equations Used

$$F_{stat} = \frac{\mathrm{var}(x)}{\mathrm{var}(y)}$$

$$\mathrm{var}_{pooled} = \frac{n_x \,\mathrm{var}(x) + n_y \,\mathrm{var}(y)}{n_x + n_y - 2}$$

$$t_{stat} = \frac{\bar{x} - \bar{y}}{\sqrt{\frac{\mathrm{var}_{pooled}}{n_x} + \frac{\mathrm{var}_{pooled}}{n_y}}}$$

C.2 Student T-Test on Maximum Rut Depth Measurements

Laps	50 (x)	51 (y)	52 (z)
15	5.6	4.3	4.9
30	6.9	4.2	6.7
50	7.7	5.2	7.1
100	9.8	7.8	7.5
150	9.6	7.5	7.4
200	11.7	8.5	8.2
300	12.1	9.8	9.2
400	12.2	10.1	8.9
500	12.2	10.1	9.2
Average	9.76	7.50	7.68
Variance	6.38	5.80	1.94

Number of Samples n	9

F stat	Var x/y	0.91
	Var y/z	2.99
	Var x/z	3.29

Since F stat are less than critical value from Fstat table….use pool variance t test. **F stat = 4.5**

Pool Var xy	6.85
Pool Var yz	4.35
Pool Var xz	4.68

T stat	Txy	1.83	**Same Set**
	Tyz	-0.18	**Same Set**
	Txz	2.04	**Same Set**

If T stat is less than critical T value from table then reults are from same population. **T value = 2.12**

Conclusion

Since all three T stat values are less than the critical value of 2.12, all rut depth data from all three stations is statistically from the same population.

Equations Used

$$F_{stat} = \frac{\text{var}(x)}{\text{var}(y)}$$

$$\text{var}_{pooled} = \frac{n_x \,\text{var}(x) + n_y \,\text{var}(y)}{n_x + n_y - 2}$$

$$t_{stat} = \frac{\bar{x} - \bar{y}}{\sqrt{\frac{\text{var}_{pooled}}{n_x} + \frac{\text{var}_{pooled}}{n_y}}}$$

APPENDIX D
ORIGINAL STRAINS – SECOND PAVEMENT

This appendix presents the original principal strain and shear strain data from the second pavement. The sudden drop in strain magnitude after 187,000 laps can be seen. This occurred after the one month break. The modified values were determined by adding the difference between the original strains values at 187,000 and 188,000 laps to the value at 203,000 laps.

For example, in the case of the vertical compressive strain at Station 38: The strain dropped from 589με at 187,000 laps to 503με at 188,000 laps, a difference of 86με. Thus the modified strain value at 203,000 laps was 557με plus the 87με difference. The new strain was 643με.

D.1 Original and Modified Strain Data

Table D. 1 Original principal strains (as presented in body of thesis)

			Laps (x1000)													
	Station	Coil	0	1	2	5	10	20	50	100	170	187	188	203	250	300
Average Strains (Tension -ve)	38	Vertical	401	432	429	479	477	479	528	549	573	589	503	557	528	507
		Transverse	-72	-104	-82	-108	-131	-140	-183	-172	-185	-188	-179	-164	-171	-160
		Longitudinal	-335	-426	-444	-583	-729	-822	-936	-1089	-1160	-1204	-992	-984	-948	-893
	39	Vertical	421	481	482	477	502	509	531	543	560	556	534	541	532	491
		Transverse	-123	-122	-112	-118	-144	-147	-213	-247	-274	-278	-240	-237	-236	-221
		Longitudinal	-445	-483	-530	-564	-592	-627	-717	-817	-848	-865	-803	-788	-684	-800
	40	Vertical	408	456	466	446	465	469	515	539	548	564	493	544	533	513
		Transverse	-53	-75	-52	-72	-81	-93	-117	-116	-98	-131	-96	-119	-121	-105
		Longitudinal	-448	-556	-486	-512	-548	-550	-654	-819	-744	-786	-711	-745	-865	-745

Table D. 2 Modified principal strain (modified values highlighted)

			Laps (x1000)												
	Station	Coil	0	1	2	5	10	20	50	100	170	187	204	250	300
Average Strains (Tension -ve)	38	Vertical	401	432	429	479	477	479	528	549	573	589	643	614	615
		Transverse	-72	-104	-82	-108	-131	-140	-183	-172	-185	-188	-173	-180	-169
		Longitudinal	-335	-426	-444	-583	-729	-822	-936	-1089	-1160	-1204	-1157	-1160	-1154
	39	Vertical	421	481	482	477	502	509	531	543	560	556	563	554	524
		Transverse	-123	-122	-112	-118	-144	-147	-213	-247	-274	-278	-275	-274	-259
		Longitudinal	-445	-483	-530	-564	-592	-627	-717	-817	-848	-865	-850	-806	-862
	40	Vertical	408	456	466	446	465	469	515	539	548	564	615	604	584
		Transverse	-53	-75	-52	-72	-81	-93	-117	-116	-98	-131	-154	-156	-140
		Longitudinal	-448	-556	-486	-512	-548	-550	-654	-819	-744	-786	-820	-940	-920

Table D. 3 Original transverse shear strains

			Laps (x1000)													
	Station	Value	0	1	2	5	10	20	50	100	170	187	188	203	250	300
Avergage Maximum Transverse Shear Strain	38	Raw Strain	473	536	511	587	608	619	711	721	758	777	682	721	699	667
		Normalised	1.000	1.133	1.080	1.241	1.285	1.309	1.503	1.524	1.603	1.643	1.442	1.524	1.478	1.410
	39	Raw Strain	544	603	594	595	646	656	744	790	834	834	774	778	768	712
		Normalised	1.000	1.108	1.092	1.094	1.188	1.206	1.368	1.452	1.533	1.533	1.423	1.430	1.412	1.309
	40	Raw Strain	461	531	518	518	546	562	632	655	646	695	589	663	654	618
		Normalised	1.000	1.152	1.124	1.124	1.184	1.219	1.371	1.421	1.401	1.508	1.278	1.438	1.419	1.341

Table D. 4 Modified transverse shear strains (modified values highlighted)

			Laps (x1000)												
	Station	Value	0	1	2	5	10	20	50	100	170	187	204	250	300
Avergage Maximum Transverse Shear Strain	38	Raw Strain	473	536	511	587	608	619	711	721	758	777	816	794	784
		Normalised	1.000	1.133	1.080	1.241	1.285	1.309	1.503	1.524	1.603	1.643	1.725	1.679	1.658
	39	Raw Strain	544	603	594	595	646	656	744	790	834	834	838	828	783
		Normalised	1.000	1.108	1.092	1.094	1.188	1.206	1.368	1.452	1.533	1.533	1.540	1.522	1.439
	40	Raw Strain	461	531	518	518	546	562	632	655	646	695	769	760	724
		Normalised	1.000	1.152	1.124	1.124	1.184	1.219	1.371	1.421	1.401	1.508	1.668	1.649	1.570

Table D. 5 Original longitudinal shear strains

			Laps (x1000)													
	Station	Value	0	1	2	5	10	20	50	100	170	187	188	203	250	300
Avergage Maximum Longitudinal Shear Strain	38	Raw Strain	736	858	873	1062	1206	1301	1464	1638	1733	1793	1495	1541	1476	1400
		Normalised	1.000	1.166	1.186	1.443	1.639	1.768	1.989	2.226	2.355	2.436	2.031	2.094	2.005	1.902
	39	Raw Strain	866	964	1012	1041	1094	1136	1248	1360	1408	1421	1337	1329	1216	1291
		Normalised	1.000	1.113	1.169	1.202	1.263	1.312	1.441	1.570	1.626	1.641	1.544	1.535	1.404	1.491
	40	Raw Strain	856	1012	952	958	1013	1019	1169	1358	1292	1350	1204	1289	1398	1258
		Normalised	1.000	1.182	1.112	1.119	1.183	1.190	1.366	1.586	1.509	1.577	1.407	1.506	1.633	1.470

Table D. 6 Modified longitudinal shear strains (modified values highlighted)

			Laps (x1000)												
	Station	Value	0	1	2	5	10	20	50	100	170	187	204	250	300
Avergage Maximum Longitudinal Shear Strain	38	Raw Strain	736	858	873	1062	1206	1301	1464	1638	1733	1793	1800	1774	1769
		Normalised	1.000	1.166	1.186	1.443	1.639	1.768	1.989	2.226	2.355	2.436	2.446	2.410	2.404
	39	Raw Strain	866	964	1012	1041	1094	1136	1248	1360	1408	1421	1413	1360	1386
		Normalised	1.000	1.113	1.169	1.202	1.263	1.312	1.441	1.570	1.626	1.641	1.632	1.570	1.600
	40	Raw Strain	856	1012	952	958	1013	1019	1169	1358	1292	1350	1435	1544	1504
		Normalised	1.000	1.182	1.112	1.119	1.183	1.190	1.366	1.586	1.509	1.577	1.676	1.804	1.757

D.2 Original and Modified Shear Strain Plots

This section shows the transverse and longitudinal shear strain plots over loading laps. The original and modified strain plots are presented.

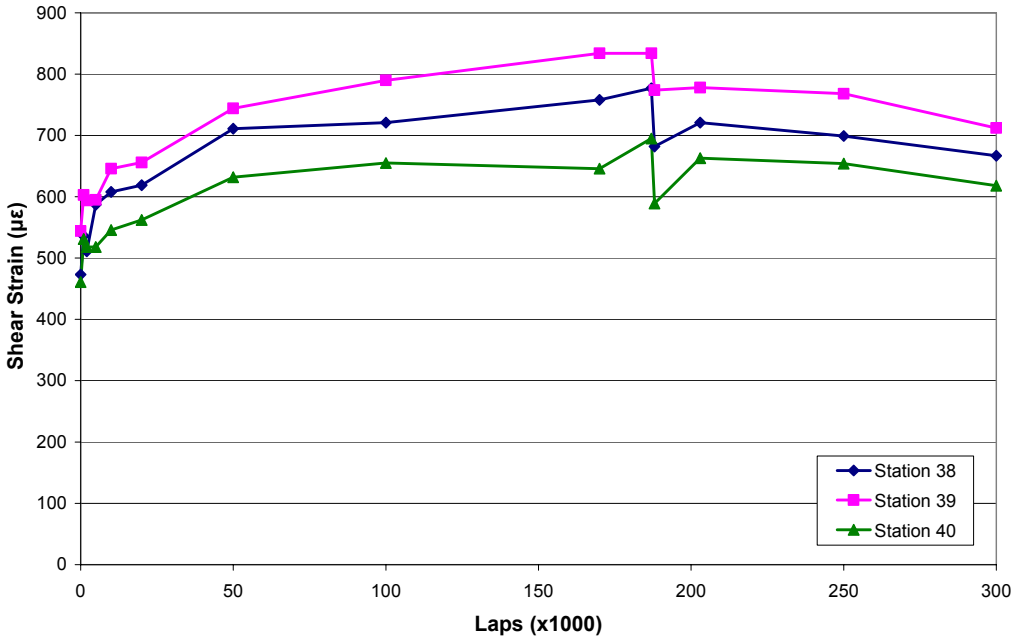

Figure D. 1 Original transverse shear strains over loading laps

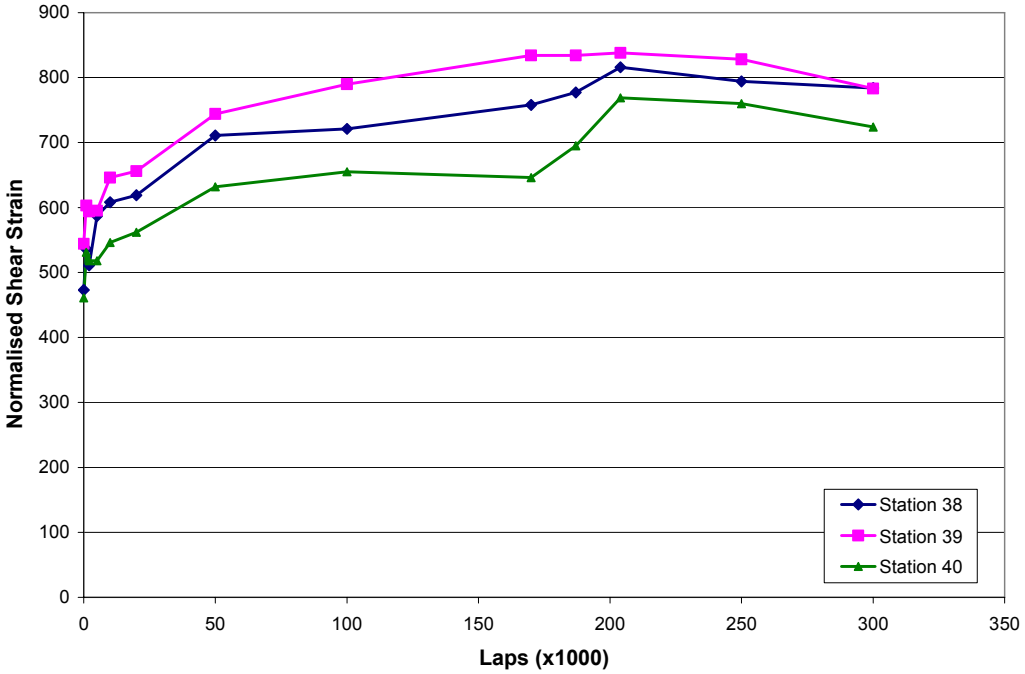

Figure D. 2 Modified transverse shear strains over loading laps

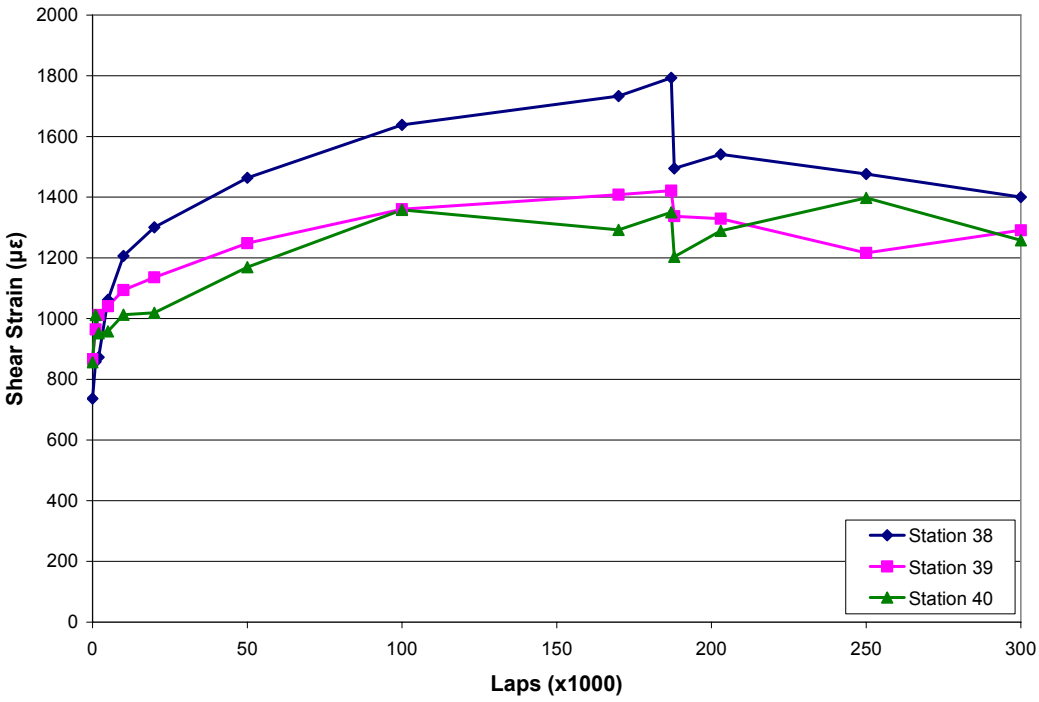

Figure D. 3 Original longitudinal shear strain over loading laps

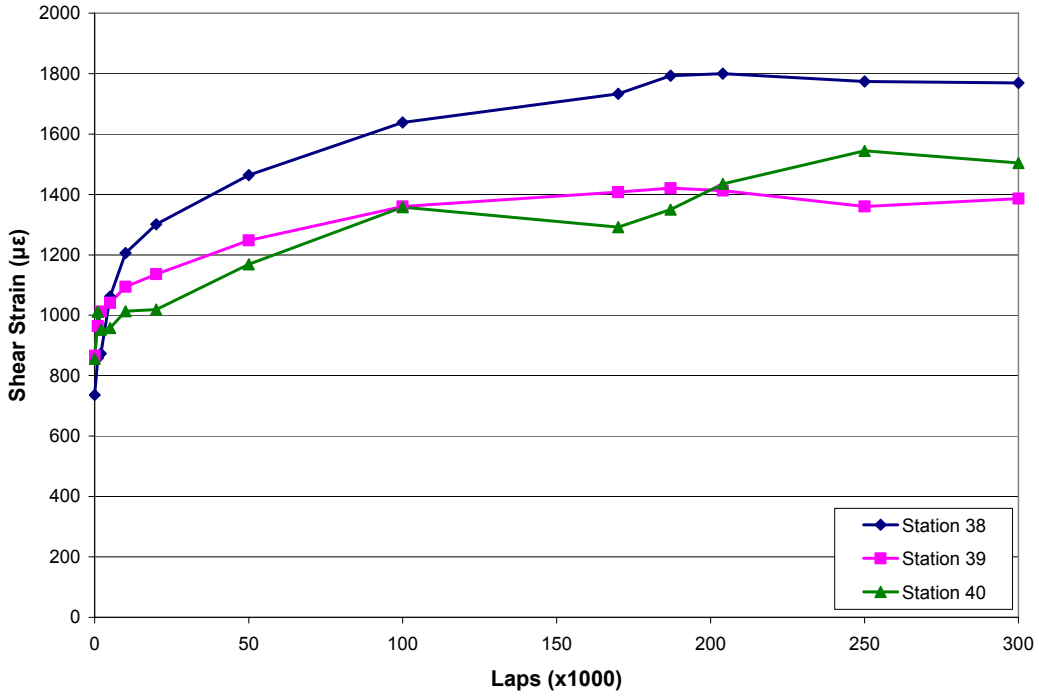

Figure D. 4 Modified longitudinal shear strain over loading laps